

DYNAMIC INVESTIGATION AND REHABILITATION OF EXISTING
RAILWAY TRUSS BRIDGE UNDER HIGH SPEED TRAIN LOADINGS FOR
PASSENGER COMFORT

A THESIS SUBMITTED TO
THE GRADUATE SCHOOL OF NATURAL AND APPLIED SCIENCES
OF
MIDDLE EAST TECHNICAL UNIVERSITY

BY

GÜNDÜZ MUTLU

IN PARTIAL FULFILLMENT OF THE REQUIREMENTS
FOR
THE DEGREE OF MASTER OF SCIENCE
IN
CIVIL ENGINEERING

FEBRUARY 2008

Approval of the thesis:

**DYNAMIC INVESTIGATION AND REHABILITATION OF EXISTING
RAILWAY TRUSS BRIDGE UNDER HIGH SPEED TRAIN LOADINGS FOR
PASSENGER COMFORT**

Submitted by **GÜNDÜZ MUTLU** in partial fulfillment of the requirements for
the degree of **Master of Science in Civil Engineering Department, Middle
East Technical University** by,

Prof. Dr. Canan Özgen
Dean, Graduate School of **Natural and Applied Sciences**

Prof. Dr. Güney Özcebe
Head of Department, **Civil Engineering**

Prof. Dr. Çetin Yılmaz
Supervisor, **Civil Engineering Dept., METU**

Asst. Prof. Dr. Alp Caner
Co-Supervisor, **Civil Engineering Dept., METU**

Examining Committee Members:

Asst. Prof Dr. Ahmet Türer
Civil Engineering Dept., METU

Prof. Dr. Çetin Yılmaz
Civil Engineering Dept., METU

Asst. Prof Dr. Alp Caner
Civil Engineering Dept., METU

Asst. Prof. Dr. Özgür Kurç
Civil Engineering Dept., METU

Deniz Hanhan, M.S.
Deha Proje Ltd. Şti.

Date:

08 / 02 / 2008

I hereby declare that all information in this document has been obtained and presented in accordance with academic rules and ethical conduct. I also declare that, as required by these rules and conduct, I have fully cited and referenced all material and results that are not original to this work.

Name, Last Name : Gündüz Mutlu

Signature :

ABSTRACT

DYNAMIC INVESTIGATION AND REHABILITATION OF EXISTING RAILWAY TRUSS BRIDGE UNDER HIGH SPEED TRAIN LOADINGS FOR PASSENGER COMFORT

Mutlu, Gündüz

M.Sc. Department of Civil Engineering

Supervisor: Prof. Dr. Çetin Yılmaz

Co-Supervisor: Asst. Prof Dr. Alp Caner

March 2008, 108 pages

In Turkey, big investments are made to improve the existing train lines for use of new high speed trains. Most of the bridges on the existing train lines are typical and in this thesis one of the standard types, the classic steel truss bridge is investigated. This thesis presents the dynamic investigation of standard type existing truss bridge for passenger comfort criteria under the high speed train loadings. Two different computational analysis models have been developed to idealize the vehicle-bridge modeling to evaluate the passenger comfort that were influenced by dynamic vibrations on bridges induced by trains. Field tests of this bridge have been conducted by two separate institutes, Middle East Technical University and Turkish State Railways, to determine the state of the bridge under existing low-speed train loadings. Eigenvalue and Time history analysis of the LARSA 4D structural analysis program has been used to investigate the vehicle-bridge interactions. The solutions obtained from the analysis have been evaluated with the experimental results. Different rehabilitation options are analytically studied to improve the serviceability of

standard steel truss bridges per Eurocode 1990:2002, Eurocode 1991-2:2003, UIC 774-3 and UIC 776-1. The focus of this research is to define a relationship between span weight per meter and passenger comfort as well as the stiffness of this type of bridge.

Keywords: Bridge, High-Speed Train, Rehabilitation, Passenger Comfort, Measurement

ÖZ

MEVCUT KAFES KİRİŞ TİPİ TREN YOLU KÖPRÜSÜNÜN HIZLI TREN YÜKLERİ ALTINDA YOLCU KONFORU İÇİN DİNAMİK İNCELEME VE İYİLEŞTİRMESİ

Mutlu, Gündüz

Yüksek Lisans, İnşaat Mühendisliği Bölümü

Tez Yöneticisi: Prof. Dr. Çetin Yılmaz

Ortak Tez Yöneticisi: Yrd. Doç. Dr. Alp Caner

Mart 2008, 108 sayfa

Türkiyede mevcut tren hatlarına, yeni hızlı trenlerin kullanılabilmemesi için çok büyük yatırımlar yapılmıştır. Mevcut tren hatları üzerinde bulunan köprülerden çoğu tipiktir ve bu tezde standart tiplerden bir tanesi olan çelik kafes kiriş köprü tipi incelenmiştir. Bu tez köprünün, hızlı tren yüklemeleri altında, yolcu konforu kriterinin göz önüne alındığı dinamik incelemeleri içermektedir. Hızlı tren geçişi sırasında köprüde oluşan dinamik titreşimlerden etkilenen yolcu konforunu irdeleyebilmek amacı ile Tren-Köprü etkileşimini idealleştirecek iki farklı bilgisayar analiz modeli oluşturulmuştur. Köprünün mevcut durumda çalışmakta olan klasik tren yükleri altındaki durumunu belirleyebilmek amacı ile Saha testleri iki farklı kurum, Orta Doğu Teknik Üniversitesi ve T.C. Devlet Demiryolları, tarafından gerçekleştirilmiştir. Tren-Köprü etkileşimlerini inceleyebilmek için LARSA 4D yapısal analiz yazılımının Eigenvalue ve zaman alanı analizleri kullanılmıştır. Analizlerden elde edilen sonuçlar saha testlerinden elde edilen sonuçlar ile birlikte değerlendirilmiştir. Çelik kiriş köprünün servis durumunu, Eurocode 1990:2002, Eurocode 1991-

2:2003, UIC 774-3 ve UIC 776-1 yönetmeliklerine göre geliştirebilmek için farklı iyileştirme seçenekleri analitik olarak incelenmiştir. Bu araştırmanın amacı birim metredeki köprü ağırlığı ve rijitliği ile yolcu konforu arasında bir ilişki tanımlamaktır.

Anahtar Kelimeler: Köprü, Hızlı Tren, İyileştirme, Yolcu Konforu, Ölçüm

To my family

ACKNOWLEDGEMENTS

It is a great pleasure for me to complete my Master thesis and have the opportunity to thank all who were always nearby me during the whole studies.

First of all, I would like to thank my advisor Prof. Dr. Çetin Yılmaz, who directed me to the area of bridges and high-speed trains, for his expert guidance. Working with him has been a rewarding experience.

I am also thankful to my co-advisor Asst. Prof. Dr. Alp Caner, for his valuable knowledge, great patience, motivating ability shown at the hopeless moments and continuous guidance.

My thanks also go to Asst. Prof. Dr. Ahmet Türer, for his valuable criticism and encouragement at various stages of this thesis.

For my dearest wife and parents, I can never thank them enough with any words for their endless love and supports. They have always understood me at hard times and shared all stressful days and nights with me.

TABLE OF CONTENTS

ABSTRACT.....	iv
ÖZ	vi
DEDICATION	viii
ACKNOWLEDGEMENTS.....	ix
TABLE OF CONTENTS.....	x
LIST OF TABLES.....	xii
LIST OF FIGURES	xiv
LIST OF SYMBOLS AND ABBREVIATIONS	xxii
CHAPTER	
1. INTRODUCTION	1
1.1. History	1
1.2. The Objectives and Scope of The Study.....	3
2. LITERATURE REVIEW	5
3. ANALYSIS PROCEDURE	11
3.1. Description of The Bridge	11
3.2. Field Testing.....	13
3.2.1. Testing Equipment.....	13
3.3. Computer Modeling	14
3.3.1. Moving Force Model	15
3.3.2. Moving Suspension Mass Model	20
3.4. Analysis Specifications	27
3.4.1. Dynamic Analysis Parameters.....	30
3.5. Rehabilitation	35
3.6. Computational Analysis Methods	35
3.6.1. Non-Linear Time History Analysis.....	35
3.6.2. Eigenvalue analysis.....	36

4. FIELD TEST AND ANALYSIS RESULTS	37
4.1. Introduction	37
4.2. Field Test Results	40
4.3. Moving Force Model Analysis Results	43
4.4. Moving Suspension Mass Model Analysis Results	50
4.5. Moving Force Model and Moving Suspension Mass Model Analysis Results Comparison	54
4.6. Eigenvalue Analysis Results	56
5. DISCUSSION ON RESULTS	59
5.1. Introduction	59
5.2. Discussion on Field Test Results	59
5.3. Discussion on Moving Force Model Analysis Results	60
5.4. Discussion on Moving Suspension Mass Model Analysis Results	62
5.5. Discussion on Moving Force Model and Moving Suspension Mass Model Analysis Results Comparison	63
5.6. Discussion on Eigenvalue Analysis Results	65
6. SUMMARY AND CONCLUSION	66
REFERENCES	68
APPENDICES	
A. SELECTIVE ANALYSIS RESULTS	72

LIST OF TABLES

TABLES

Table 3.1	Properties of German ICE, Japanese SKS, and French TGV High-Speed Railway Trains.....	26
Table 3.2	Values of Damping to be assumed for design purposes	30
Table 3.3	Application of HSLM-A and HSLM-B Trains.....	34
Table 3.4	HSLM-A Train Loading Cases	34
Table 4.1	Recommended levels of comfort	38
Table 4.2	Limiting values of deck twist	39
Table 4.3	Joint Acceleration (m/sec^2) values at midspan of bridge with different sections and mass dampers under HSLM-A10 train loading with varying speeds ...	44
Table 4.4	Max Joint Acceleration values at midspan of bridge with different sections and mass dampers under HSLM-A10 train loadings	44
Table 4.5	Joint Displacement (m) values of different sections with different mass dampers under HSLM-A10 train loading with varying speeds.....	46
Table 4.6	Max Joint Displacement values at midspan of bridge with different sections and mass dampers under HSLM-A10 train loadings	46
Table 4.7	Joint Rotation values at midspan of bridge with different sections and mass dampers under HSLM-A10 train loading with varying speeds	48
Table 4.8	Max Joint Rotation values at midspan of bridge with different sections and mass dampers under HSLM-A10 train loadings	48
Table 4.9	% Decrease of Joint Acceleration values at midspan of bridge with the effect of mass dampers under HSLM-A10 train loadings	50
Table 4.10	Joint Acceleration (m/sec^2) values at midspan of bridge with different sections under HSLM-A10 train loading with varying speeds.....	51
Table 4.11	Joint Displacement (m) values at midspan of bridge with different sections under HSLM-A10 train loading with varying speeds.....	52

Table 4.12	Joint Rotation (mm/3m) values at midspan of bridge with different sections under HSLM-A10 train loading with varying speeds.....	53
Table 4.13	First five modes of the model without rehabilitation	56
Table 4.14	First Natural Frequencies and Periods of sections with varying mass increments	58

LIST OF FIGURES

FIGURES

Figure 3.1	General view of Steel Truss Bridge from ground	12
Figure 3.2	Entrance of the Steel Truss Bridge	12
Figure 3.3	A wireless accelerometer node.....	14
Figure 3.4	Dynamic model of train-bridge system.....	14
Figure 3.5	Example of a model of a track/structure system.....	16
Figure 3.6	Train loading models	17
Figure 3.7	Resistance k of the track per unit length as a function of the longitudinal displacement u of the rails.....	18
Figure 3.8	Defined Moving Force Model at Larsa 4D	19
Figure 3.9	Section of the Moving Force model	20
Figure 3.10	Moving suspension mass model/sprung mass model	20
Figure 3.11	Equivalent Spring Force vs. Displacement graph obtained by using Runge-Kutta algorithm.....	24
Figure 3.12	Velocity vs. Displacement graph obtained by using Runge-Kutta algorithm.....	24
Figure 3.13	Velocity vs. Time graph obtained by using Runge-Kutta algorithm	25
Figure 3.14	Displacement vs. Time graph obtained by using Runge-Kutta algorithm	25
Figure 3.15	Section of the Moving Suspension Mass Model	27
Figure 3.16	Defined Moving Suspension Mass Model at Larsa 4D.....	27
Figure 3.17	Flow chart for determining whether a dynamic analysis is required or not.....	29
Figure 3.18	Additional damping $\Delta\zeta$ [%] as a function of span length L	30

Figure 3.19	HSLM-A Train Spacing	33
Figure 3.20	Load Model 71 and characteristic values for vertical loads	33
Figure 4.1	Maximum permissible vertical deflection δ for railway bridges with 3 or more successive simply supported spans corresponding to a permissible vertical acceleration of $b_v = 1 \text{ m/sec}^2$ in a coach for speed V [km/h]	38
Figure 4.2	Definition of deck twist	38
Figure 4.3	X-Z cross section of the analysis model.....	39
Figure 4.4	Y-Z cross section of the analysis model.....	40
Figure 4.5	Measured Acceleration record from the truss bridge, scaled down to $1/10^{\text{th}}$ of magnitude	41
Figure 4.6	Minimum and Maximum accelerations recorded from the truss bridge	42
Figure 4.7	Free vibration stabilization diagram	42
Figure 4.8	Max Joint Acceleration values at midspan of bridge with different sections and mass dampers under HSLM-A10 train loadings.....	45
Figure 4.9	Trendline of Max Joint Acceleration at midspan of bridge with different per meter weight	45
Figure 4.10	Max Joint Displacement values at midspan of bridge with different sections and mass dampers under HSLM-A10 train loadings.....	47
Figure 4.11	Trendline of Max Joint Displacement at midspan of bridge with different per meter weight	47
Figure 4.12	Max Joint Rotation values at midspan of bridge with different sections and mass dampers under HSLM-A10 train loadings.....	49
Figure 4.13	Trendline of Max Joint Rotation at midspan of bridge with different per meter weight	49
Figure 4.14	Max Joint Acceleration values with trendline at midspan of bridge with different sections under HSLM-A10 train loadings.....	51

Figure 4.15	Max Joint Displacement values with trendline at midspan of bridge with different sections under HSLM-A10 train loadings.....	52
Figure 4.16	Max Joint Rotation values with trendline at midspan of bridge with different sections under HSLM-A10 train loadings.....	53
Figure 4.17	Max Joint Rotation with assumed values of mass damper effects at midspan of bridge with different sections under HSLM-A10 train loadings	54
Figure 4.18	Max Joint Acceleration values at midspan of bridge with different sections under HSLM-A10 train loadings	54
Figure 4.19	Max Joint Displacement values at midspan of bridge with different sections under HSLM-A10 train loadings	55
Figure 4.20	Max Joint Rotation values at midspan of bridge with different sections under HSLM-A10 train loadings	55
Figure 4.21	Spring Force values at the midspan of the existing bridge under HSLM-A10 train loading with a speed of 70 m/hr	56
Figure 4.22	First bending mode of existing steel bridge with concrete deck.....	57
Figure 4.23	First torsional mode of existing steel bridge with concrete deck.....	57
Figure A.1	Joint acceleration vs. time graphic of E1 analysis model with a speed of 75 m/sec.....	72
Figure A.2	Joint acceleration vs. time graphic of E1-5 analysis model with a speed of 75 m/sec.....	73
Figure A.3	Joint acceleration vs. time graphic of E1-10 analysis model with a speed of 75 m/sec.....	73
Figure A.4	Joint acceleration vs. time graphic of E2 analysis model with a speed of 75 m/sec.....	74
Figure A.5	Joint acceleration vs. time graphic of E2-5 analysis model with a speed of 75 m/sec.....	74
Figure A.6	Joint acceleration vs. time graphic of E2-10 analysis model with a speed of 75 m/sec.....	75

Figure A.7	Joint acceleration vs. time graphic of E3 analysis model with a speed of 75 m/sec.....	75
Figure A.8	Joint acceleration vs. time graphic of E3-5 analysis model with a speed of 75 m/sec.....	76
Figure A.9	Joint acceleration vs. time graphic of E3-10 analysis model with a speed of 75 m/sec.....	76
Figure A.10	Joint acceleration vs. time graphic of E4 analysis model with a speed of 75 m/sec.....	77
Figure A.11	Joint acceleration vs. time graphic of E4-5 analysis model with a speed of 75 m/sec.....	77
Figure A.12	Joint acceleration vs. time graphic of E4-10 analysis model with a speed of 75 m/sec.....	78
Figure A.13	Joint acceleration vs. time graphic of E5 analysis model with a speed of 75 m/sec.....	78
Figure A.14	Joint acceleration vs. time graphic of E5-5 analysis model with a speed of 75 m/sec.....	79
Figure A.15	Joint acceleration vs. time graphic of E5-10 analysis model with a speed of 75 m/sec.....	79
Figure A.16	Combined Joint acceleration vs. time graphic of analysis models without mass damping under a speed of 75 m/sec	80
Figure A.17	Combined Joint acceleration vs. time graphic of analysis models with 5% mass damping under a speed of 75 m/sec	80
Figure A.18	Combined Joint acceleration vs. time graphic of analysis models with 10% mass damping under a speed of 75 m/sec.....	81
Figure A.19	Joint Displacement vs. time graphic of E1 analysis model with a speed of 75 m/sec.....	81
Figure A.20	Joint Displacement vs. time graphic of E1-5 analysis model with a speed of 75 m/sec.....	82
Figure A.21	Joint Displacement vs. time graphic of E1-10 analysis model with a speed of 75 m/sec.....	82
Figure A.22	Joint Displacement vs. time graphic of E2 analysis model with a speed of 75 m/sec.....	83

Figure A.23	Joint Displacement vs. time graphic of E2-5 analysis model with a speed of 75 m/sec.....	83
Figure A.24	Joint Displacement vs. time graphic of E2-10 analysis model with a speed of 75 m/sec.....	84
Figure A.25	Joint Displacement vs. time graphic of E3 analysis model with a speed of 75 m/sec.....	84
Figure A.26	Joint Displacement vs. time graphic of E3-5 analysis model with a speed of 75 m/sec.....	85
Figure A.27	Joint Displacement vs. time graphic of E3-10 analysis model with a speed of 75 m/sec.....	85
Figure A.28	Joint Displacement vs. time graphic of E4 analysis model with a speed of 75 m/sec.....	86
Figure A.29	Joint Displacement vs. time graphic of E4-5 analysis model with a speed of 75 m/sec.....	86
Figure A.30	Joint Displacement vs. time graphic of E4-10 analysis model with a speed of 75 m/sec.....	87
Figure A.31	Joint Displacement vs. time graphic of E5 analysis model with a speed of 75 m/sec.....	87
Figure A.32	Joint Displacement vs. time graphic of E5-5 analysis model with a speed of 75 m/sec.....	88
Figure A.33	Joint Displacement vs. time graphic of E5-10 analysis model with a speed of 75 m/sec.....	88
Figure A.34	Combined Joint displacement vs. time graphic of analysis models without mass damper under a speed of 75 m/sec.....	89
Figure A.35	Combined Joint displacement vs. time graphic of analysis models with 5% mass damper under a speed of 75 m/sec.....	89
Figure A.36	Combined Joint displacement vs. time graphic of analysis models with 10% mass damper under a speed of 75 m/sec.....	90
Figure A.37	Joint rotation vs. time graphic of E1 analysis model with a speed of 75 m/sec	90
Figure A.38	Joint rotation vs. time graphic of E1-5 analysis model with a speed of 75 m/sec	91

Figure A.39	Joint rotation vs. time graphic of E1-10 analysis model with a speed of 75 m/sec	91
Figure A.40	Joint rotation vs. time graphic of E2 analysis model with a speed of 75 m/sec	92
Figure A.41	Joint rotation vs. time graphic of E2-5 analysis model with a speed of 75 m/sec	92
Figure A.42	Joint rotation vs. time graphic of E2-10 analysis model with a speed of 75 m/sec	93
Figure A.43	Joint rotation vs. time graphic of E3 analysis model with a speed of 75 m/sec	93
Figure A.44	Joint rotation vs. time graphic of E3-5 analysis model with a speed of 75 m/sec	94
Figure A.45	Joint rotation vs. time graphic of E3-10 analysis model with a speed of 75 m/sec	94
Figure A.46	Joint rotation vs. time graphic of E4 analysis model with a speed of 75 m/sec	95
Figure A.47	Joint rotation vs. time graphic of E4-5 analysis model with a speed of 75 m/sec	95
Figure A.48	Joint rotation vs. time graphic of E4-10 analysis model with a speed of 75 m/sec	96
Figure A.49	Joint rotation vs. time graphic of E5 analysis model with a speed of 75 m/sec	96
Figure A.50	Joint rotation vs. time graphic of E5-5 analysis model with a speed of 75 m/sec	97
Figure A.51	Joint rotation vs. time graphic of E5-10 analysis model with a speed of 75 m/sec	97
Figure A.52	Combined Joint rotation vs. time graphic of analysis models without mass damper under a speed of 75 m/sec	98
Figure A.53	Combined Joint rotation vs. time graphic of analysis models with 5% mass damper under a speed of 75 m/sec	98
Figure A.54	Combined Joint rotation vs. time graphic of analysis models with 10% under a speed of 75 m/sec	99

Figure A.55	Joint acceleration vs. time graphic of E1 analysis model with a speed of 70 m/sec.....	100
Figure A.56	Joint acceleration vs. time graphic of E2 analysis model with a speed of 70 m/sec.....	100
Figure A.57	Joint acceleration vs. time graphic of E3 analysis model with a speed of 70 m/sec.....	101
Figure A.58	Joint acceleration vs. time graphic of E4 analysis model with a speed of 70 m/sec.....	101
Figure A.59	Joint acceleration vs. time graphic of E5 analysis model with a speed of 70 m/sec.....	102
Figure A.60	Joint displacement vs. time graphic of E1 analysis model with a speed of 70 m/sec.....	102
Figure A.61	Joint displacement vs. time graphic of E2 analysis model with a speed of 70 m/sec.....	103
Figure A.62	Joint displacement vs. time graphic of E3 analysis model with a speed of 70 m/sec.....	103
Figure A.63	Joint displacement vs. time graphic of E4 analysis model with a speed of 70 m/sec.....	104
Figure A.64	Joint displacement vs. time graphic of E5 analysis model with a speed of 70 m/sec.....	104
Figure A.65	Joint rotation vs. time graphic of E1 analysis model with a speed of 70 m/sec	105
Figure A.66	Joint rotation vs. time graphic of E2 analysis model with a speed of 70 m/sec	105
Figure A.67	Joint rotation vs. time graphic of E3 analysis model with a speed of 70 m/sec	106
Figure A.68	Joint rotation vs. time graphic of E4 analysis model with a speed of 70 m/sec	106
Figure A.69	Joint rotation vs. time graphic of E5 analysis model with a speed of 70 m/sec	107
Figure A.70	Combined Joint acceleration vs. time graphic of analysis models with a speed of 70 m/sec	107
Figure A.71	Combined Joint acceleration vs. time graphic of analysis models with a speed of 70 m/sec	108

Figure A.72 Combined Joint acceleration vs. time graphic of
analysis models with a speed of 70 m/sec 108

LIST OF SYMBOLS AND ABBREVIATIONS

TGV	: Train a Grande Vitesse
TCDD	: Turkish State Railways
EN	: Eurocode
IAPF	: Spanish Code
MTMD	: Multi Tuned Mass Damper
TMD	: Tuned Mass Damper
METU	: Middle East Technical University
Ghz	: Gigahertz
v	: Speed
m_{vk}	: Half mass of the k^{th} train car
c_{vk}	: Damping coefficient of vertical bolster spring of the k^{th} train car
k_{vk}	: Stiffness coefficient of vertical bolster spring of the k^{th} train car
m_b	: Mass of bogie
I_b	: Moment of inertia of bogie
c_b	: Damping coefficient of axle springs
k_b	: Stiffness coefficient of axle springs
m_w	: Mass of wheel set
l_w	: Half distance of wheel base
d	: Regular spacing of group of axles
e_v	: Eccentricity of the train loading
L	: Span Length
LM	: Load Model
Φ_3	: Dynamic factor for railway Load Model 71,SW/0 and SW/2
φ',φ''	: Dynamic enhancement of static loading for real trains

Φ'_{dyn}	: Dynamic enhancement of static loading for real train determined from a dynamic analysis
L_{Φ}	: Determinant length (length associated with Φ)
$Y_{\text{dyn}}, Y_{\text{stat}}$: Maximum dynamic response and maximum corresponding static response at any particular point
Max	: Maximum
a	: Distance between rail supports, distributed loads length
n_0	: First natural bending frequency of the bridge loaded by permanent actions [Hz]
n_t	: First natural torsional frequency of the structure
ζ	: Lower limit of percentage of critical damping (%), or damping ratio
$\Delta\zeta$: Additional damping (%)
ζ_{Total}	: Total damping (%)
w_i, w_j	: Natural frequencies in radian per second
a_0	: Mass proportional coefficient of Rayleigh Damping
a_1	: Stiffness proportional coefficient of Rayleigh Damping
v_i	: Resonant Speed
λ_i	: Principal wavelength of frequency of excitation
E1	: Existing state of the truss bridge with a substitution of concrete deck on for timber sleepers
Ei	: i times of the E1 section, where $i=2, 3, 4$ and 5

CHAPTER 1

INTRODUCTION

1.1. History

Increasing population on the world causes to an increasing demand on the public transportation. Driven by a developing economy and supported by a technological evolutions, this issue results to modernization of railway networks. The High-Speed Trains were started to be constructed at late 50's.

High-speed rail is a type of passenger rail transport that operates significantly faster than the normal speed of rail traffic. Specific definitions include 200-320 km/h - depending on whether the track is upgraded or new - by the European Union and above 145 km/h by the United States Federal Railroad Administration, but there is no single standard, and lower speeds can be required by local constraints. Today world's fastest high speed train is the JR-Maglev with a top speed of 581 km/h in Japan.

While high-speed rail is designed for passenger travel, some high speed systems offer also some kind of freight service. For instance, the French mail service La Poste owns a few special TGV trains for carrying postal freight.

Railways were the first form of mass transportation, and until the development of the motorcar in the early 20th century had an effective

monopoly on land transport. Railway companies in Europe and the United States used streamlined trains since 1933 for high speed services with an average speed of up to 130 km/h and top speed of more than 160 km/h. With this service they were able to compete with the upcoming airplanes. World War II stopped these services. In 1957, the Odakyu Electric Railway in Greater Tokyo launched its Romancecar 3000 SSE. This set a world record for narrow gauge trains at 145 km/h, giving Japanese designer's confidence they could safely build even faster trains at standard gauge. Desperate for transport solutions due to overloaded trains between Tokyo and Osaka, Japan, the idea of high speed rail was born.

The world's first "high-speed train" was Japan's Tōkaidō Shinkansen, officially opened in October 1964, with construction commencing in 1959. The 0 Series Shinkansen, built by Kawasaki Heavy Industries, had achieved speeds of 200 km/h on the Tokyo–Nagoya–Kyoto–Osaka route.

The countries that have trains with maximum operation speeds currently at over 200 km/h are as follows: [3]

Belgium	China	Finland
France	Germany	Italy
Japan	Norway	Portugal
Russia	South Korea	Spain
Sweden	Switzerland	Taiwan
United Kingdom	United States	

In Turkey TCDD was founded in 1927. Although all the lines were connected at the time of TCDD creation, they did not constitute a network suitable for an efficient transportation. Large parts of Anatolia had no railways and some large cities were still not connected. A

development program was prepared by the government and entrusted to TCDD to carry it over. On average, TCDD doubled the size of the network (from about 4000 km in 1924 to 8500 km today). After the Second World War, Turkey shifted its priorities from rail to road transportation. In the 1990's, urban networks, from light rail to heavy metro were inaugurated in most of the large Turkish cities. Transportation needs in large cities and road congestion brought about the latest shift in TCDD strategy. [2] In the early 2000's, TCDD forgo its network expansion strategy and focused instead on the upgrade and modernization of mainlines with High-Speed Railways.

The Turkish State Railways started building high-speed rail lines in 2003. The commercial high speed trains are expected to reach top speeds of 250-300 km/h on these tracks. The first ten high speed train sets were purchased from CAF of Spain, and have a maximum speed of 250 km/h.

1.2. The Objectives and Scope of the Study

In consequence of the increasing axle loads of the trains, modernization generally proceeds by building new lines and new bridges. Rehabilitation of the existing bridges for new lines is an alternative solution to these modernization options. This thesis aims to research the possibility of this alternative solution and create a methodology of analysis.

The majority of existing bridges in Turkey are simple span truss bridges. Therefore a sample bridge of this type is selected to be studied. Experimental data had been collected during different freight and passenger train passages. Two different computational analysis models have been developed to idealize the vehicle-bridge models to

evaluate the passenger comfort that were influenced by dynamic vibrations on bridges induced by trains.

Under the loads of High-Speed Trains, the bridges are subjected to high impacts. During studies of this thesis many useful results have been achieved. However, since there is not yet any high-speed railway line in operation for the moment now in Turkey, these theoretical results will need to be supported and proved by experimental data.

CHAPTER 2

LITERATURE REVIEW

Frýba [8] investigated an elementary theoretical model of a bridge using the integral transformation method which provides an estimation of the amplitudes of the free vibration and also gives the critical speeds at which the resonance vibration may occur. As a result of this study, simple expressions similar to dynamic impact factor which is defined as the difference between the maximum dynamic response and the maximum static deflection at midspan, has been given for the deflection, bending moment and acceleration of the bridge deck values which enable to assess the railway bridges for high speed trains. These theoretical values were satisfactorily compared with the experimental data.

By idealizing the train as a sequence of identical vehicles moving at constant speed, Biondi, Muscolino and Sofi [9] investigated the dynamic interaction between a running train, the track structure and the supporting bridge by using substructure technique. The rails and the bridge are modeled as Bernoulli–Euler beams and the ballast is characterized as a viscoelastic foundation. Consequently, an accurate and efficient model has been developed.

Another study has been made by Museros, Romero, Poy and Alarcón [10] to eliminate the difference between the results of a moving load model and more sophisticated model analysis on short bridges. They concluded that the maximum accelerations of the deck are not

significantly affected from the load distribution through the sleepers and ballast layer and the train-bridge interaction causes reductions of considerable importance in the maximum displacements and accelerations of short bridges.

Turer [11] measured the vibration level of two steel bridges, by using wireless accelerometer nodes, with different span lengths and structural types during conventional train passage. Simple interactions between train speed and transverse beam spacing were evaluated for possible resonance conditions. As a result, simple evaluation results have supported the findings obtained from measurements indicating that existing bridges would likely run into serious resonance, safety and serviceability problems if tried to be used for fast or high-speed trains.

Another vibration measurement has been made by De Roeck, Maeck and Teughels [12] to validate the previously developed numerical models at a high speed train bridge in Antoing. A dynamic displacement of 2 mm for a span of 50 m and a bridge acceleration of 1 m/sec² has been measured which were very small values when compared with usual values of other bridge measurements. This situation has been associated with the stiffness of the bridge.

Xia and Zhang [13] studied the dynamic interaction between high-speed train and bridge by theoretical analysis and field experiment. Each vehicle was composed of a body, two bogies and four wheel-sets and the spring-dashpot suspensions between three components. Each of the bodies, bogies and wheels respectively has, five, five and three degrees of freedom systems. Consequently vehicles were modeled by 27 degrees of freedom and the bridge was modeled by modal superposition technique. The whole recorded histories of the China-Star high-speed train on the Qin-Shen Special Passenger Railway in

China were applied on the computational model and the calculated results were compared with the measured data. Consequently, a well match has been achieved between the calculated and the measured data.

Heiden, Bokan, Simões da Silva, Greiner, Pirchere and Pircher [14] discussed the organization of part 2 of Eurocode 1 and the annex A2 of Eurocode 0, with special emphasis on the design checks associated with dynamic effects and train-bridge interaction, a discussion some additional rules recently imposed in the German regulations and the application of these rules to a composite trussed railway bridge which was currently being designed for the German rail network. It was found that the type of bridge that presented at the study complies with both of the requirements.

A paper of Geier and Österreicher [15] presents a combined assessment method that can be applied to evaluate railway bridges subject to dynamic stress in accordance with Eurocode 1. The objective of the method described in the paper was to assess the adherence to permissible structural acceleration by taking into account dynamic magnification factors based on a computer model. As a conclusion, the effects of boundary beams, ballast and rails had a major influence on the dynamic properties of the structure as far as short to medium span railway bridges are concerned.

Another dynamic experiment on the Antoin Bridge has been executed and reported by Xia, De Roeck, Zhang and Maeck. [16] In the experiments, the dynamic responses of the bridge such as the deflections, the accelerations and the strains were measured by a laser velocity displacement transducer accelerometers and strain gauges, respectively. Many useful results have been obtained and reported from the analysis of the recorded data.

A valuable study on modeling has been made by Delgado and dos Santos. [17] The railway traffic on bridges was performed by two different methodologies. The first model contains a set of moving masses which the effects of the moving forces and masses implied. In the second model both the structural behavior of the train and the interaction with the bridge were involved. The main aim of the study was to evidence the importance of different parameters such as stiffness and mass of the bridge, stiffness of the train; in order to investigate the structural behavior of the bridge and the riding comfort. Various parameters have been studied with a railway bridge, such as: the stiffness and length of the bridge, the existence of ballast, structural damping and irregularities in the track. In the parametric study the stiffness and irregularities were found to be the most important parameters inducing the response.

Goicolea, Dominguez, Navarro and Gabaldon [18] proposed a general revision of available methods for dynamic calculation, as well as a description of the provisions in the new codes IAPF and Eurocode 1 for actions on bridges. Also they proposed a simplified method for dynamic analysis of portal frames. In this study several simplified or sophisticated models of analysis were described for the purpose of the design of high speed railroad bridges which requires consideration of the dynamic vibration under moving loads because of the real possibility of resonance.

An investigation has been made by Ju and Lin [19] to determine the resonant characteristics of three-dimensional bridges under high-speed train loadings. Multi-span bridges with high piers and simply supported beams were used in the dynamic finite element analysis. It has been concluded that to avoid resonance, the dominated train frequencies and the bridge natural frequencies should be as different as possible, especially for the first dominated train frequency and the first bridge

natural frequency in each direction. This study also indicated that a suitable axial stiffness between two simple beams can reduce vibrations at a near-resonance condition.

Yang, Yau and Hsu [20] developed a train model to investigate the vibration of simple beams subjected to the passage of high speed trains as a composition of two subsystems of wheel loads of constant intervals, with one consisting of all the front wheel front wheel assemblies and the other rear assemblies. By an analytical approach, the key parameters that govern the dynamic responses of the beams were identified, using the moving load assumption. As a result, several design parameters have been obtained to avoid resonance situation.

Lin, Asce, Wan and Chen [21] researched applicability of multiple tuned mass dampers to suppress train-induced vibration on bridges. A railway bridge has been modeled as an Euler-Bernoulli beam and a train has been simulated as a series of moving forces, moving masses, or moving suspension masses. An MTMD system has been designed to alter the bridge dynamic characteristics to avoid excessive vibrations. As a result, simply supported bridges of the Taiwan High-Speed Railway under real trains show that the proposed MTMD is more effective and reliable than a single TMD in reducing dynamic responses during resonant speeds, as the train axle arrangement is regular.

In this study, modeling of the vehicle-bridge system is in a great importance, since the main scope is to determine the relation between the bridge span weight per meter and passenger comfort. Moving Force Model and Moving Suspension Models have been used as like in the Lin, Asce, Wan and Chen's [21] study by combining the train and bridge parameters of Eurocode 1991-2 [5] and UIC 774-3. [6]

With this study the effectiveness comparison of the mass incrementing and section strengthening on the passenger comfort criteria's which have been defined by Eurocode 1990 [4], has been made. Details about modeling process will be given in the next chapter.

CHAPTER 3

ANALYSIS PROCEDURE

3.1. Description of the Bridge

The truss bridge studied in this thesis is on the river Kızılırmak near the town of Irmak and located on Ankara-Sivas railway line. The bridge was built in 1927 and has three spans with a 4.8 m. width, 6.5 m. height, and a span length of 50 m. each. ST37 were used as the structural material in the whole bridge. The abutments and the two intermediate piers are seems to be straight with a nearly zero degree slope.

The bridge has two longitudinal built-up beams under the rails, 30x30 cm timber sleepers between them and ten transverse built-up beams. At the time of testing, structural sections were at good condition, free from cracks and not affected from any corrosion effects. The bridge has not had any expansion joint between the bridge deck and the approach roadway.



Figure 3.1 General view of Steel Truss Bridge from ground



Figure 3.2 Entrance of the Steel Truss Bridge

3.2. Field Testing

The bridge has been tested by two separate institutes, at the same time, under different types of passenger and freight train loadings. One of them was Middle East Technical University and the other was Turkish State Railways.

3.2.1. Testing Equipment

MicroStrain's G-link[®] Wireless accelerometer nodes, shown in Figure 3.3, were used for the testing by the METU testing staff. G-Link[®] is a high-speed, triaxial acceleration node, designed to operate as part of an integrated wireless sensor network system. Every node in the wireless network is assigned a unique 16 bit address, so a single host transceiver can address thousands of multichannel sensor nodes. The frequency agile system enables simultaneous real-time streaming from the personal computer from up to 16 nodes in the range of 2.4 GHz range. Wireless accelerometer nodes are widely used to monitor tilt and vibration in a wide range of machines and structures.

Wireless accelerometers were installed at different transverse beams and the acceleration of the nodes were measured and recorded to identify the frequencies and mode shapes.

A mechanical accelerometer like vertical seismometer and an infrared deflection reader have been used by Turkish state railways field test staff.

The first and third spans have been tested by two of the field test staff for ambient and during train passing conditions.



Figure 3.3 A wireless accelerometer node

3.3. Computer Modeling

The dynamic model for train-bridge interaction system is composed of a train model and a bridge model that are linked by an assumed wheel-track relation. [1] The vehicle model consists of locomotives and passenger or freight cars. The bridge models are generally consists of multi-span girders, piers and foundations as shown in Figure 3.4.

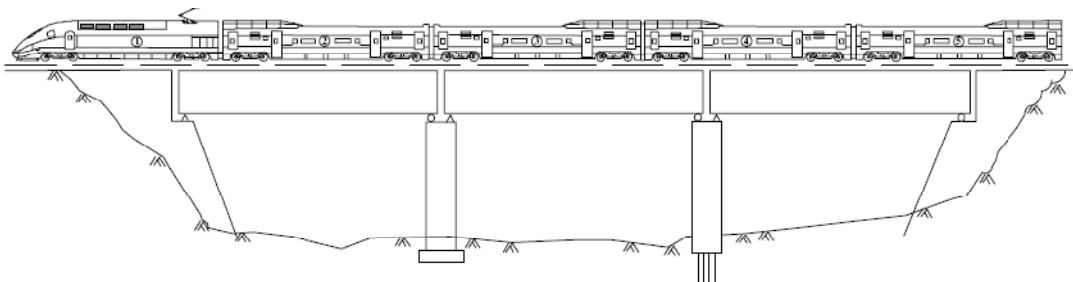


Figure 3.4 Dynamic model of train-bridge system [1]

When the bridge carries a railway, the track will be laid on the bridge deck and the forces from the wheels of a train will be transmitted to the bridge deck through the track. [1] The piers are assumed to be rigid and the effects of the piers is neglected to define a methodology for common type simple span bridges, therefore only one of the span has been modeled.

During the analysis two different computational bridge models have been developed to investigate the vehicle-bridge interactions.

3.3.1. Moving Force Model

Moving Forces has been modeled to investigate dynamic impacts of high-speed trains. The model has been determined based upon item 6.5.4.4 of EN 1991-2 to investigate the static impacts of high-speed trains. [5] An example model as per EN91-2 has been given in Figure 3.5. In this model the steel beams has been defined as line elements. The concrete deck has been defined as a finite shell element as shown in Figure 3.8. Fictitious rigid elements have been defined to between these two line elements and the transverse beams as shown in Figure 3.9. The aim of using fictitious rigid elements was to assume a perfect bonding between the deck and the steel beams and behave as a composite structure. Nowadays many chemical bonding materials prove that this assumption is acceptable.

Vehicle has been modeled as separate single moving loads which are defined under each wheels of the train as shown in Figure 3.6.

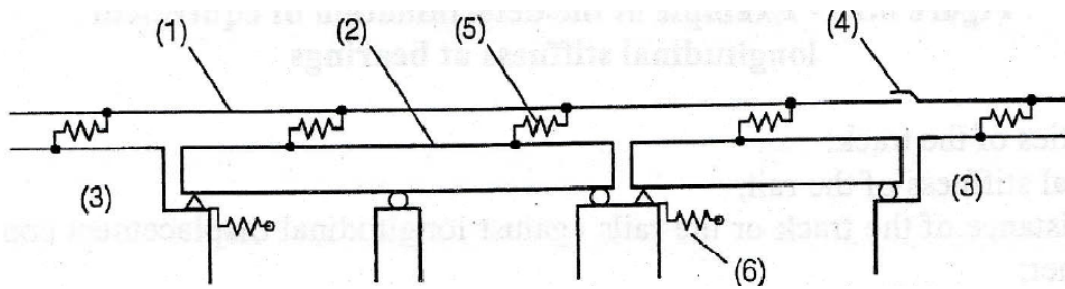


Figure 3.5 Example of a model of a track/structure system [5]

Where;

- (1) Track
- (2) Superstructure
- (3) Embankment
- (4) Rail expansion device (if present)
- (5) Longitudinal non-linear springs reproducing the longitudinal load/displacement behavior of the track
- (6) Longitudinal springs reproducing the longitudinal stiffness K of a fixed support to the deck taking into account the stiffness of the foundation, piers and bearings etc.

The bridge does not contain a rail expansion device. Therefore the 4th item has not been used in the analysis. The 6th item has also been neglected because of analyzing of the single simple span.

The behavior of the non-linear springs can be obtained as per the Figure 3.7 which is taken from UFC 774-3 item 1.2.1.2. [6]

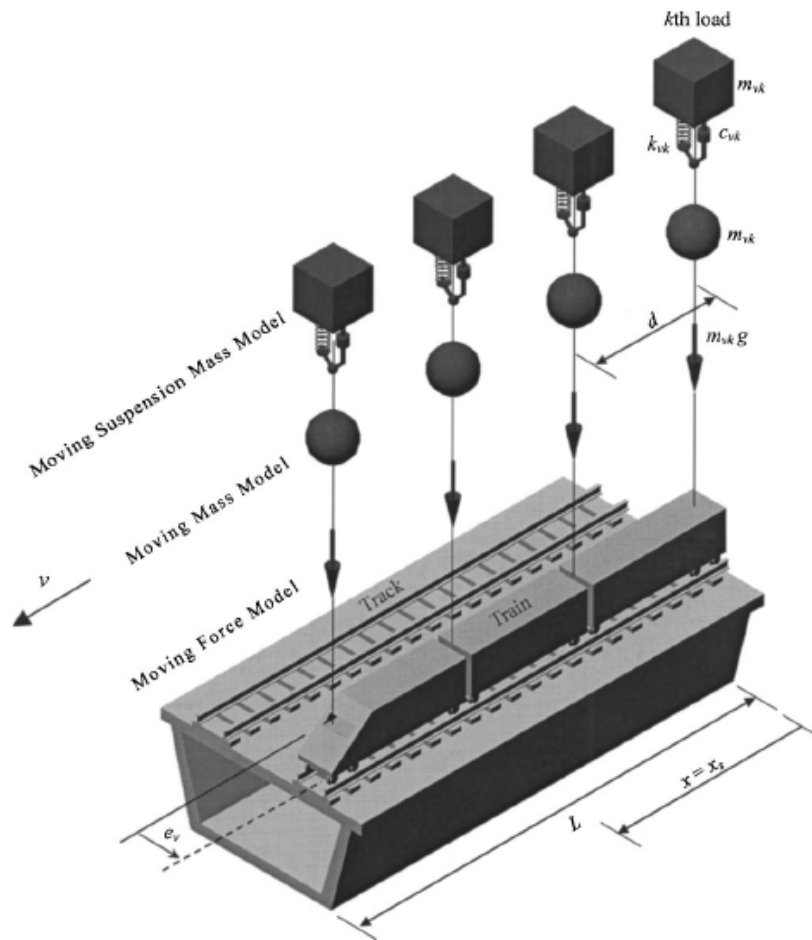


Figure 3.6 Train loading models [21]

As per item 1.2.2 of UFC 774-3 the displacement u_0 at the beginning of the plastic zone is 0,5 mm, and the resistance k is 40 kN/m for unloaded track and 60 kN/m for loaded track. In the literature most of the moving mass models do not contains tracks and the loads are directly applied to the bridge deck. In this thesis to simplify the analysis the moving force model does not also contains tracks and non-linear springs.

Common use for the term "Track" refers to everything from the top of the structural support to the top of the rail. Tracks are divided most

practically into categories of ballasted and un-ballasted tracks. Ballasted track is any track which contains ballast. Un-ballasted track is everything else. Un-ballasted track subcategories are:

- Direct Fixation Track
 - Discrete Fasteners Bolted to the support
 - Embedded Rail Track
 - Continuously Supported Rail
 - Embedded Block Track and Embedded Tie Track
- Open Deck Track

Direct fixation track is a system where the rail fastens directly to the track support. [22] The high-speed train track in this thesis has been assumed to be fastened to the deck with direct fixation method that does not contains any ballasts or sleepers. Direct fixation is most widely used when the clearance is a major critical design issue as in this bridge model.

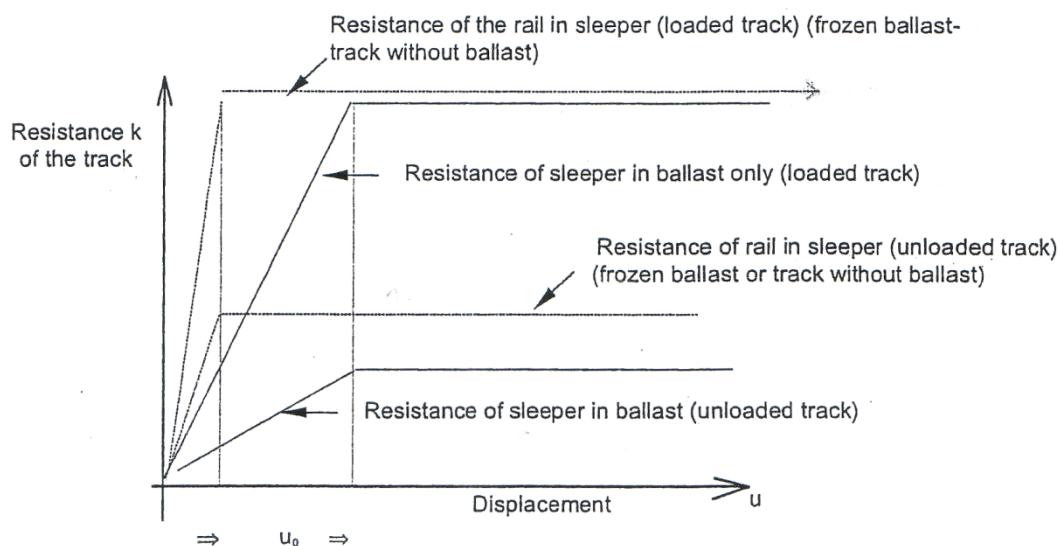


Figure 3.7 Resistance k of the track per unit length as a function of the longitudinal displacement u of the rails [5]

The existing bridge was not suitable for the direct fixation method with its timber sleepers because this method needs a more continuous surface to be applied. Therefore a 250 mm. thick reinforced concrete deck has been assumed to be used on the bridge instead of the existing timber sleepers. Since there are several methods to improve the strength of the bridge, the effect of this deck element on the structural stability and strength of the bridge has not been included to the scope of this thesis.

The section of the track-bridge interaction model has been defined as shown in Figure 3.5.

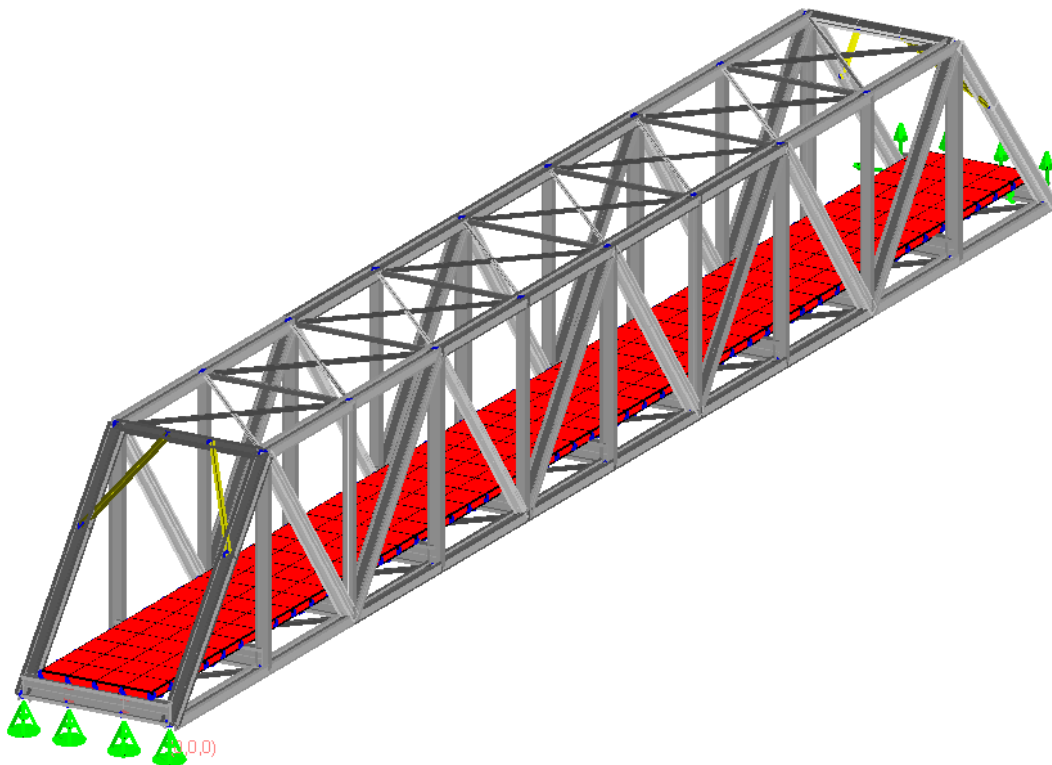


Figure 3.8 Defined Moving Force Model at Larsa 4D

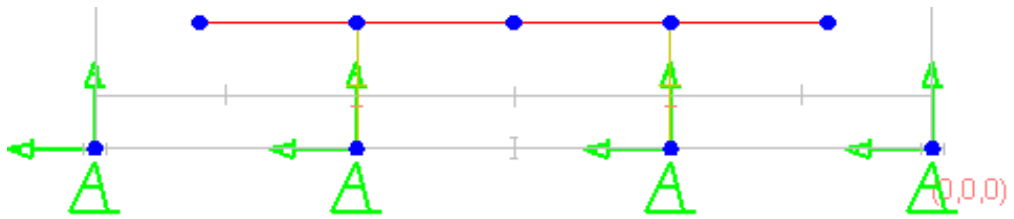


Figure 3.9 Section of the Moving Force Model

3.3.2. Moving Suspension Mass Model

The advance in computation technologies and because of the emergence of high-performance computers, it becomes feasible to have a more realistic modeling of the vehicle instead of simple moving force modeling.

This model is consists of defined half masses of a train car, a spring and a dashpot system as seen in Figure 3.10.

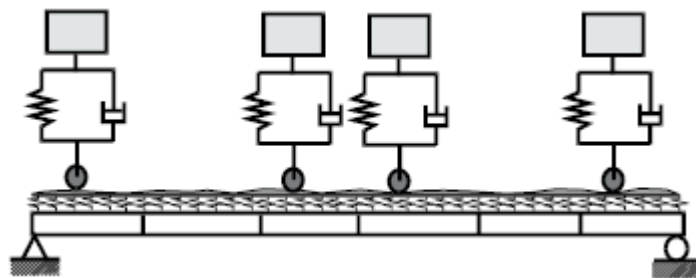


Figure 3.10 Moving suspension mass model/sprung mass model [22]

This model, has been defined as nearly same as the first Moving Loads model. Vehicle has been modeled with moving suspension mass elements at each of the slab joints at a height of train's center of gravity as shown on Figure 3.16. The height of center of gravity is

assumed as 1 m from the slab. Relatively Elastic members have been defined between the masses on the longitudinal location to provide the stability of the model. To check the sensitivity of the elasticity on the passenger comfort criteria's three analysis has been executed by different elastic elements which have relative elasticity's of 1/100, 1/1000 and 1/10000 times of the rigid elements. Larsa 4D software has given an error at the analysis execution when the relativity was 1/10000. The difference between the results of analysis with 1/100 and 1/1000 relativity for joint acceleration was nearly 3%.

As seen from Figure 3.14, an analysis structure has been developed by masses whole over the bridge on each of the joint under the track. The total weight of these masses on the bridge is nearly same as total weight of the bridge. Considering that the total weight of the vehicle is not as much as the total weight of the masses, the calculated modal frequency with this model will not be realistic. Regarding that the modal frequency is directly affecting the damping ratio. This means this will give better but unrealistic results. Therefore the vehicle has been statically modeled by HSLM-A10 train on the bridge by masses to identify the damping ratio and calculate the Rayleigh damping constants.

It is not possible to define exact moving loads one at a time over a bridge with Larsa 4D time history analysis. Therefore masses have been defined at all joints over the bridge. Compression only springs have been defined to prevent the effect of load-free masses at anytime of the analysis.

The spring coefficient and the damping coefficient of the axle springs have been selected based on the French TGV trains. [21] The details of some of the most common High-speed railway trains are have been given at Table 3.1. From these real parameters c_b and k_b values has

been used with HSLM-A10 train loading to be able to compare the previous analysis results.

A Mass-Spring-Dashpot system has been modeled as one equivalent nonlinear curve at the structural analysis software. An ideal mass-spring-dashpot system with mass m , spring constant k , and viscous dashpot of damping coefficient c can be described with the following formula:

$$F_s = -kx \dots\dots\dots (3.1)$$

$$F_d = -cv = -c\dot{x} = -c \frac{dx}{dt} \dots\dots\dots (3.2)$$

By treating the mass as a body and applying Newton's second law,

$$\sum F = ma = m\ddot{x} = m \frac{d^2x}{dt^2} \dots\dots\dots (3.3)$$

Where a is the acceleration of the mass and x is the displacement of the mass relative to initial state.

The above equations combine to form the equation of motion, a second order differential equation for displacement x as a function of time t .

$$m\ddot{x} = mg - kx - c\dot{x} \dots\dots\dots (3.4)$$

This equation can be converted to a first order equation of motion by using v instead of x' .

$$m\dot{v} = mg - k\frac{v}{t} - cv \dots\dots\dots (3.5)$$

$$\dot{v} = g + \frac{v}{m} \left(-\frac{k}{t} - c \right) \dots\dots\dots (3.6)$$

Runge-Kutta algorithm has been used to solve the differential equation of the spring-dashpot system modeling and define an equivalent nonlinear spring curve.

The Runge-Kutta algorithm is widely used to approximately solve a differential equation numerically. The algorithm is known to be very accurate and well-behaved for a wide range of problems.

Considering the Equation 3.6;

$$\dot{v} = f(t, v) \dots\dots\dots (3.7)$$

with initial condition $v(0) = 0$, supposing that v_n is the speed at the time t_n . The Runge-Kutta formula takes v_n and t_n and calculates an approximation for v_{n+1} at a brief time later, $t_n + h$. It uses a weighted average of approximated values of $f(t, v)$ at several times within the interval $(t_n, t_n + h)$. The formula is given by;

$$v_{n+1} = v_n + \frac{h}{6} (a + 2b + 2c + d) \dots\dots\dots (3.8)$$

where;

$$a = f(t_n, v_n) \dots\dots\dots (3.9)$$

$$b = f(t_n + \frac{h}{2}, v_n + \frac{h}{2} a) \dots\dots\dots (3.10)$$

$$c = f(t_n + \frac{h}{2}, v_n + \frac{h}{2} b) \dots\dots\dots (3.11)$$

$$d = f(t_n + h, v_n + hc) \dots\dots\dots (3.12)$$

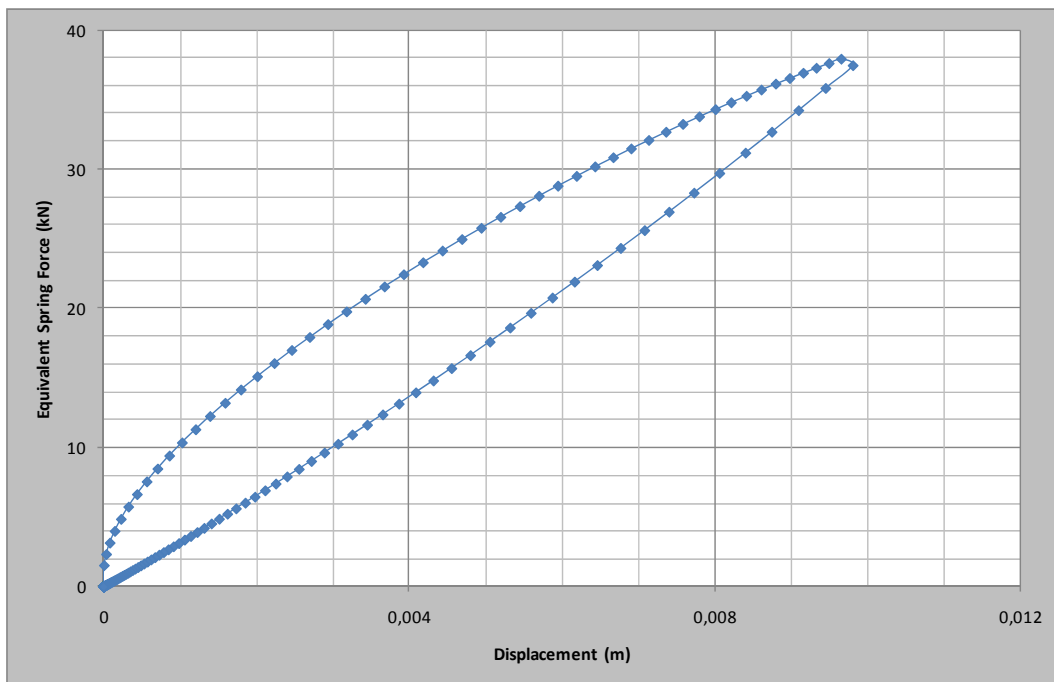


Figure 3.11 Equivalent Spring Force vs. Displacement graph obtained by using Runge-Kutta algorithm

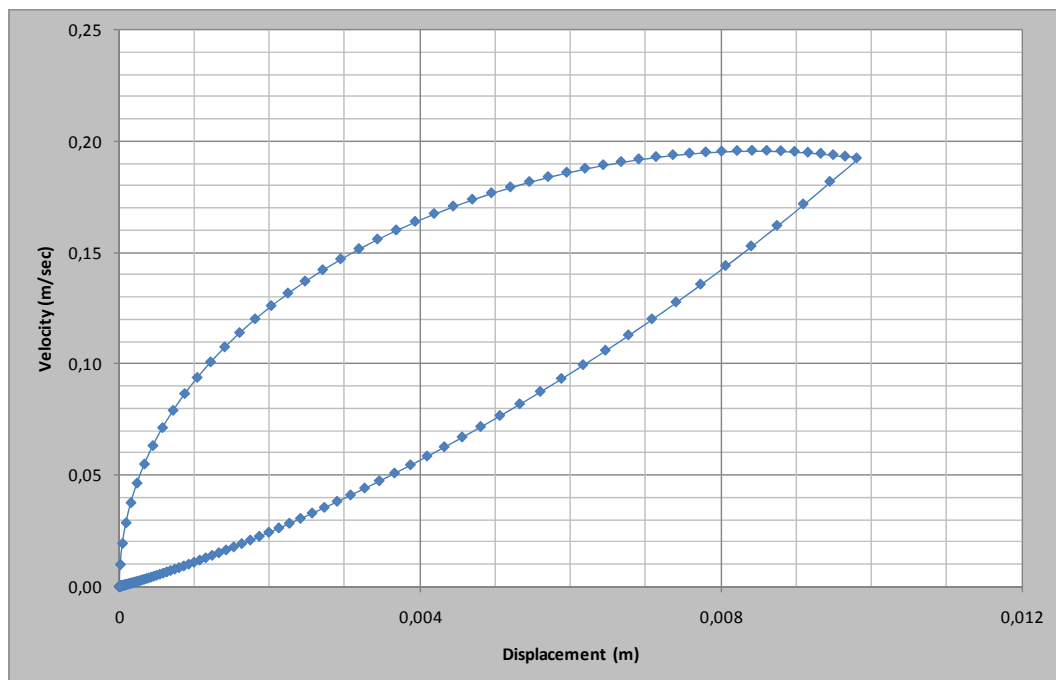


Figure 3.12 Velocity vs. Displacement graph obtained by using Runge-Kutta algorithm

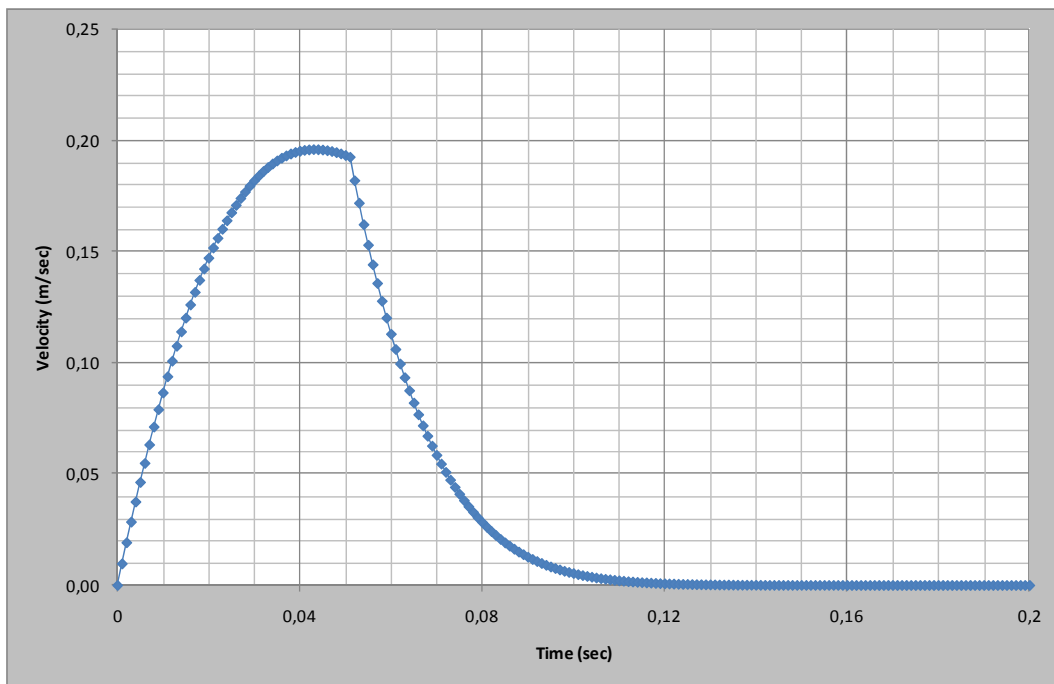


Figure 3.13 Velocity vs. Time graph obtained by using Runge-Kutta algorithm

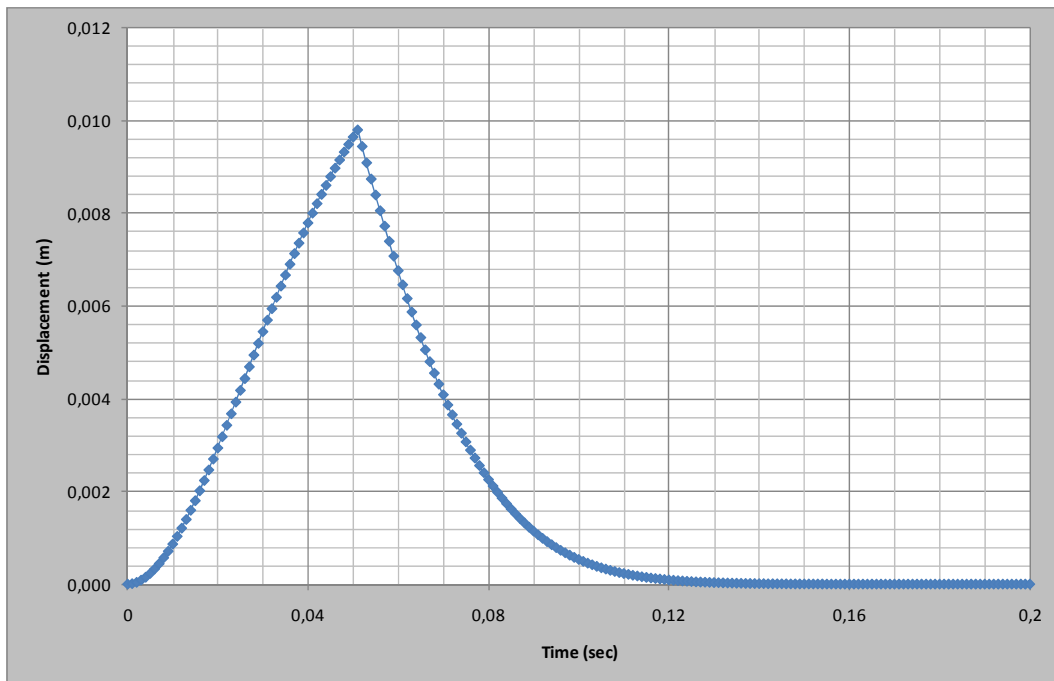


Figure 3.14 Displacement vs. Time graph obtained by using Runge-Kutta algorithm

An assumption has been made to obtain the given graphs about the contact duration of the train wheel and the track. Contact duration has been used as 0,05 sec during the calculations.

With reference to Figure 3.7 unloading behavior of the defined nonlinear spring curve for moving suspension mass model has been neglected. The reason is that the unloading behavior does not impact to any part of the train which means when the spring starts to unload; no part of the train will be over the spring.

The aim of this modeling was to determine the beneficial mass damping effect of the train when the train is over the bridge.

Table 3.1 Properties of German ICE, Japanese SKS, and French TGV High-Speed Railway Trains [19]

Train properties	ICE	SKS	TGV
Number of bogie	52	64	52
Car spacing, a (m)	26.4	25.0	18.7
$(v_c)_{n=1}$ (km/h)	338	320	240
$(v_c)_{n=7}$ (km/h)	169	160	120
m_v (kg)	27,000	20,875	27,000
c_v (N s/m)	22,700	90,200	96,700
κ_v (N/m)	660,000	530,000	664,000
m_b (kg)	3,000	3,040	3,000
I_b (kg-m ²)	4,000	3,930	4,000
c_b (N s/m)	78,400	78,400	78,400
κ_b (N/m)	2,360,000	2,360,000	2,360,000
m_w (kg)	1,800	1,780	1,800
l_w (m)	1.5	1.25	1.5

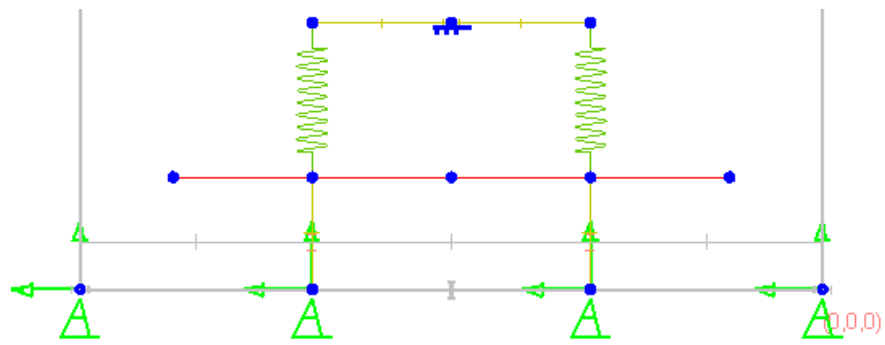


Figure 3.15 Section of the Moving Suspension Mass Model

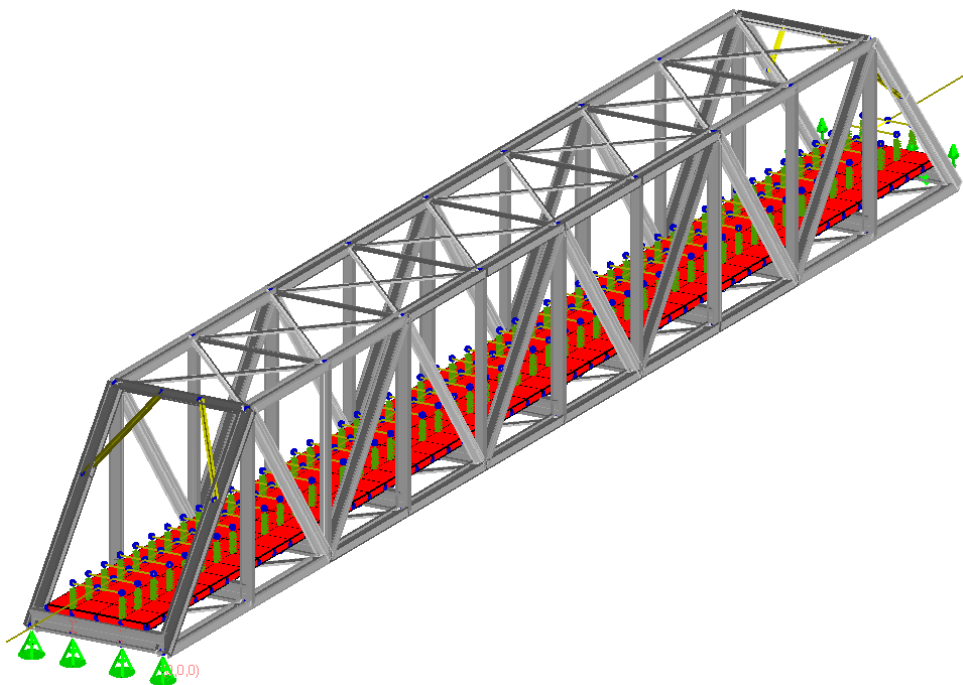


Figure 3.16 Defined Moving Suspension Mass Model at Larsa 4D

3.4. Analysis Specifications

Dynamic effect calculations have been made per Eurocode 1991-2:2003 section 6.4.6. The critical loading has been determined by selecting the most effective case from the loadings mentioned below.

- $LM71 \times \Phi_3 \dots\dots\dots (3.13)$

- $HSLM \times (1 + \varphi'_{dyn} + \varphi'') \dots\dots\dots (3.14)$

As per EN 1991-2 section 6.4.5;

$$\Phi_3 = \frac{2,16}{\sqrt{L_\Phi} - 0,2} + 0,73 \dots\dots\dots (3.15)$$

EN 1991-2 section 6.4.6.5 indicates;

$$\varphi'_{dyn} = \max \left| y_{dyn} / y_{stat} \right| - 1 \dots\dots\dots (3.16)$$

and as per EN 1991-2 Annex C;

$$\varphi'' = \frac{\alpha}{100} \left[56e^{-\left(\frac{L_\Phi}{10}\right)^2} + 50 \left(\frac{L_\Phi n_0}{80} - 1 \right) e^{-\left(\frac{L_\Phi}{20}\right)^2} \right] \dots\dots\dots (3.17)$$

$$\varphi'' \geq 0$$

where:

n_0 is the first natural bending frequency of the bridge loaded by permanent actions [Hz]

L_Φ is the determinant length [m]

α is a coefficient for speed

$$\text{with: } \alpha = \frac{v}{22} \text{ if } v \leq 22 \text{ m/s}$$

$$\alpha = 1 \text{ if } v > 22 \text{ m/s} \dots\dots\dots (3.18)$$

Dynamic analysis requisite has been determined by using the flow chart at the EN 1991-2 Figure 6.9 which is shown below at Figure 3.17.

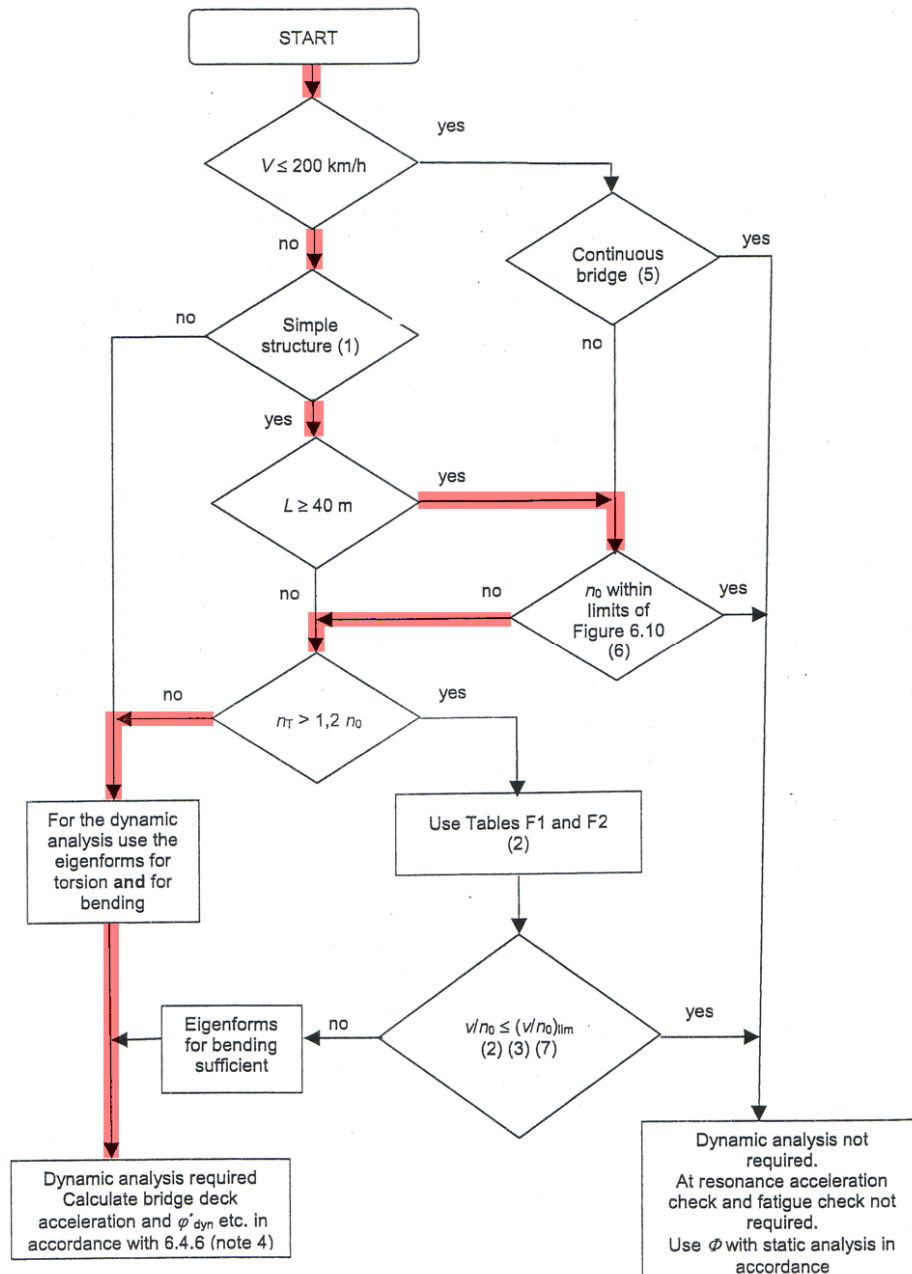


Figure 3.17 Flow chart for determining whether a dynamic analysis is required or not

3.4.1. Dynamic Analysis Parameters

- **Damping Ratio:**

Table 3.2 Values of damping to be assumed for design purposes [4]

Bridge Type	ζ Lower Limit of percentage of critical damping [%]	
	Span $L < 20\text{m}$	Span $L \geq 20\text{m}$
Steel and composite	$\zeta = 0.5 + 0.125 (20 - L)$	$\zeta = 0.5$
Prestressed concrete	$\zeta = 1.0 + 0.07 (20 - L)$	$\zeta = 1.0$
Filler beam and reinforced concrete	$\zeta = 1.5 + 0.07 (20 - L)$	$\zeta = 1.5$

$$\zeta_{\text{TOTAL}} = \zeta + \Delta\zeta \dots\dots\dots (3.19)$$

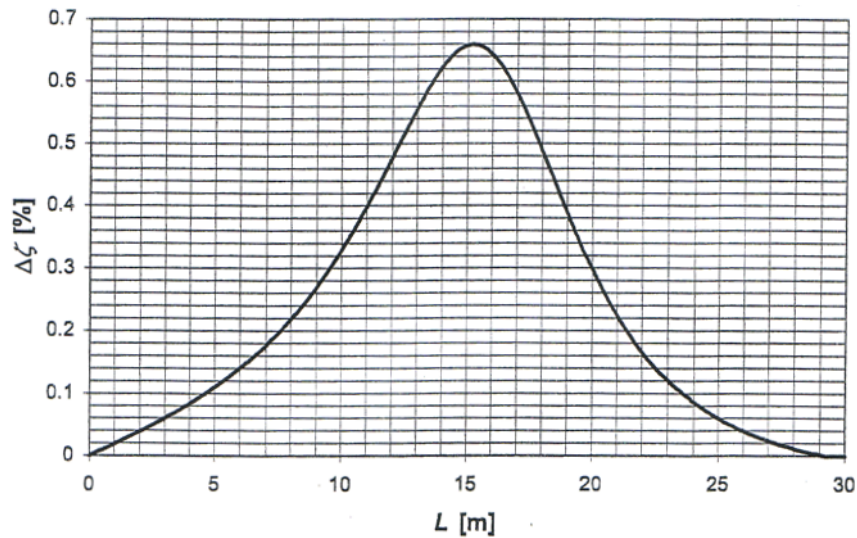


Figure 3.18 Additional damping $\Delta\zeta$ [%] as a function of span length L

where:

$$\Delta\zeta = \frac{0,0187L - 0,00064L^2}{1 - 0,0441L - 0,0044L^2 + 0,000255L^3} [\%] \dots\dots\dots (3.20)$$

As indicated at section 3.1 the bridge type is steel and the span length is 50 m, by using these bridge characteristics ζ has been calculated as 0.5% from the Table 3.2 shown above.

As per Figure 3.18 shown above and equation 3.20, $\Delta\zeta$ has been calculated as a negligible value, therefore total damping ratio (ζ_{Total}) has been determined as 0.5%.

Larsa 4D analysis software uses Rayleigh damping coefficients to define the damping ratio of the model to the system. Rayleigh damping contains two coefficient which are proportional to mass and stiffness as seen at equations 3.21 and 3.22. These coefficients have been calculated by using total damping ratio.

$$a_0 = \zeta \frac{2\omega_i\omega_j}{\omega_i + \omega_j} \dots\dots\dots (3.21)$$

$$a_1 = \zeta \frac{2}{\omega_i + \omega_j} \dots\dots\dots (3.22)$$

$$w_1 = f_1 \times 2\pi = 4.28 \times 2\pi = 31.35$$

$$w_2 = f_2 \times 2\pi = 16.35 \times 2\pi = 142.57$$

By these calculations Rayleigh damping coefficients has been determined as;

Mass proportional coefficient $a_0 = 0.057$

Stiffness proportional coefficient $a_1 = 5.75 \times 10^{-5}$

- **Train Speed**

Dynamic analysis has been executed with different train speeds, starting from 40 m/sec up to 83 m/sec with 10 m/sec intervals.

Resonance in a structure is the condition to have a harmonic excitation source acting on a structure at frequencies matching one or multiple major natural vibration modes of that structure. Resonance condition of major modes might have high dynamic mass, combined with low damping ratios generally generates extreme deformations causing the structure to get damaged. [11]

As per En 1991-2 section 6.4.6.2 train speeds which might cause a resonance situation can be calculated as follows:

$$v_i = n_0 \lambda_i \dots\dots\dots (3.23)$$

v_i is the Resonant Speed [m/sec]
 n_0 is the first natural frequency of the unloaded structure,
 λ_i is the principal wavelength of frequency of excitation and may be estimated by:

$$\lambda_i = \frac{d}{i} \dots\dots\dots (3.24)$$

d is the regular spacing of groups of axles
 $i = 1, 2, 3$ or 4 .

$v_1 = 134.73$ m/sec	$v_2 = 67.37$ m/sec
$v_3 = 44.91$ m/sec	$v_4 = 33.68$ m/sec

From the above calculated possible resonant speeds, v_2 appears between the analysis train speed intervals 45 m/sec and 70 m/sec which is the closest analysis speed to the v_2 , has been expected to be the most critical speed.

- **Train Loading**

HSLM-A and HSLM-B train loading cases have been determined according to Table 3.3. Dynamic analysis has been executed by using HSLM-A train loading since the span length of the bridge is greater than 7m.

The procedure to determine the critical HSLM-A train loading for a steel bridge with 50 m span length does not defined at EN 1991-2. Therefore the dynamic analysis has been performed on the existing section of the bridge with a train speed of 80 m/sec for all of the HSLM-A and LM-71 train loadings. From these selective results HSLM-A10 loading has been determined as critical train loading by evaluating the analysis results.

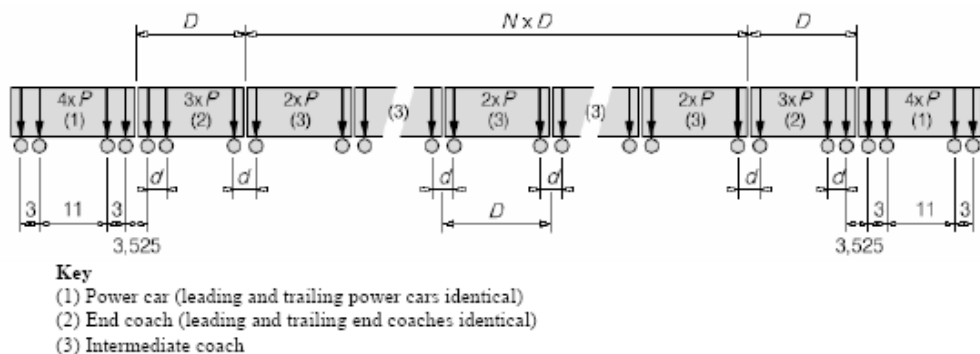


Figure 3.19 HSLM-A Train Spacing [4]

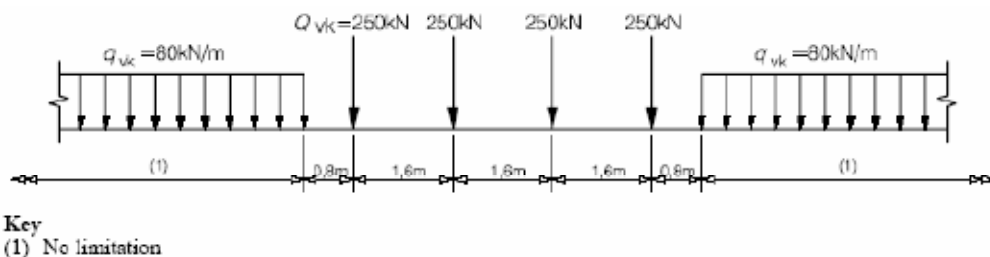


Figure 3.20 Load Model 71 and characteristic values for vertical loads [4]

Table 3.3 Application of HSLM-A and HSLM-B [4]

Structural configuration	Span	
	L < 7m	L ≥ 7m
Simply supported span ^a	HSLM-B ^b	HSLM-A ^c
Continuous structure ^a or Complex structure	HSLM-A Trains A1 to A10 inclusive ^d	HSLM-A Trains A1 to A10 inclusive ^d
<p>^a Valid for bridges only longitudinal line beam or simple plate behavior with negligible skew effects on rigid supports</p> <p>^b For simply supported spans with a span of up to 7 m a single critical Universal Train from HSLM-B may be used for the analysis in accordance with 6.4.6.1.1(5).</p> <p>^c For simply supported spans with a span of 7 m or greater a single critical Universal train for HSLM-A may be used for the dynamic analysis in accordance with annex E (Alternatively Universal trains A1 to A10 inclusive may be used).</p> <p>^d All trains A1 to A10 inclusive should be used in the design.</p> <p>^e Any structure that does not comply with Note a above. For example a skew structure, bridge with significant torsional behaviour, half through structure with significant floor and main girder vibration modes etc. In addition, for complex structures with significant floor vibration modes (e.g. half through or through bridges with shallow floors) HSLM-B should also be applied.</p>		

Table 3.4 HSLM-A Train Loading Cases [4]

Universal Train	Number of Intermediate coaches N	Coach length D [m]	Bogie axle spacing d [m]	Point Force P [kN]
A1	18	18	2.00	170
A2	17	19	3.50	200
A3	16	20	2.00	180
A4	15	21	3.00	190
A5	14	22	2.00	170
A6	13	23	2.00	180
A7	13	24	2.00	190
A8	12	25	2.50	190
A9	11	26	2.00	210
A10	11	27	2.00	210

3.5. Rehabilitation

The limit values of EN 1991-2 for a railroad could not be provided by Dynamic analysis results of the existing bridge. Therefore a specific rehabilitation methodology with two different methods has been defined and investigated to find the most effective rehabilitation method.

The first method contains mass increments which are 5% and 10% of total weight of the bridge. Mass increments are modeled as thicker deck sections at mid span of the existing truss bridge.

Thickening of the steel sections of the bridge has been used as second rehabilitation method. Double (E2), Triple (E3), Quadruple (E4) and Quintuple (E5) sections have been modeled and analyzed.

A relationship between span weight per meter and passenger comfort as well as the stiffness has been defined by using these rehabilitation methods.

3.6. Computational Analysis Methods

3.6.1. Non-Linear Time History Analysis

The nonlinear time history analysis is an extension of the linear time history analysis in which elements with geometric nonlinearity (e.g. cables) and elements with material nonlinear behavior (e.g. nonlinear elastic and inelastic springs) can be included. The use of such an advanced analysis method also may be the most cost effective approach to estimate the response of a structure to dynamic loads when nonlinear behavior needs to be accounted for realistically.

The most common applications of nonlinear time history in structural engineering are dynamic response to seismic and blast loadings when the structure includes elements with geometric nonlinearity like cables, or protective devices like seismic isolators, or elements with material nonlinearity such as inelastic springs with energy dissipater characteristics.

The nonlinear time history analysis is carried out by using the Newmark-Beta time integration algorithm with the Newton-Raphson method using iterations within each integration time step. The number of iterations performed within each time step is controlled by user specified convergence criteria.

The nonlinear time history analysis requires significant computational effort and computer time.

3.6.2. Eigenvalue Analysis

The eigenvalue analysis is performed to extract the un-damped free-vibration mode shapes and frequencies of a structure. The eigenvalue analysis is important as a precursor to any dynamic analysis because knowledge of the structure's natural frequencies and modes can help to characterize its dynamic response.

CHAPTER 4

FIELD TEST AND ANALYSIS RESULTS

4.1. Introduction

In this chapter the results of field tests, moving force model and moving suspension mass model analysis results have been presented. The passenger comfort criteria have been defined with the joint acceleration, joint displacement and joint rotation values in Eurocode 1991-2. Therefore the maximum values at the midspan of the steel truss bridge and in addition to these values the frequency and mode shapes have been presented in this section.

Joint acceleration has been limited to 5 m/sec^2 as per traffic safety for Directly Fixed tracks and also a limitation has been defined for passenger comfort as in Table 4.1 which has been taken from Eurocode 1990:2005 Annex A2 item 4.4.3.1.

Joint Displacement has been limited to $L/600 \text{ mm}$ where L is the span length of the bridge as per traffic safety criteria and also a limitation has been defined for passenger comfort as in Figure 4.1 which has been taken from Eurocode 1990:2005 Annex A2 item 4.4.3.2.3.

Joint Rotation has been defined as the relative deformation of a joint according to a joint which is 3 m far and on the other side of the track. Joint rotation is limited as in Figure 4.2 which has been taken from Eurocode 1990:2005 Annex A2 item 4.4.2.2.2.

Table 4.1 Recommended levels of comfort [4]

Level of Comfort	Vertical acceleration b_v (m/s ²)
Very good	1,0
Good	1,3
Acceptable	2,0

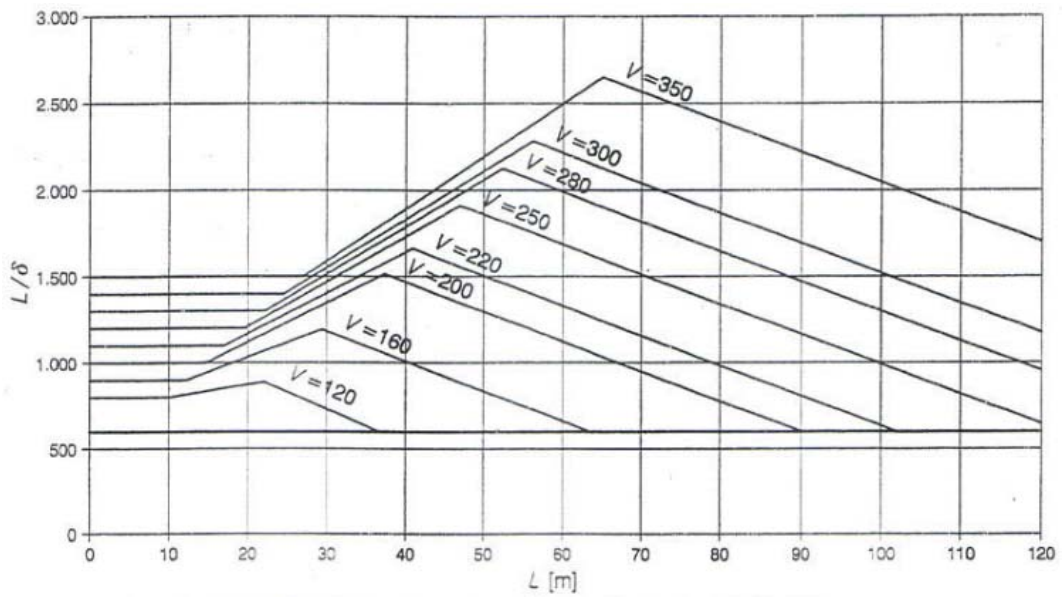


Figure 4.1 Maximum permissible vertical deflection δ for railway bridges with 3 or more successive simply supported spans corresponding to a permissible vertical acceleration of $b_v = 1 \text{ m/sec}^2$ in a coach for V [km/h] [4]

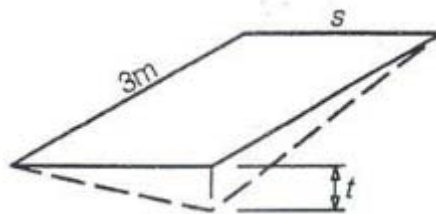


Figure 4.2 Definition of deck twist

Table 4.2 Limiting values of deck twist

Speed range V (km/h)	Maximum twist t (mm/3m)
$V \leq 120$	$t \leq t_1$
$120 < V < 200$	$t \leq t_2$
$V > 200$	$t \leq t_3$

The recommended values for the set of t are;

$$t_1 = 4.5$$

$$t_2 = 3.0$$

$$t_3 = 1.5$$

In this study a total of 600 different graphics has been obtained for the passenger comfort criteria's mentioned above. 72 selective graphics has been reported for the critical speeds of the analysis methods. The reported values are calculated at the mid-span joint which is marked at the Figure 4.3 and 4.4.

Section improvements and mass increments are indicated as Ex-y where x is the sectional coefficient and y is the mass damping coefficient as percent. For example E2-5 indicates that the truss steel sections have been doubled and a 5% of the total weight of truss bridge has been used as mass increment during the analysis. For an analysis without a mass increment no indicators has been used. (E1)

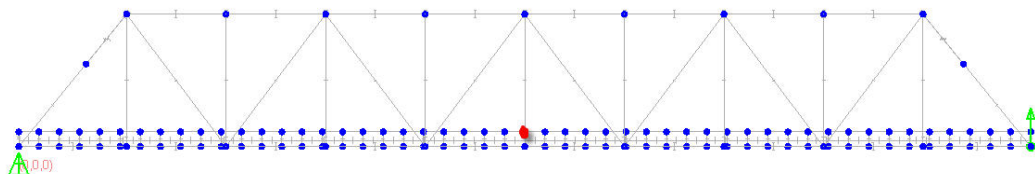


Figure 4.3 X-Z cross section of the analysis model

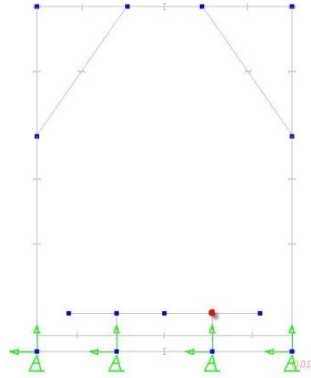


Figure 4.4 Y-Z cross section of the analysis model

4.2. Field Test Results

Field test has been conducted by two separate institutes, METU and Turkish State Railways. The records of the Turkish State Railways could not be taken as per the privacy policy of the institute. The displacements at the midspan of the bridge under several train loadings have been shared as an on-site information which are at a magnitude of 1.25 to 2.00 cm records.

One of a sample data during train crossing is given in Figure 4.4 which is recorded and post-processed by Asst. Prof. Dr. Ahmet Türer from METU. The recorded accelerations have been scaled down to $1/10^{\text{th}}$ of their original magnitude to be able to observe the relative magnitudes of the accelerations. The transverse direction acceleration record has also been shifted by 0.5g to be able to see the three direction groups separately. The minimum and maximum accelerations recorded during train crossing are summarized in Figure 4.5.

Post-processing of the recorded ambient and train crossing data by Dr. Türer gave relatively better results but only the first bending mode has been able to be extracted. In an attempt to better capture the

frequency and damping ratios of modes, the recorded data has been added one after another in the form of a single recording. A longer data record formed in this manner gave better information as shown in Figure 4.3 regarding the stability of frequencies; however, in the cost of losing mode shapes. [11]

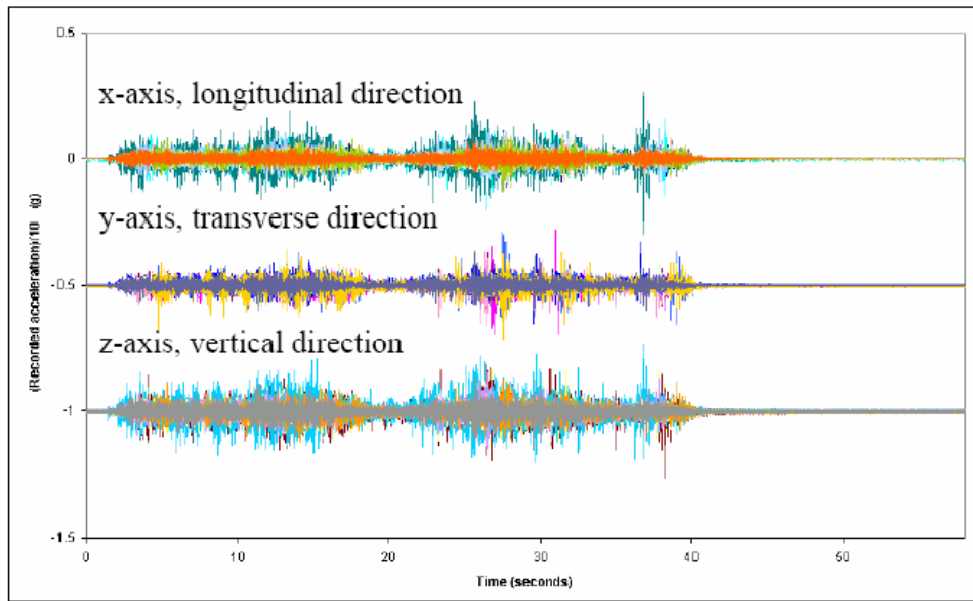


Figure 4.5 Measured Acceleration record from the truss bridge, scaled down to 1/10th of magnitude (By courtesy of Dr. Türer)

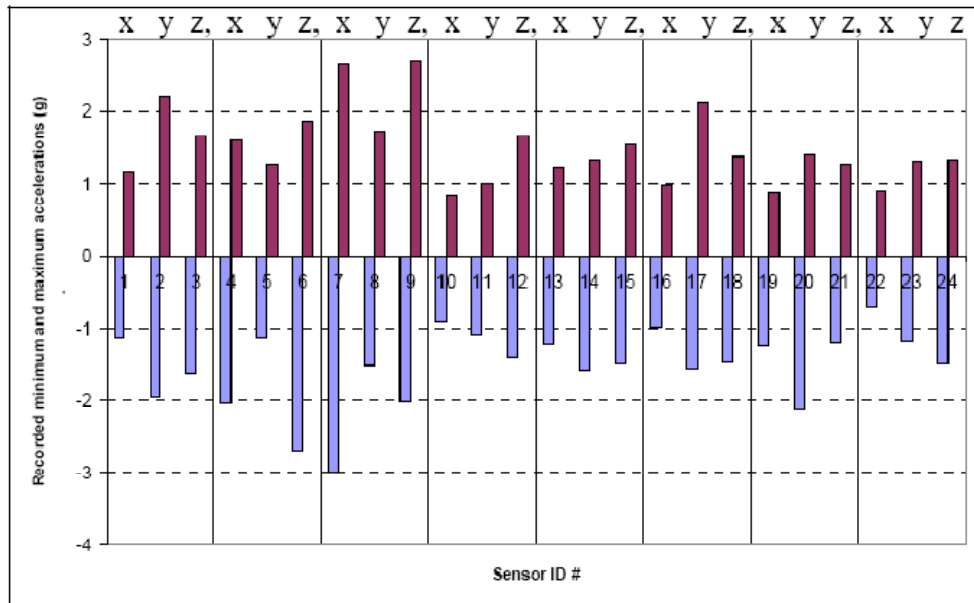


Figure 4.6 Minimum and Maximum accelerations recorded from the truss bridge (By courtesy of Dr. Türer)

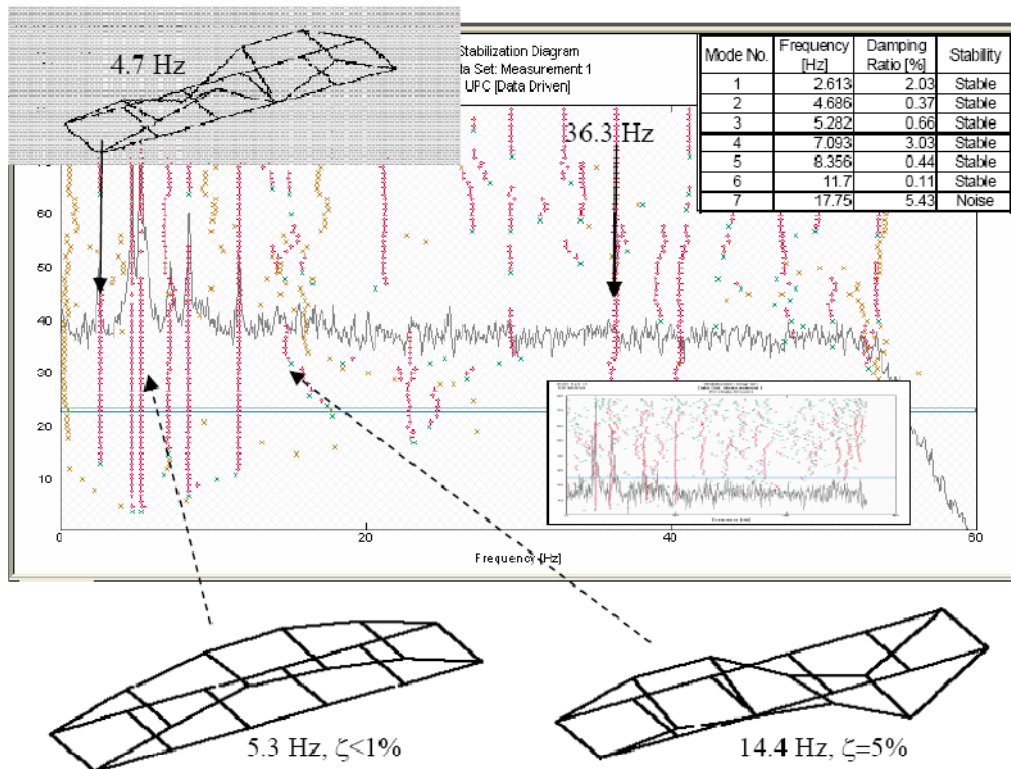


Figure 4.7 Free vibration stabilization diagram (By courtesy of Dr. Türer)

4.3. Moving Force Model Analysis Results

Moving Force Model has been analyzed with the Non-Linear Time History analysis of Larsa 4D.

The procedure to determine the critical HSLM-A train loading for a steel bridge with 50 m span length does not defined at EN 1991-2. Therefore the model has been analyzed under all of the HSLM-A from A1 to A10 and LM-71 train loadings.

Instead of an analyze with 5 different sections with 3 mass increment condition under 11 different train loadings with 10 increasing speed case that makes a 1.650 times of non-linear time history analysis run which might take a 15 days to complete, a section for all trains with all speed cases which makes also 110 run, has been made to identify the most critical train.

HSLM-A10 has been identified as the critical train and further 140 times of non-linear time history analysis run has been made to complete the analysis.

Table 4.3 Joint Acceleration (m/sec²) values at midspan of bridge with different sections and mass increments under HSLM-A10 train loading with varying speeds

Section	Mass Damping	Speed								
		40	45	50	55	60	65	70	75	80
E1	0.00%	15.46	14.74	27.54	12.53	26.60	22.58	27.16	30.45	22.71
	5.00%	7.35	8.70	9.98	4.14	6.55	8.88	13.00	15.86	10.07
	10.00%	4.60	5.29	7.40	2.95	5.38	6.77	12.09	6.89	5.51
E2	0.00%	9.79	11.31	16.00	8.30	14.23	12.96	16.29	17.49	12.98
	5.00%	4.05	5.00	5.12	1.77	4.14	4.62	4.77	7.84	6.81
	10.00%	2.13	3.22	2.83	1.41	2.05	2.58	4.17	4.49	6.46
E3	0.00%	7.79	10.18	11.68	6.23	10.22	10.33	13.78	12.81	9.37
	5.00%	2.28	3.24	3.57	1.71	2.64	3.04	3.08	3.74	4.72
	10.00%	1.45	1.54	1.95	0.85	1.66	1.85	2.04	3.31	3.56
E4	0.00%	6.35	7.85	9.14	4.51	7.68	8.04	10.46	9.88	8.55
	5.00%	1.53	2.56	2.67	1.07	1.87	2.94	2.17	2.66	2.57
	10.00%	0.68	1.16	1.32	0.80	1.10	1.32	1.32	1.46	1.62
E5	0.00%	5.10	6.53	7.67	3.61	5.91	6.91	8.70	8.11	7.31
	5.00%	1.34	2.09	2.03	0.94	1.60	2.18	1.96	2.19	1.97
	10.00%	0.75	0.83	1.22	0.51	1.12	1.27	1.00	1.11	1.27

Table 4.4 Max Joint Acceleration values at midspan of bridge with different sections and mass increments under HSLM-A10 train loadings

Sections	Mass Damping	Max Acceleration
E1	0.00%	30.45
	5.00%	15.86
	10.00%	12.09
E2	0.00%	17.49
	5.00%	7.84
	10.00%	6.46
E3	0.00%	13.78
	5.00%	4.72
	10.00%	3.56
E4	0.00%	10.46
	5.00%	2.94
	10.00%	1.62
E5	0.00%	8.70
	5.00%	2.19
	10.00%	1.27

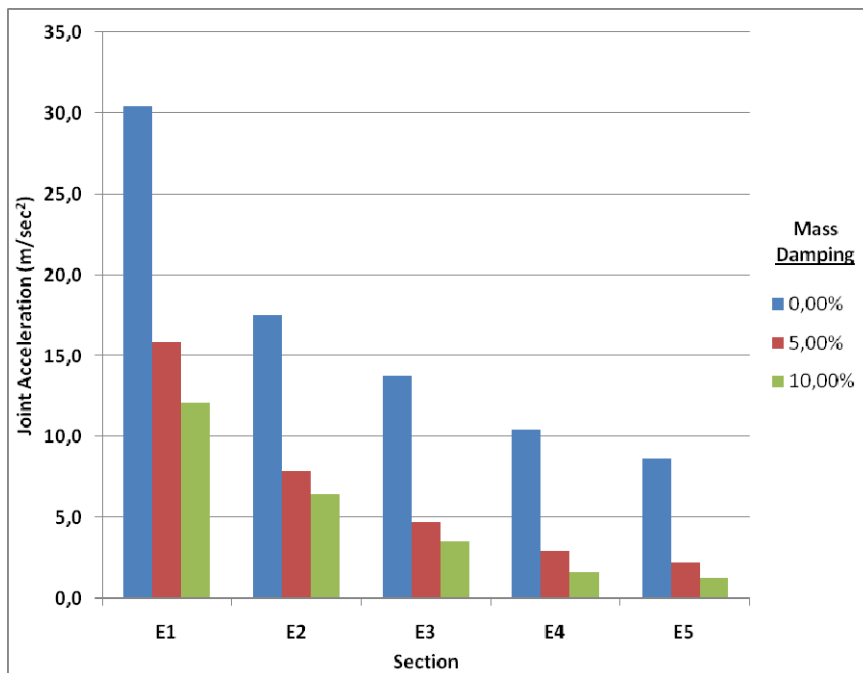


Figure 4.8 Max Joint Acceleration values at midspan of bridge with different sections and mass increments under HSLM-A10 train loadings

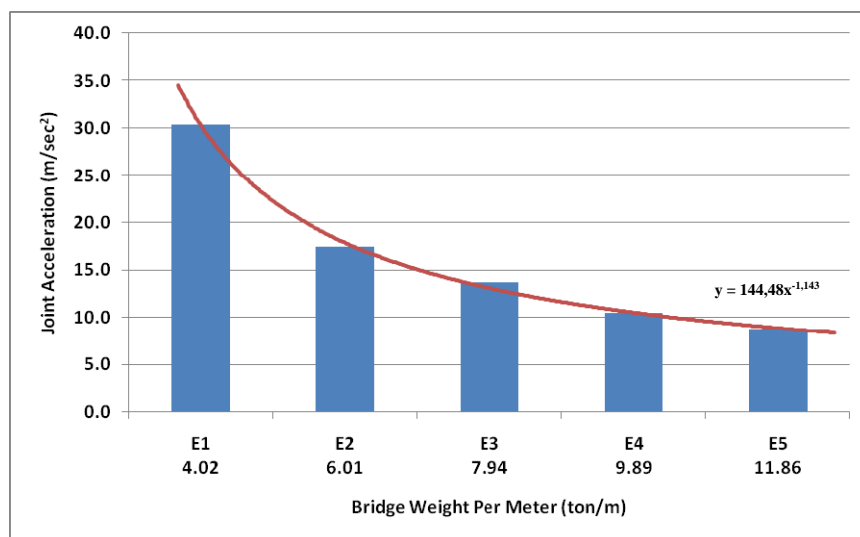


Figure 4.9 Trendline of Max Joint Acceleration at midspan of bridge with different per meter weight

Table 4.5 Joint Displacement (m) values of different sections with different mass increments under HSLM-A10 train loading with varying speeds

Section	Mass Damping	Speed								
		40	45	50	55	60	65	70	75	80
E1	0.00%	0.00102	0.00043	0.00276	0.00116	0.00055	0.00149	0.00616	0.01553	0.00477
	5.00%	0.00179	0.00046	0.00181	0.00102	0.00106	0.00557	0.00993	0.01010	0.00071
	10.00%	0.00208	0.00073	0.00200	0.00031	0.00400	0.00459	0.01557	0.00234	0.00030
E2	0.00%	0.00034	0.00008	0.00076	0.00034	0.00128	0.00084	0.00007	0.00085	0.00198
	5.00%	0.00121	0.00020	0.00052	0.00040	0.00098	0.00016	0.00039	0.00220	0.00308
	10.00%	0.00015	0.00081	0.00019	0.00079	0.00061	0.00035	0.00151	0.00296	0.00656
E3	0.00%	0.00027	0.00064	0.00016	0.00024	0.00061	0.00130	0.00022	0.00033	0.00059
	5.00%	0.00025	0.00011	0.00053	0.00020	0.00100	0.00063	0.00008	0.00058	0.00124
	10.00%	0.00067	0.00018	0.00034	0.00030	0.00058	0.00013	0.00026	0.00099	0.00145
E4	0.00%	0.00014	0.00071	0.00041	0.00030	0.00028	0.00043	0.00029	0.00008	0.00049
	5.00%	0.00018	0.00009	0.00029	0.00010	0.00048	0.00080	0.00009	0.00024	0.00061
	10.00%	0.00018	0.00006	0.00028	0.00020	0.00048	0.00032	0.00019	0.00064	0.00093
E5	0.00%	0.00003	0.00026	0.00016	0.00020	0.00004	0.00037	0.00032	0.00013	0.00034
	5.00%	0.00017	0.00040	0.00009	0.00010	0.00038	0.00079	0.00012	0.00024	0.00033
	10.00%	0.00015	0.00010	0.00037	0.00010	0.00065	0.00040	0.00002	0.00039	0.00074

Table 4.6 Max Joint Displacement values at midspan of bridge with different sections and mass increments under HSLM-A10 train loadings

Sections	Mass Damping	Max Displacement
E1	0.00%	0.00853
	5.00%	0.01010
	10.00%	0.01557
E2	0.00%	0.00198
	5.00%	0.00308
	10.00%	0.00656
E3	0.00%	0.00113
	5.00%	0.00124
	10.00%	0.00145
E4	0.00%	0.00077
	5.00%	0.00080
	10.00%	0.00093
E5	0.00%	0.00037
	5.00%	0.00056
	10.00%	0.00074

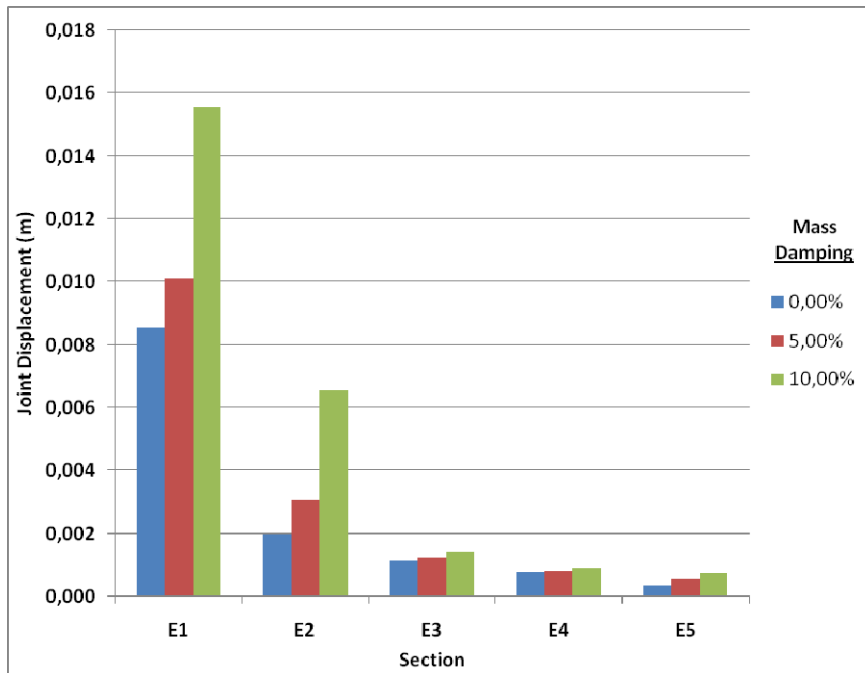


Figure 4.10 Max Joint Displacement values at midspan of bridge with different sections and mass increments under HSLM-A10 train loadings

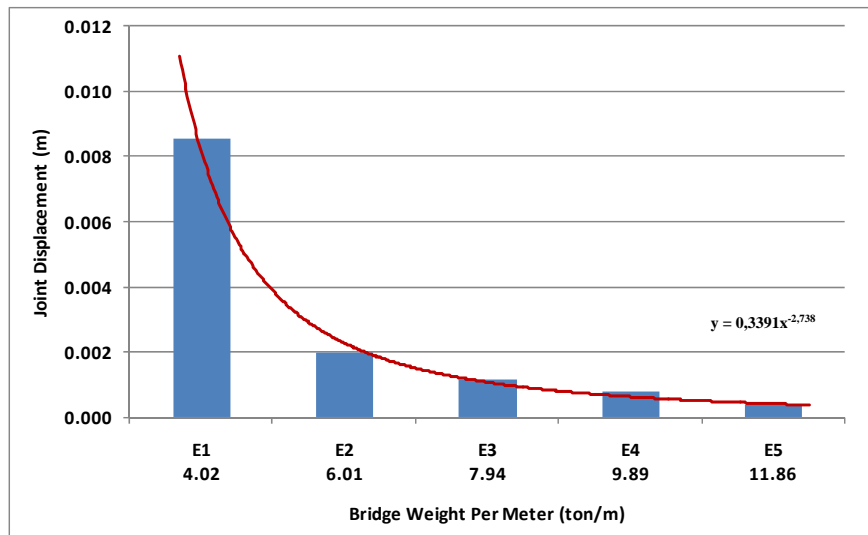


Figure 4.11 Trendline of Max Joint Displacement at midspan of bridge with different per meter weight

Table 4.7 Joint Rotation values at midspan of bridge with different sections and mass increments under HSLM-A10 train loading with varying speeds

Section	Mass Damping	Speed								
		40	45	50	55	60	65	70	75	80
E1	0.00%	0.865	0.817	0.851	0.732	1.010	0.938	0.974	1.020	0.716
	5.00%	0.836	0.856	0.798	0.730	1.000	0.909	0.976	1.136	0.821
	10.00%	0.815	0.895	0.839	0.725	1.007	0.887	0.650	0.988	0.853
E2	0.00%	0.279	0.291	0.294	0.251	0.341	0.317	0.313	0.350	0.266
	5.00%	0.286	0.326	0.292	0.252	0.338	0.301	0.306	0.356	0.306
	10.00%	0.340	0.333	0.311	0.251	0.346	0.307	0.283	0.345	0.257
E3	0.00%	0.150	0.188	0.166	0.136	0.200	0.201	0.170	0.175	0.167
	5.00%	0.154	0.181	0.170	0.177	0.200	0.183	0.188	0.190	0.196
	10.00%	0.152	0.175	0.177	0.200	0.208	0.186	0.193	0.191	0.208
E4	0.00%	0.119	0.129	0.114	0.100	0.120	0.119	0.301	0.141	0.107
	5.00%	0.110	0.120	0.122	0.100	0.130	0.124	0.126	0.123	0.113
	10.00%	0.111	0.123	0.128	0.100	0.129	0.129	0.121	0.127	0.116
E5	0.00%	0.076	0.093	0.083	0.100	0.090	0.077	0.089	0.093	0.079
	5.00%	0.086	0.103	0.097	0.100	0.099	0.096	0.079	0.106	0.088
	10.00%	0.083	0.091	0.097	0.100	0.111	0.097	0.090	0.093	0.076

Table 4.8 Max Joint Rotation values at midspan of bridge with different sections and mass increments under HSLM-A10 train loadings

Sections	Mass Damping	Max Rotation
E1	0.00%	1.210
	5.00%	1.136
	10.00%	1.007
E2	0.00%	0.367
	5.00%	0.356
	10.00%	0.346
E3	0.00%	0.201
	5.00%	0.200
	10.00%	0.192
E4	0.00%	0.181
	5.00%	0.130
	10.00%	0.129
E5	0.00%	0.124
	5.00%	0.118
	10.00%	0.111

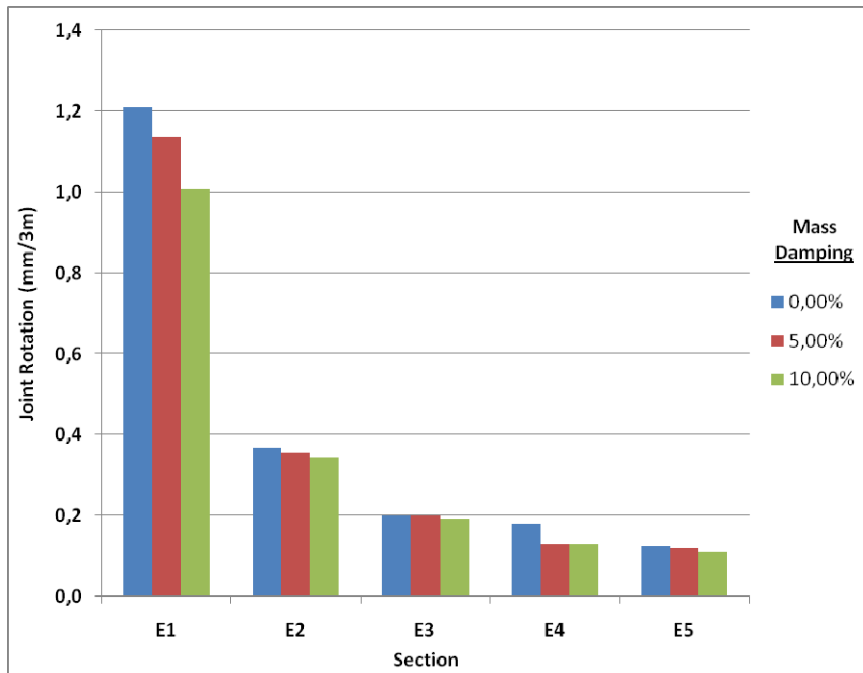


Figure 4.12 Max Joint Rotation values at midspan of bridge with different sections and mass increments under HSLM-A10 train loadings

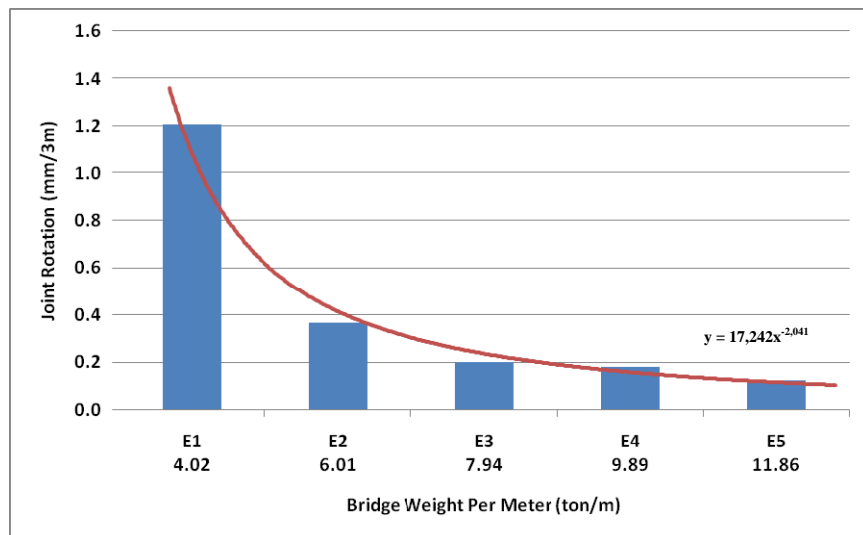


Figure 4.13 Trendline of Max Joint Rotation at midspan of bridge with different per meter weight

Table 4.9 % Decrease of Joint Acceleration values at midspan of bridge with the effect of mass increments under HSLM-A10 train loadings

Sections	Mass Damping	Max Acceleration	Decrease (%)
E1	0.00%	30.45	
	5.00%	15.86	47.91%
	10.00%	12.09	60.30%
E2	0.00%	17.49	
	5.00%	7.84	55.18%
	10.00%	6.46	63.08%
E3	0.00%	13.78	
	5.00%	4.72	65.71%
	10.00%	3.56	74.17%
E4	0.00%	10.46	
	5.00%	2.94	71.91%
	10.00%	1.62	84.52%
E5	0.00%	8.70	
	5.00%	2.19	74.79%
	10.00%	1.27	85.41%

4.4. Moving Suspension Mass Model Analysis Results

Moving Suspension Mass Model has also been analyzed with the Non-Linear Time History analysis of Larsa 4D. The aim of this model's analyze was to investigate the general behavior and to compare the results with the moving force model analysis results. Therefore analyze has just been executed for existing situation of the bridge under HSLM-A10 train loading with 10 different speeds.

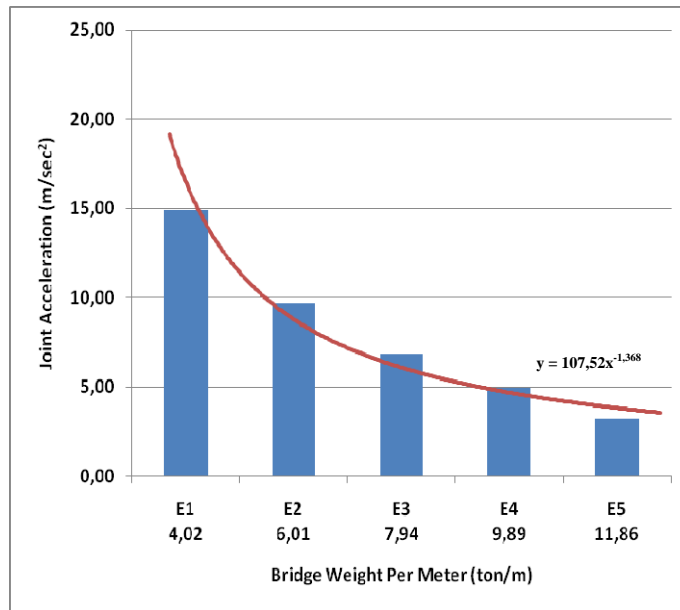


Figure 4.14 Max Joint Acceleration values with trendline at midspan of bridge with different sections under HSLM-A10 train loadings

Table 4.10 Joint Acceleration (m/sec²) values at midspan of bridge with different sections under HSLM-A10 train loading with varying speeds

Section	Speed									Max
	40	45	50	55	60	65	70	75	80	
E1	3.51	14.89	10.60	10.55	8.38	6.66	9.56	7.83	5.88	14.89
E2	1.30	9.73	7.96	5.41	4.10	4.43	3.57	4.51	3.69	9.73
E3	1.29	6.88	5.29	5.16	4.11	3.30	3.64	4.02	3.31	6.88
E4	0.96	4.99	3.86	3.75	3.00	3.31	3.10	2.47	1.89	4.99
E5	0.91	3.22	2.51	2.45	2.85	1.95	3.09	1.82	1.40	3.22

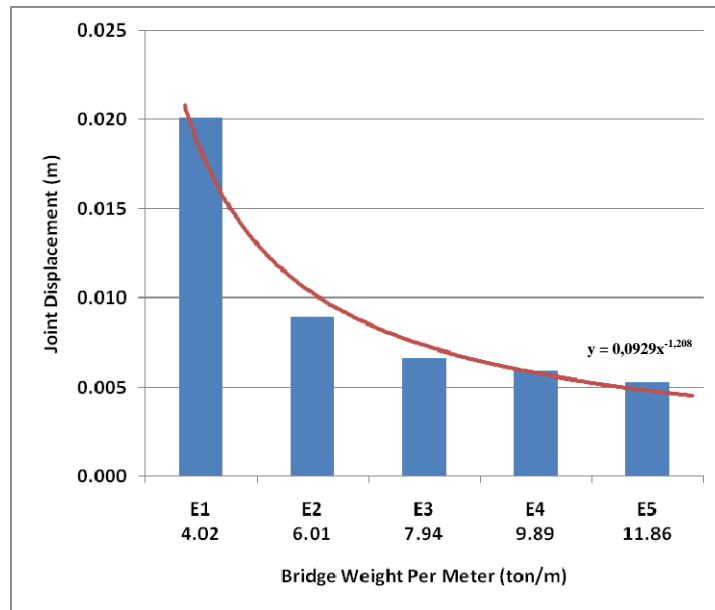


Figure 4.15 Max Joint Displacement values with trendline at midspan of bridge with different sections under HSLM-A10 train loadings

Table 4.11 Joint Displacement (m) values at midspan of bridge with different sections under HSLM-A10 train loading with varying speeds

Section	Speed									Max
	40	45	50	55	60	65	70	75	80	
E1	0.00486	0.02014	0.01696	0.01482	0.00936	0.00826	0.00868	0.01016	0.01005	0.02014
E2	0.00179	0.00895	0.00820	0.00734	0.00503	0.00478	0.00440	0.00473	0.00414	0.00895
E3	0.00207	0.00667	0.00570	0.00486	0.00415	0.00369	0.00371	0.00410	0.00346	0.00667
E4	0.00108	0.00596	0.00522	0.00397	0.00356	0.00318	0.00318	0.00247	0.00232	0.00596
E5	0.00100	0.00494	0.00531	0.00200	0.00265	0.00189	0.00255	0.00200	0.00133	0.00531

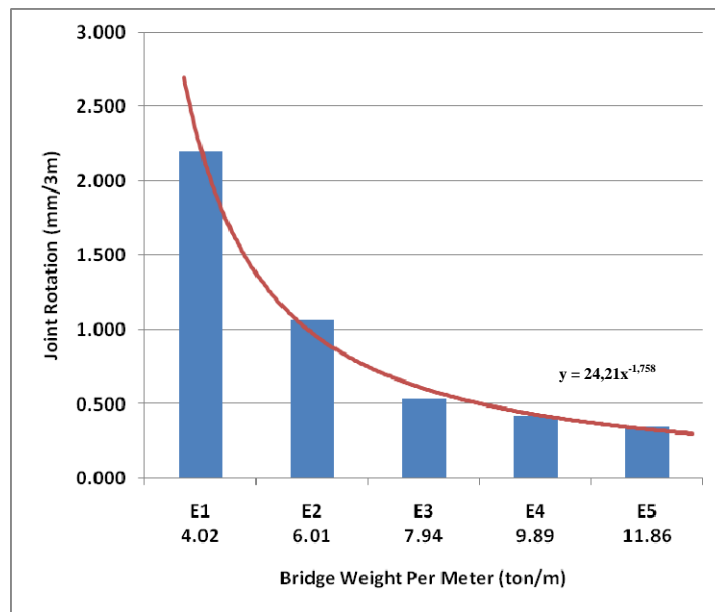


Figure 4.16 Max Joint Rotation values with trendline at midspan of bridge with different sections under HSLM-A10 train loadings

Table 4.12 Joint Rotation (mm/3m) values at midspan of bridge with different sections under HSLM-A10 train loading with varying speeds

Section	Speed									Max
	40	45	50	55	60	65	70	75	80	
E1	0.452	1.813	1.797	1.479	1.112	1.247	2.200	1.022	1.440	2.200
E2	0.202	1.068	0.978	0.723	0.487	0.642	0.579	0.523	0.380	1.068
E3	0.152	0.525	0.537	0.482	0.256	0.298	0.294	0.235	0.268	0.537
E4	0.068	0.420	0.393	0.372	0.171	0.211	0.252	0.187	0.227	0.420
E5	0.100	0.352	0.297	0.248	0.160	0.157	0.179	0.144	0.088	0.352

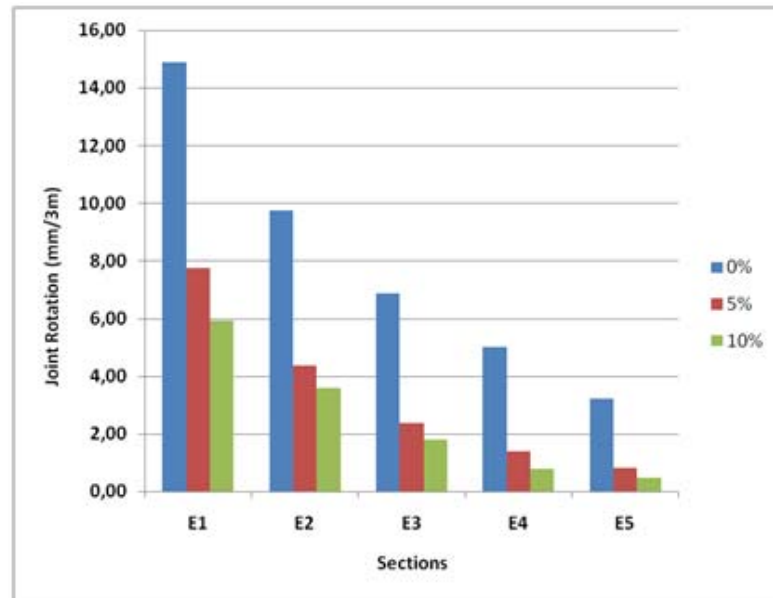


Figure 4.17 Max Joint Rotation with assumed values of mass increment effects at midspan of bridge with different sections under HSLM-A10 train loadings

4.5. Moving Force Model and Moving Suspension Mass Model Analysis Results Comparison

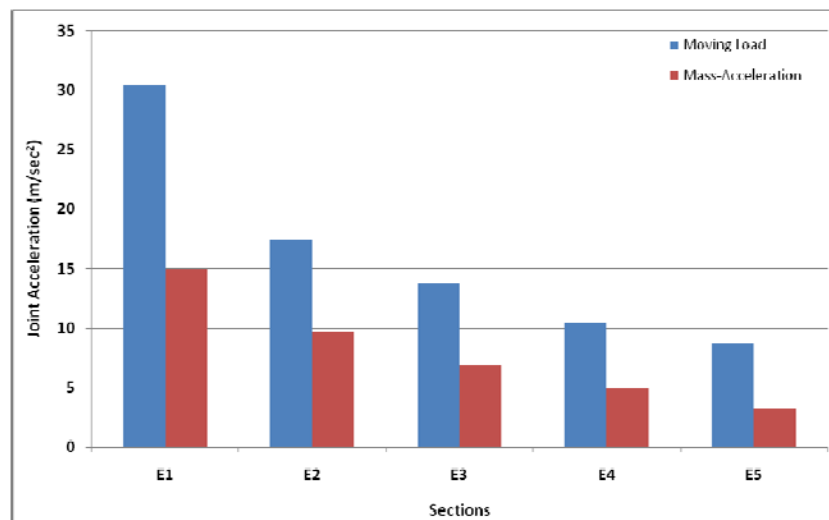


Figure 4.18 Max Joint Acceleration values at midspan of bridge with different sections under HSLM-A10 train loadings

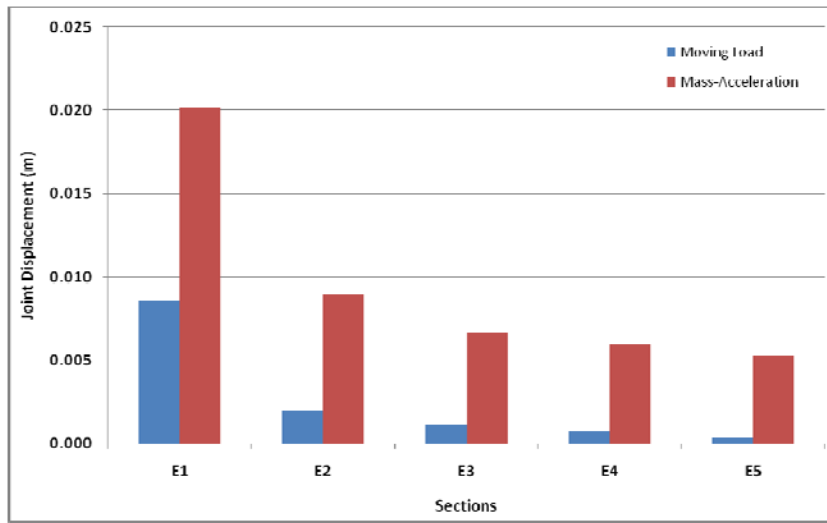


Figure 4.19 Max Joint Displacement values at midspan of bridge with different sections under HSLM-A10 train loadings

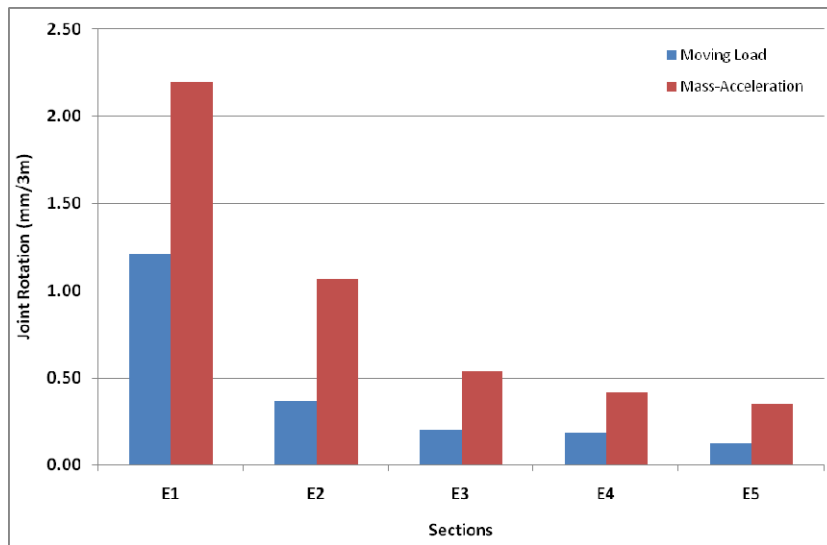


Figure 4.20 Max Joint Rotation values at midspan of bridge with different sections under HSLM-A10 train loadings

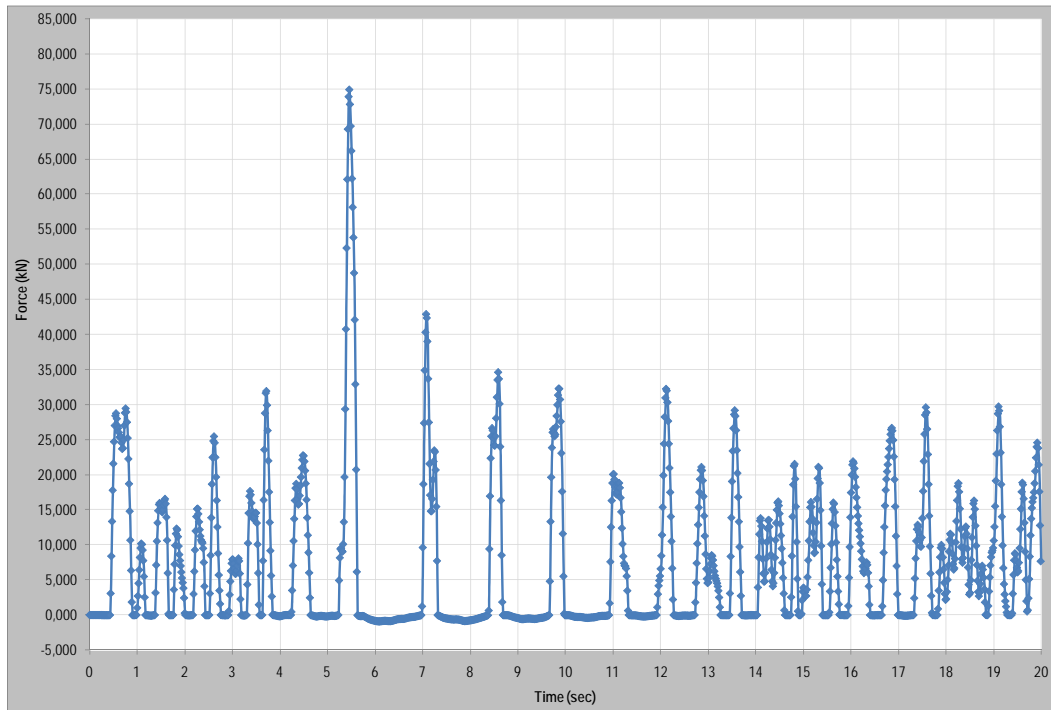


Figure 4.21 Spring Force values at the midspan of the existing bridge under HSLM-A10 train loading with a speed of 70 m/hr

4.6. Eigenvalue Analysis Results

First five eigenmodes of the existing bridge with concrete deck has been given in table 4.13.

Table 4.13 First five modes of the model without rehabilitation

Eigenmode	Frequency	Period	Description
1 st	3.43	0.2917	1 st horizontal mode
2 nd	4.28	0.2337	1 st vertical bending
3 rd	4.90	0.2040	2 nd horizontal mode
4 th	7.27	0.1381	1 st torsional mode
5 th	8.45	0.1184	1 st longitudinal mode

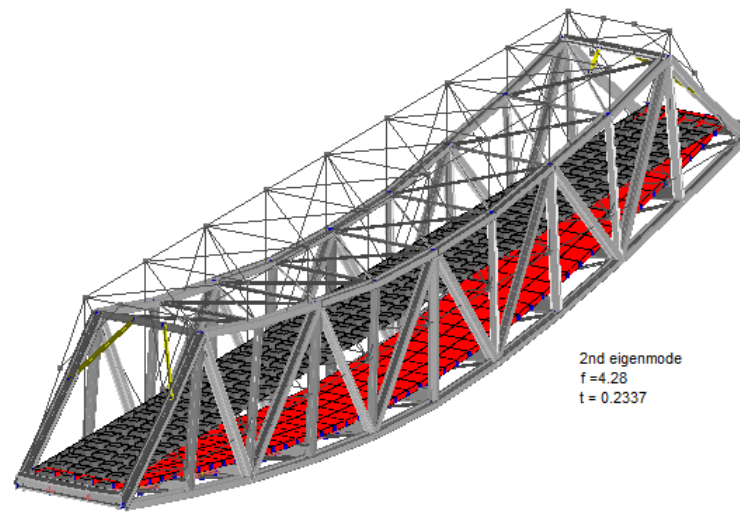


Figure 4.22 First bending mode of existing steel bridge with concrete deck

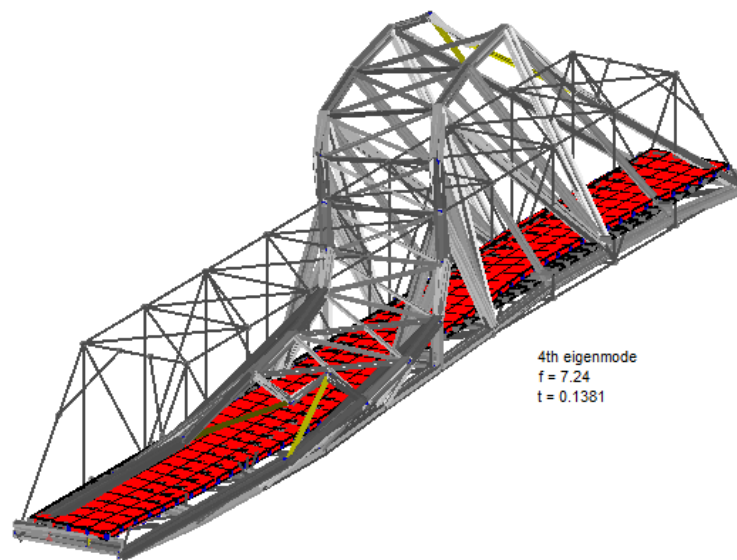


Figure 4.23 First torsional mode of existing steel bridge with concrete deck

Table 4.14 First Natural Frequencies and Periods of sections with varying mass increments

Section	Mass Increment	Fisrt Natural	
		Frequency (f)	Period (t)
E1	0 %	3,43	0,2917
	5 %	3,33	0,3007
	10 %	3,22	0,3106
E2	0 %	3,87	0,2585
	5 %	3,74	0,2675
	10 %	3,61	0,2771
E3	0 %	4,12	0,2427
	5 %	3,97	0,2517
	10 %	3,83	0,2612
E4	0 %	4,28	0,2336
	5 %	4,12	0,2426
	10 %	3,97	0,2519
E5	0 %	4,40	0,2273
	5 %	4,23	0,2363
	10 %	4,07	0,2456

CHAPTER 5

DISCUSSION ON RESULTS

5.1. Introduction

In this chapter, obtained analysis and field test results at chapter 4 will be discussed.

Modeling with too much assumption parameters might give meaningless results. In the existing state of the bridge there were lots of unknowns which were hard to assume or find a starting reference point. Therefore the field test results and the calculated results could not be compared because the bridge did not been modeled as its existing state with timber sleepers.

5.2. Discussion on Field Test Results

The dynamic measurement tests have been conducted on the steel truss bridge. Only the first mode shapes has been identified due to the selected sensor properties. From post-processed results it is understood that, the vertical accelerations appears to be higher than the defined limits of vibrations accepted for train bridges. Maximum vertical acceleration has been obtained as greater than 3g as shown in the Figure 4.5. The speed of the train is approximately calculated to be 85 km/hr. Train speeds of 95, 128, 150, 211, 259 and 320 km/hr were found to be possible resonance condition. The low damping ratio of the

steel truss bridge demonstrates that in case of a high speed train usage large deflections will have been achieved.

Overall results of the field test indicate that the bridge is not just appropriate for the high-speed train usage; it is also not allowable to usage under standard type trains with existing situations. Therefore rehabilitation becomes a must to set the bridge useful for high-speed trains.

In bridge monitoring under service conditions, usage of wireless accelerometer sensors has both advantages and disadvantages. Short setting time, wide area coverage and ease of data collection are great advantages; however the data downloading speeds and post data processing necessity for most of the readings can be count as disadvantages and should be improved for better monitoring.

5.3. Discussion on Moving Force Model Analysis Results

Moving Force Model analysis of the existing bridge with concrete deck certifies the field test results. A vertical acceleration of approximately 10 times greater than the defined limits of vibrations accepted for train bridges has been achieved as shown on Table 4.4. Maximum vertical acceleration has been obtained as greater than 3g at the field tests. The differences between the results are more likely occurred because of the substitution of the concrete deck for direct fixation on for timber sleepers but no further investigation has been made in the scope of this thesis.

From the Table 4.3 it can be obtained that the maximum vertical accelerations are occurred at train speeds of 50 m/sec and 75 m/sec which can be identified as approximate resonance speeds.

The Table 4.5 and 4.7 certifies that the train speeds of 50 m/sec and 75 m/sec are approximate resonance speeds. It can easily be seen that the maximum values of joint displacement and joint rotation are calculated at these speeds.

The Figure 4.7 shows that the allowable joint acceleration, 5 m/sec^2 , has been started to be achieved at triple section with 5% mass increment. This situation clearly figures out the poor condition of the existing bridge. It is also understood from this figure that mass increments are more effective than thickening of the steel sections. A less joint acceleration value can be obtained at double of the existing sections with a 5% mass increment instead of having five times larger sections.

Mass increment had a reverse effect on the joint displacement as shown in Figure 4.9. This effect can be explained with the application and modeling of the mass increment at just a one point which is midspan of the bridge. Joint displacement has not been an important criteria for this study because the maximum obtained joint displacement value, 0.0085 m, is far small than the maximum allowable joint displacement, 0.083 m, so that no further investigation has been made but instead of applying one big size mass increment, multiple smaller mass increments might give better results.

The maximum joint rotation has been calculated as 1.21 mm/3m which is again far small than the maximum allowable joint rotation, 3 mm/3m. It is understood from the Figure 4.11 that the mass increments are not so much effective to reduce the joint rotation. In case of a joint rotation critical bridge design, section improvement appears to be more effective than mass increments.

The relation between the span weight per meter and the maximum joint acceleration has been identified with a power trendline as shown

in Figure 4.8. Equation of the trendline signifies that to get the maximum allowable joint displacement, the optimal span weight per meter without a mass increment is 18.97 ton/m.

From the trendlines defined at Figures 4.10 and 4.12 the optimal span weight per meter has been respectively calculated as 1.67 ton/m and 2.36 ton/m. It is understood from these calculations the most critical criteria for optimal span weight for passenger comfort is the joint displacement. Therefore it can be concluded that the optimal span weight per meter calculated with moving force model is 18.97 ton/m.

5.4. Discussion on Moving Suspension Mass Model Analysis Results

From the Table 4.10 it can be obtained that the maximum vertical accelerations are occurred at train speeds of 45 m/sec and 70 m/sec which can be identified as approximate resonance speeds. It can easily be noticed that a difference of 5 m/sec has been obtained at the resonance speeds between the Moving Force Model and Moving Suspension Mass Model. This situation can be described as with addition of the high speed train's mass to the Moving Force Model, the systems frequency is decreased. Therefore as indicated with equation 3.11 and 3.12 the resonance speeds are also decreased.

The Figure 4.13 shows that the allowable joint acceleration, 5 m/sec^2 , has been started to be achieved at quadruple, E4, section. The aim of this modeling was to determine the general behavior of the model. Therefore no analysis has been executed for the mass increments but if it is assumed that the mass increments will also be effective as at the Moving Force Model, the allowable joint acceleration can be

achieved at double section with 5% mass increment as shown in Figure 4.16.

Joint displacement has not again been an important criteria for this study just like at the Moving Force Model, because the maximum obtained joint displacement value, 0.020 m, is far small than the maximum allowable joint displacement, 0.083 m.

As shown in Table 4.12 the maximum joint rotation has been calculated as 2.20 mm/3m, which is under the limit of maximum allowable joint rotation, 3 mm/3m.

The relation between the span weight per meter and the maximum joint acceleration has been identified with a power trendline as shown in Figure 4.13. Equation of the trendline signifies that to get the maximum allowable joint displacement, the optimal span weight per meter without a mass increment is 9.43 ton/m.

From the trendlines defined at Figures 4.14 and 4.15 the optimal span weight per meter has been respectively calculated as 1.09 ton/m and 0.56 ton/m. It is understood from these calculations the most critical criteria for optimal span weight for passenger comfort is the joint displacement. Therefore it can be concluded that the optimal span weight per meter calculated with Moving Suspension Mass Model is 18.97 ton/m.

5.5. Discussion on Moving Force Model and Moving Suspension Mass Model Analysis Results Comparison

Moving suspension mass model has been defined to investigate the beneficial mass damping effect of the high speed train on the bridge. As shown in the Figure 4.17 by using Moving Suspension Mass Model,

smaller maximum joint acceleration values has been obtained. This situation can be clarified as the high speed train has a positive effect on the maximum joint acceleration achieved at the midspan of the bridge.

As shown in Figures 4.18 and 4.19, greater joint displacement and rotation values are obtained with the Moving Suspension Mass Model. If compared with the joint displacement data received from Turkish State Railways these values appears to be more meaningful than obtained from the Moving Force Model analysis.

From the calculations above, the optimal span weight of the bridge per meter is calculated as 18.97 ton/m with the Moving Force Model and 9.43 ton/m Moving Suspension Mass Model. It can be concluded that considering the reality of nearly twice of an over-design situation has been occurred, the model advised at the EN 1991-2 needs to be improved.

Although, the applied loads are equal to 85 kN, it can be seen from Figure 4.20, a max effective load on the joint of 75 kN has been obtained from the analysis. This seems to be main difference between Moving Force Model and Moving Suspension Mass Model. At the Moving Force Model all the effective loads are equal to the applied load which is 85 kN.

The analysis software used, Larsa 4D, has both advantages and disadvantages. User friendly interface and copy-paste ability between the tables and MS Excel are great and time saving features; however the long processing time of the Non-Linear time history should be improved to have a better analyzing environment.

5.6. Discussion on Eigenvalue Analysis Results

Eigenvalue analysis results are given just for information only. Numerous unknown characteristics of the bridge and trains prevent us to be able to computational modeling and analyzing of the existing situation of the bridge. Assumption of this many characteristics would most probably cause meaningless analysis results. The documentation of this type of information by Turkish State Railways needs to be developed.

CHAPTER 6

SUMMARY AND CONCLUSION

In this study, a total of 250 analysis runs has been made in order to figure out the condition of the existion bridge with concrete deck, effectivity of the rehabilitation options and comparison of the Moving Force Model and Moving Suspension Mass Model analysis results. The conclusion of this study can be summarized as follows:

- The existing bridge is physically at a good condition but close to resonance condition was detected and expected to have large deformations in the resonance state.
- Overall results of the field test indicate that the bridge is not just appropriate for the high-speed train usage; it is also not allowable to usage under standard type trains with existing situations.
- The most critical passenger comfort criteria has been obtained as Joint Acceleration and maximum allowable joint acceleration value has been started to be achieved at triple section with 5% mass increment with Moving Force Model and double section with 5% mass increment with Moving Suspension Mass Model.
- Mass increments are more effective than thickening of the existing sections at joint acceleration and joint rotation criterias. Single Mass increment usage causes an incese in joint

displacement. Therefore if necessary usage of Multiple Mass increments has to be preferred.

- The optimal bridge span weight per meter without a mass increment has been calculated as 18.97 ton/m with Moving Force Model and 9.43 ton/m with Moving Suspension Mass Model. Considering the reality of nearly twice of an over-design situation has been occurred, the model advised at the EN 1991-2 needs to be improved.

The accuracy of the Moving Suspension Mass Model have been verified once again in this thesis as in the studies made in recent years.[23] The computational analysis of this thesis took a very long time to finalize. Therefore analysis softwares should be improved in this direction to have better and less time taking analysis. Finally, after several advantageous observations of the mass increments, it is hopefully expected that they are more widely and often used in the existing and new bridges.

REFERENCES

- [1] Dynamic analysis of railway bridge under high-speed trains, He Xia, Nan Zhang, Computers and Structures, 83, 1891–1901
- [2] Patrick, J., 07 March 2008, "Trains of Turkey – History / TCDD browse", <http://www.trainsofturkey.com/w/pmwiki.php/History/TCDD>, January 2007.
- [3] Wikipedia Community, 07 March 2008, "High-Speed Rail - Wikipedia The Free Encyclopedia", http://en.wikipedia.org/wiki/High-speed_rail, September 2007.
- [4] Eurocode 1990:2005 – Eurocode : "Basis on structural design", 2005, Brussels.
- [5] Eurocode 1991-2:2003 - Eurocode 1: Actions on structures - Part 2, "Traffic loads on bridges", 2003, Brussels.
- [6] UIC Code 774-3 – "Track Bridge Interaction Recommendations for Calculations 2nd edition", October 2001, Paris.
- [7] Song, K., M., Noh, H., C., and Choi, C., K., 2003," A New Three-Dimensional Finite Element Analysis Model of High-Speed Train–Bridge Interactions", Journal of Engineering Structures, 25, 1611-1626.

- [8] Fryba, L., 2001, "A Rough Assessment of Railway Bridges for High Speed Trains", *Journal of Engineering Structures*, 23, 448-556.
- [9] Biondi, B., Muscolino, G., and Sofi, A., 2005, "A Substructure Approach for the Dynamic Analysis of Train–Track–Bridge System", *Journal of Computers and Structures*, 83, 2271-2281.
- [10] Museros, P., Romero, M.L., Poy, A., and Alarcon, E., 2002, "Advances in the Analysis of Short Span Railway Bridges for High-Speed Lines", *Journal of Computers and Structures*, 80, 2121-2132.
- [11] Turer, A., "Dynamic Testing of Existing Bridges for High Speed Trains", 2007, METU, Ankara, unpublished paper.
- [12] De Roeck, G., Maeck, J., and Teughels, A., "Validation of Numerical Models by Experiments on a High Speed Railway Bridge in Antoining" Belgium.
- [13] Xia, H., Zhang, N., 2005, "Dynamic Analysis of Railway Bridge Under High-Speed Trains", *Journal of Computers and Structures*, 83, 1891-1901.
- [14] Heiden, M., Bokan, H., Simões da Silva, L., Greiner, R., Pirchere, M., Pircher, H., 2003, "Dynamic Effects of Railway Bridges for High Speed Usage: Application Example Steel-Composite Truss Bridge", IV Congresso de Construção Metálica e Mista, Lisbon.
- [15] Geier, R., Österreicher, M., "Dynamic Investigations of Railway Bridges", Vienna, Austria.

- [16]** Xia, H., Roeck, G.D., Zhang, N., Maecka, J., 2003, "Experimental analysis of a high-speed railway bridge under Thalys trains", *Journal of Sound and Vibration*, 268, 103-113.
- [17]** Delgado, M.R., dos Santos R. C., S.M., 1997, "Modeling of Railway Bridge-Vehicle Interaction on High Speed Tracks", *Journal of Computers and Structures*, Vol.63, No.3 511-523.
- [18]** Goicolea, J.M., Dominguez, J., Navarro, J.A., Gabaldon, F., 2002, "New Dynamic Analysis Methods for Railway Bridges in Codes IAPF and Eurocodes 1", *Railway Bridges Design, Construction and Maintenance Spanish group of IABSE*, 2-43, Madrid.
- [19]** Ju, S.H., Lin, H.T., 2003, "Resonance Characteristics of High-Speed Trains Passing Simply Supported Bridges", *Journal of Sound and Vibration*, 267, 1127-1141.
- [20]** Yang, Y.B., Yau, J.D., Hsu, L.C., 1997 "Vibration of Simple Beams Due to Trains Moving at High Speeds", *Journal of Engineering Structures*, Vol.19, No.11 936-944.
- [21]** Lin, C.C., Asce, M., Wang, J.F., Chen, B.L., 2005, "Train-Induced Vibration Control of High-Speed Railway Bridges Equipped with Multiple Tuned Mass Dampers", *Civil Engineering*, ASCE.
- [22]** Daniels, L.E., Tuten III, J.M., Stanford, C.L., 2001, "Definitions of Direct Fixation Track", *APTA 2001 Rail Transit Conference*, Boston
- [23]** Chopra, A., 2000, "Dynamics of Structures", Prentice Hall, New Jersey

[24] LARSA Ins., "LARSA 2000 Reference for LARSA 2000 Finite Element Analysis and Design Software", 2004, Melville, New York

APPENDIX A

SELECTIVE ANALYSIS RESULTS

A.1. Moving Force Model Analysis Graphs

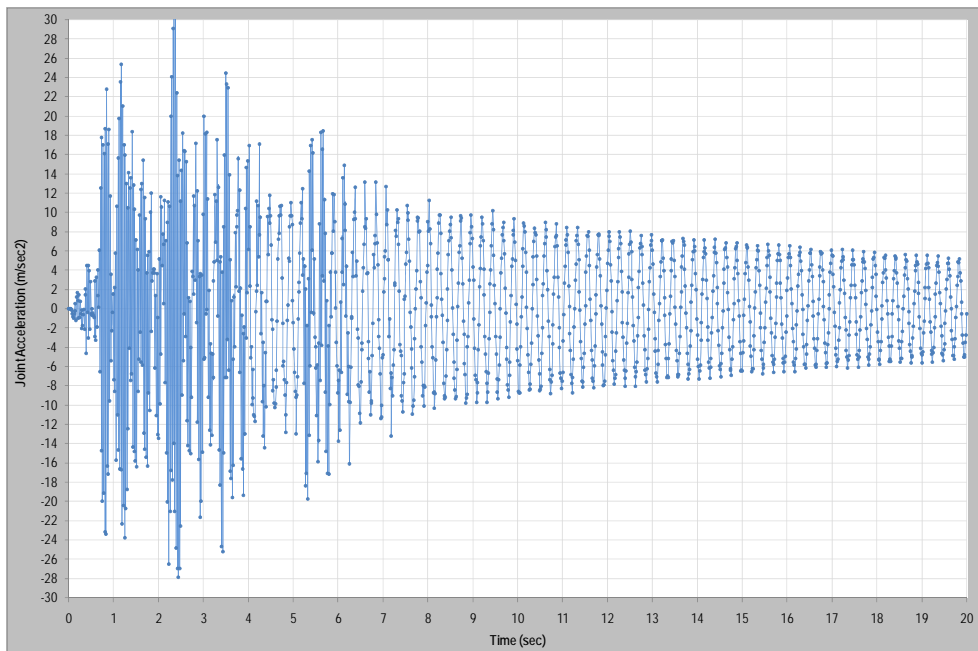


Figure A.1 Joint acceleration vs. time graphic of E1 analysis model with a speed of 75 m/sec

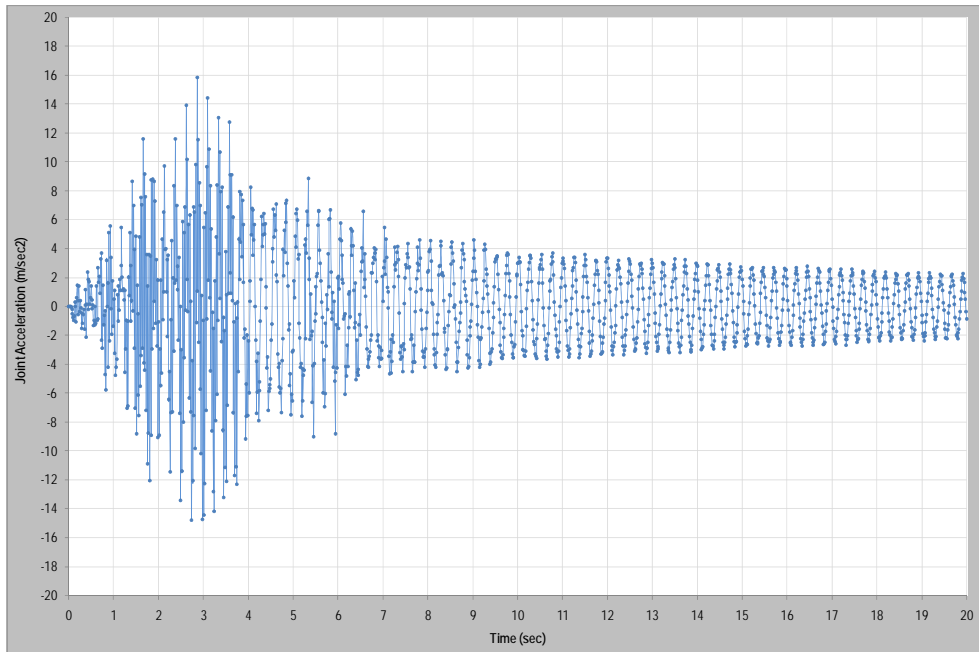


Figure A.2 Joint acceleration vs. time graphic of E1-5 analysis model with a speed of 75 m/sec

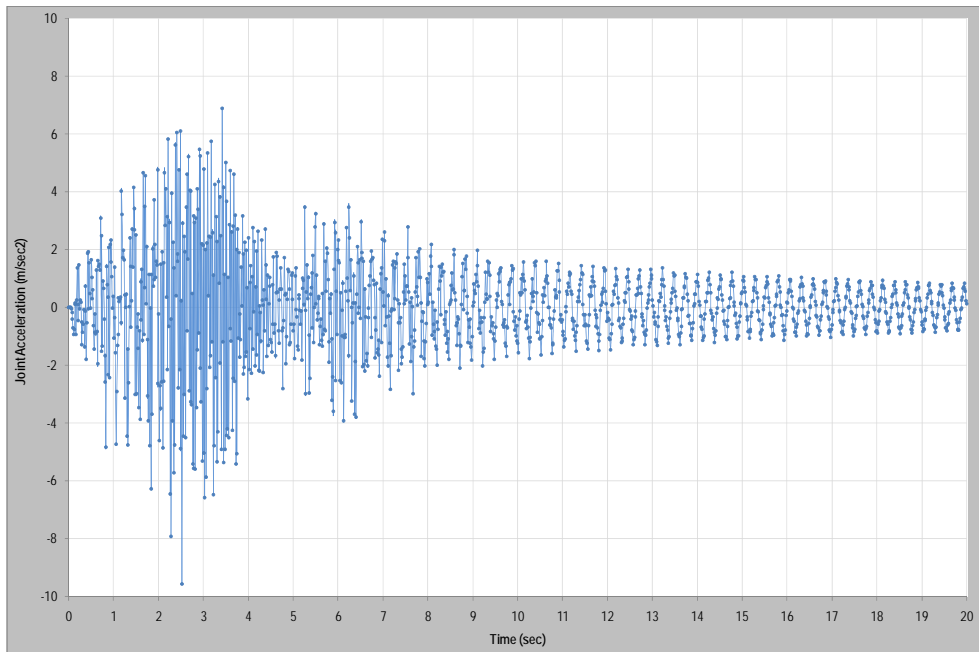


Figure A.3 Joint acceleration vs. time graphic of E1-10 analysis model with a speed of 75 m/sec

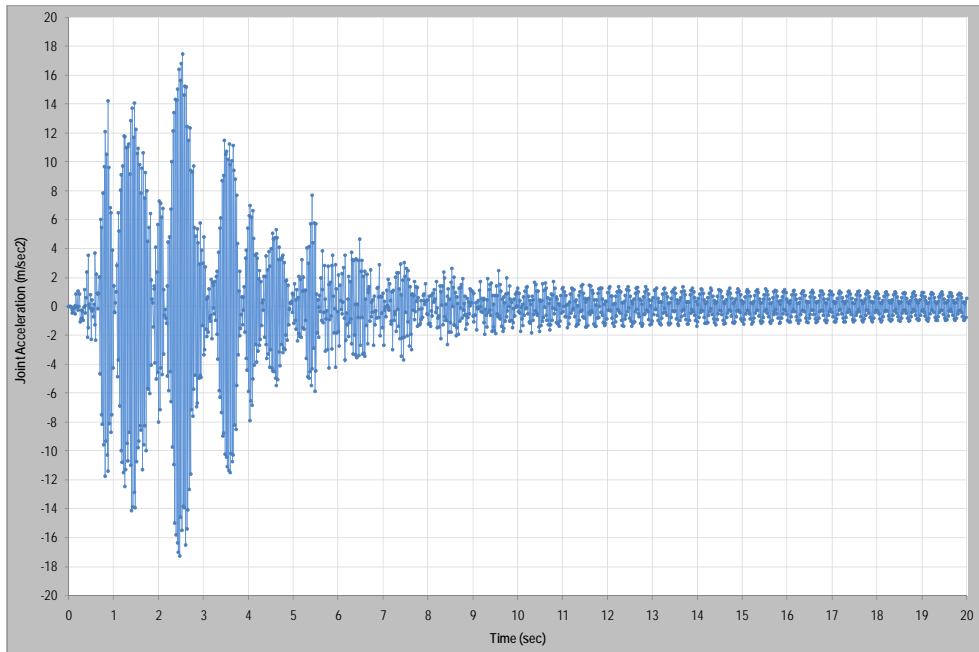


Figure A.4 Joint acceleration vs. time graphic of E2 analysis model with a speed of 75 m/sec

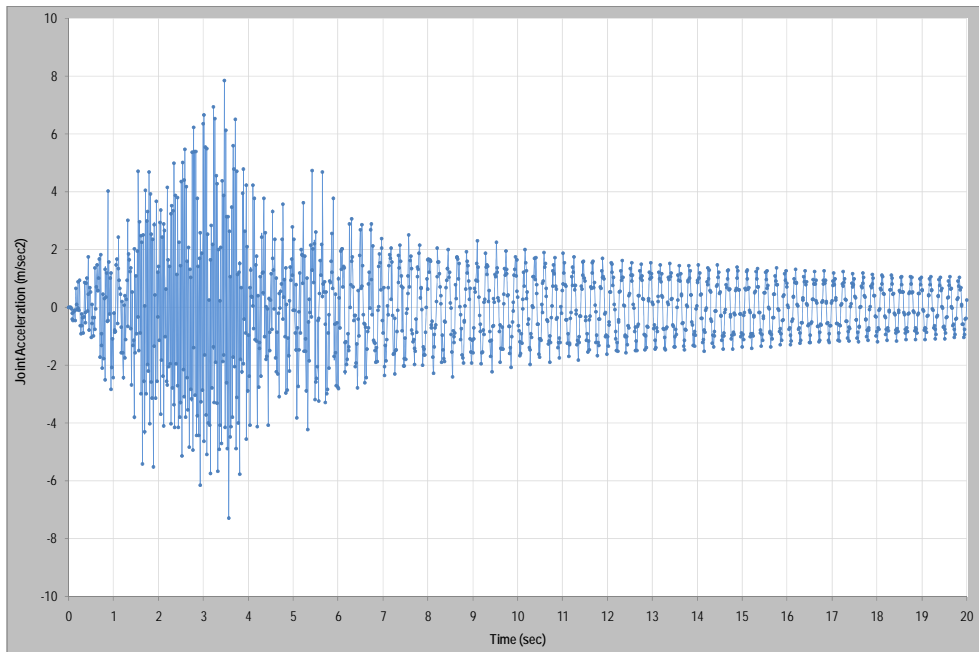


Figure A.5 Joint acceleration vs. time graphic of E2-5 analysis model with a speed of 75 m/sec

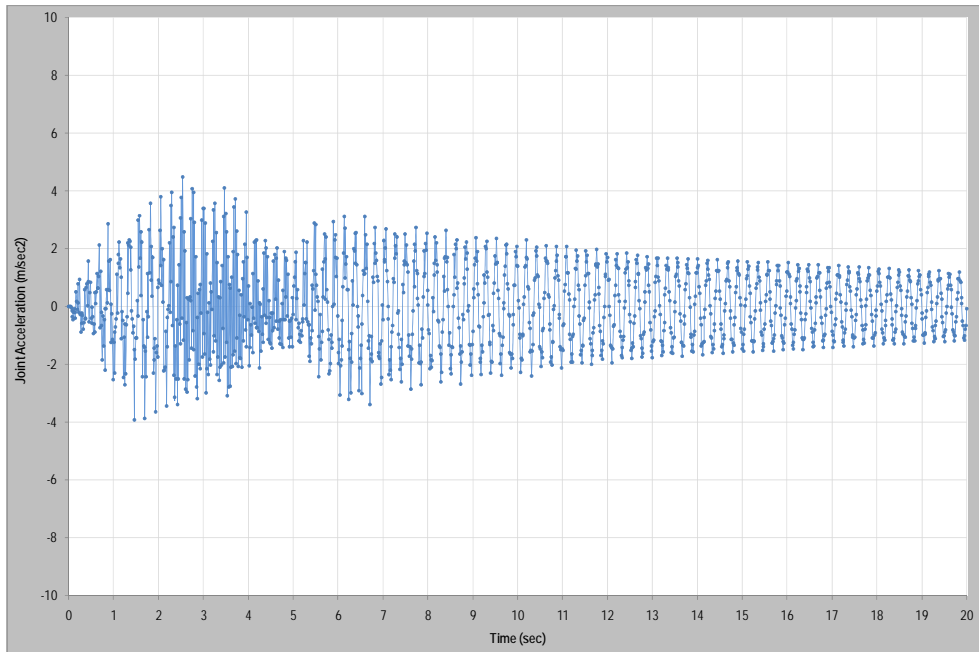


Figure A.6 Joint acceleration vs. time graphic of E2-10 analysis model with a speed of 75 m/sec

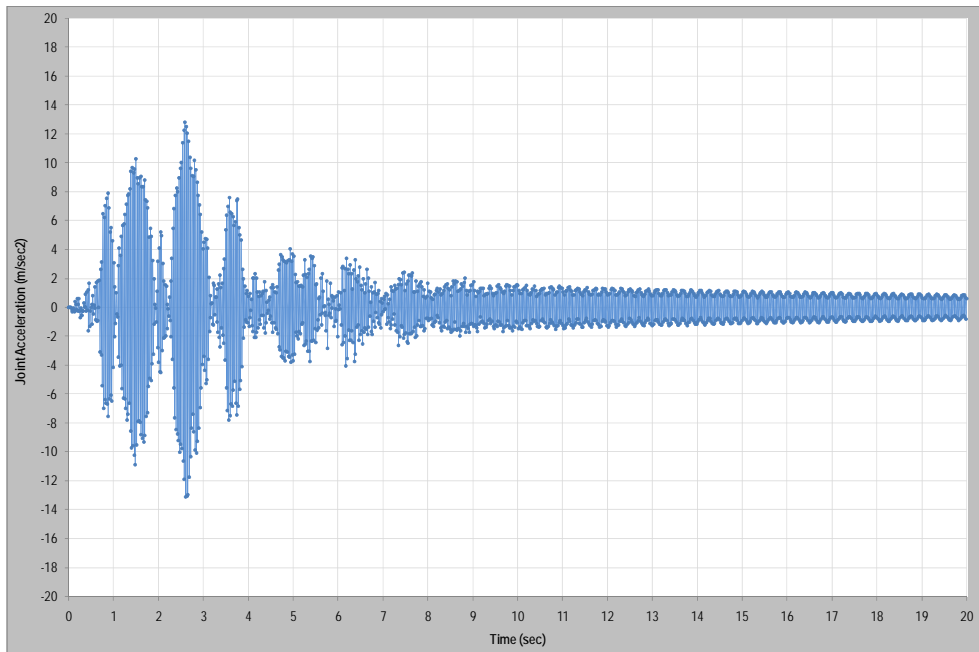


Figure A.7 Joint acceleration vs. time graphic of E3 analysis model with a speed of 75 m/sec

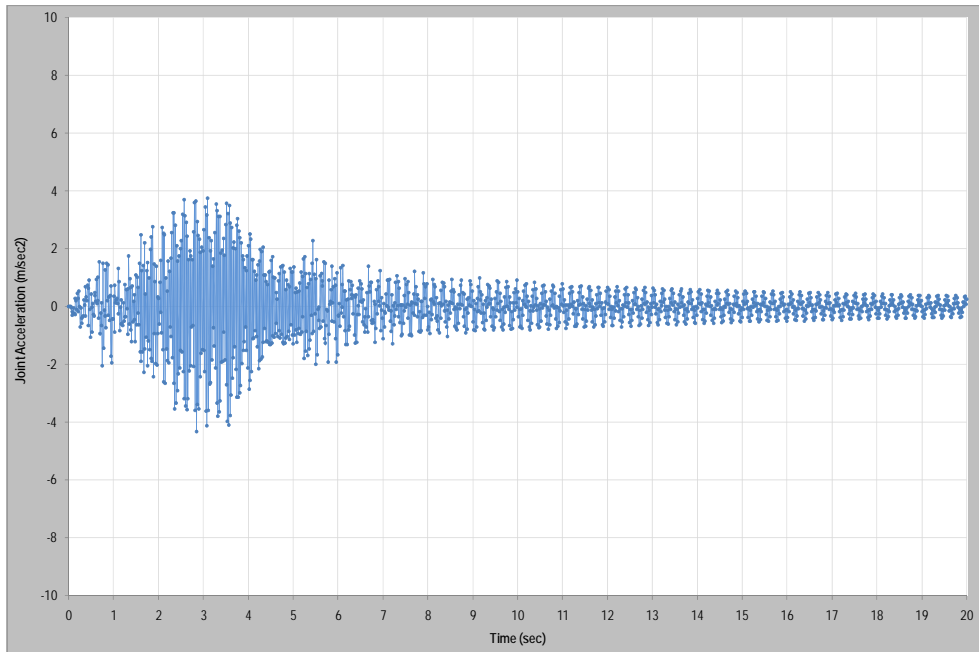


Figure A.8 Joint acceleration vs. time graphic of E3-5 analysis model with a speed of 75 m/sec

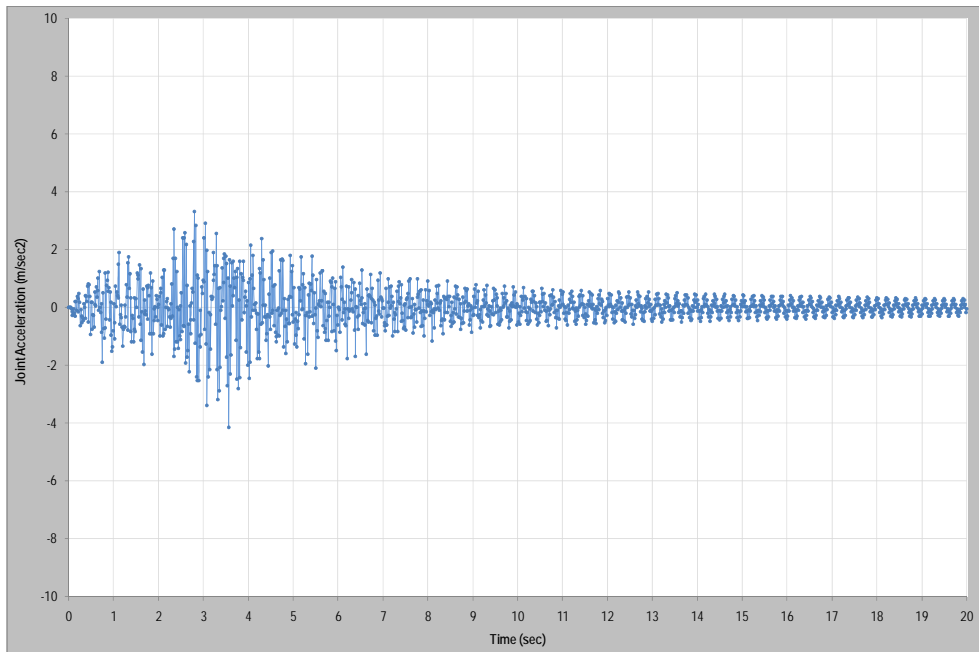


Figure A.9 Joint acceleration vs. time graphic of E3-10 analysis model with a speed of 75 m/sec

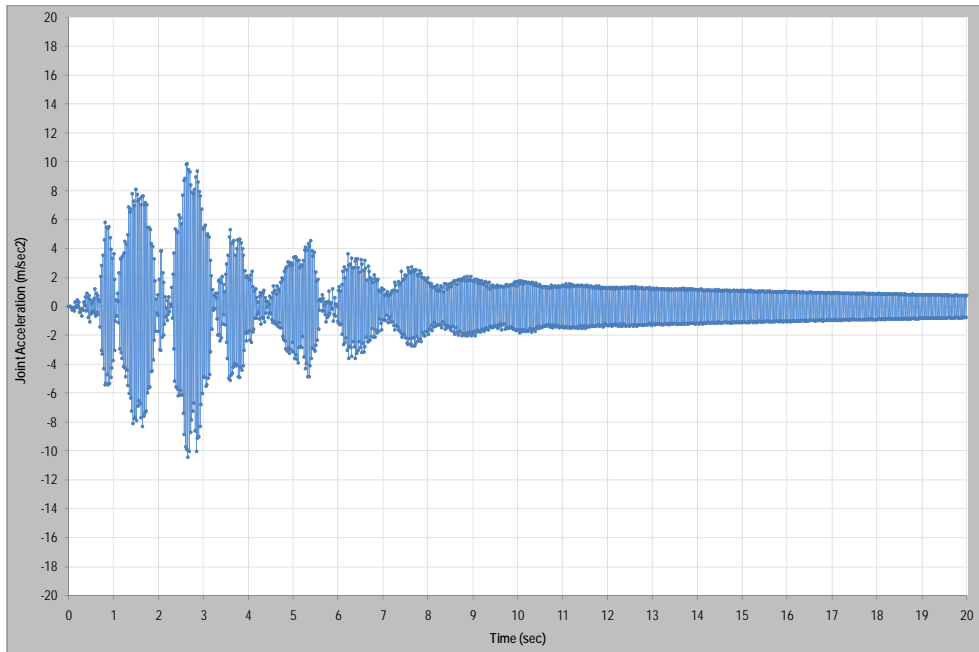


Figure A.10 Joint acceleration vs. time graphic of E4 analysis model with a speed of 75 m/sec

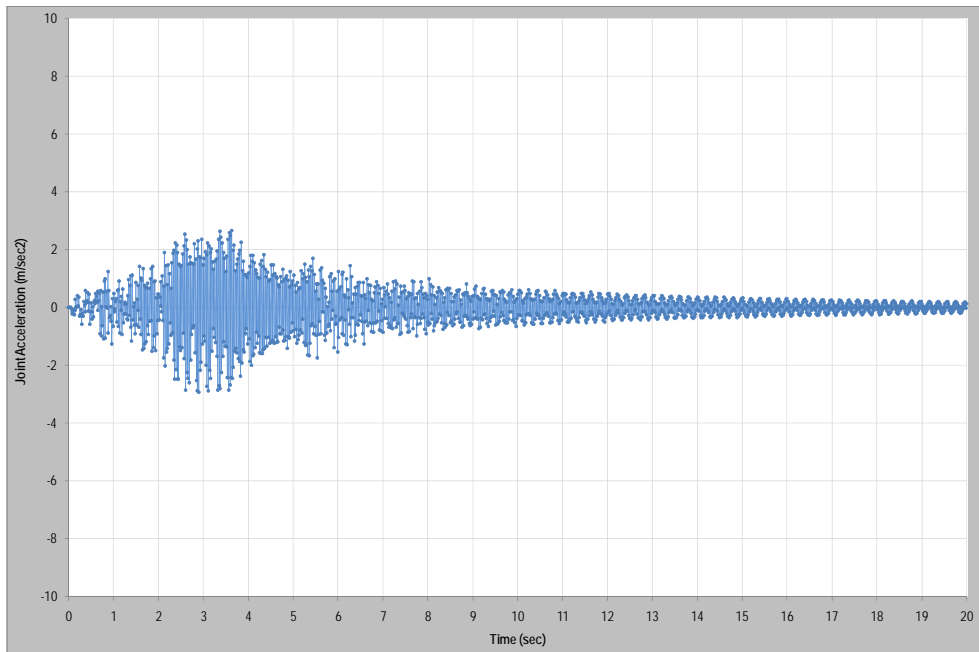


Figure A.11 Joint acceleration vs. time graphic of E4-5 analysis model with a speed of 75 m/sec

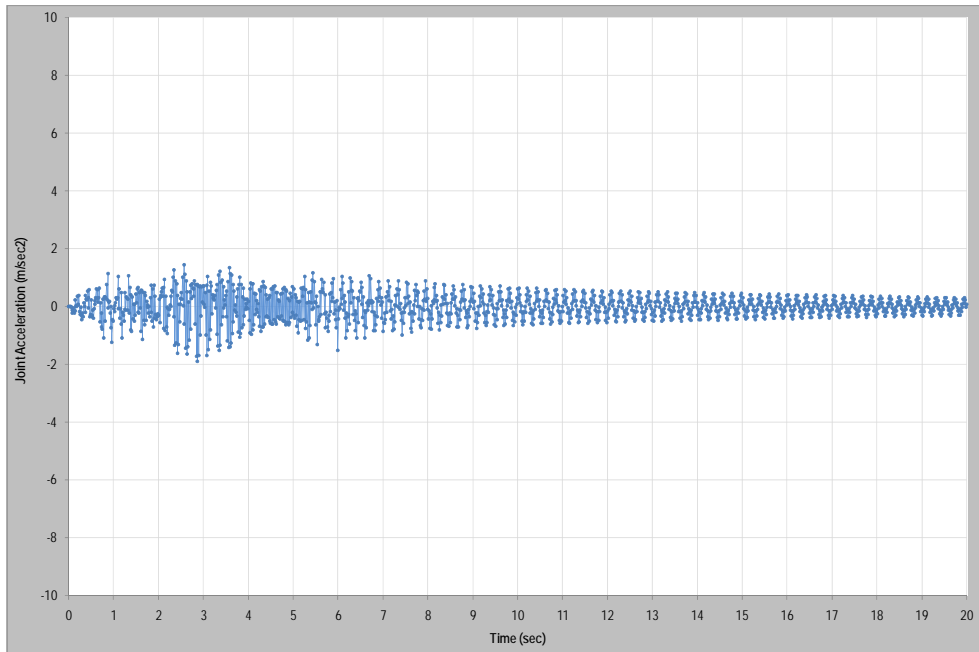


Figure A.12 Joint acceleration vs. time graphic of E4-10 analysis model with a speed of 75 m/sec

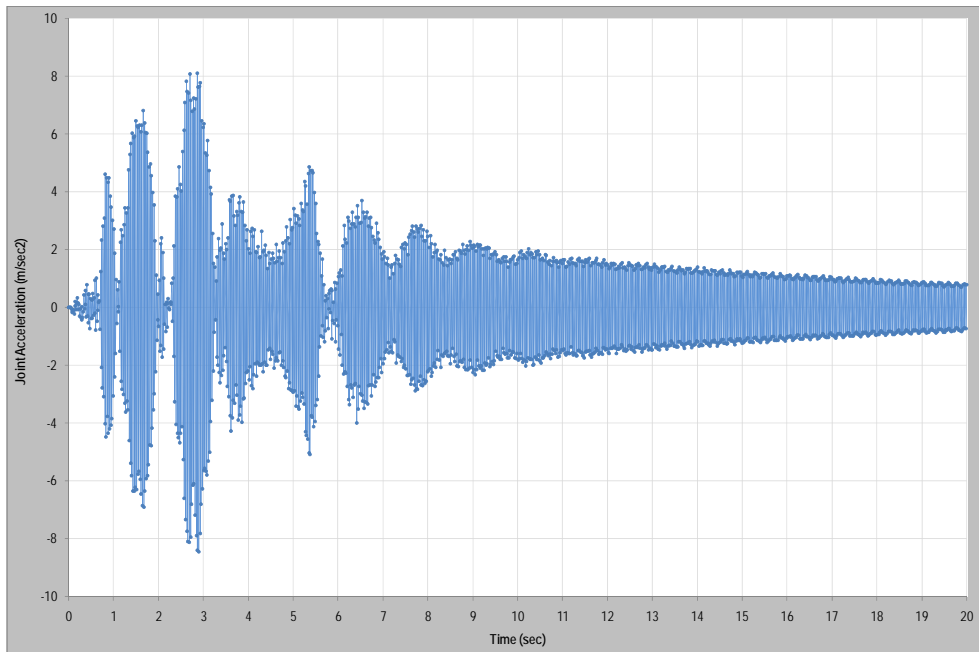


Figure A.13 Joint acceleration vs. time graphic of E5 analysis model with a speed of 75 m/sec

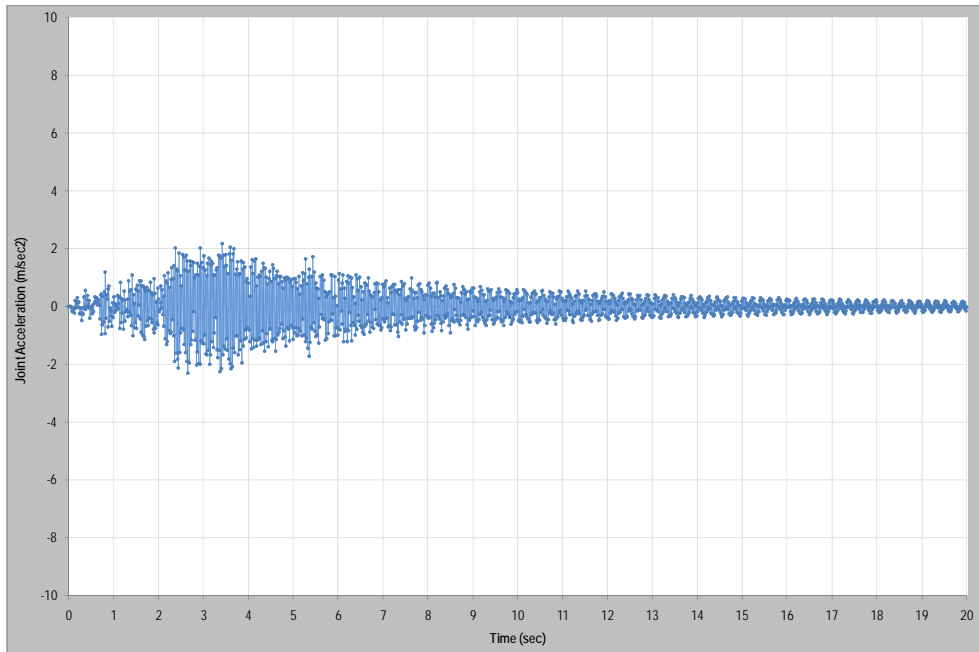


Figure A.14 Joint acceleration vs. time graphic of E5-5 analysis model with a speed of 75 m/sec

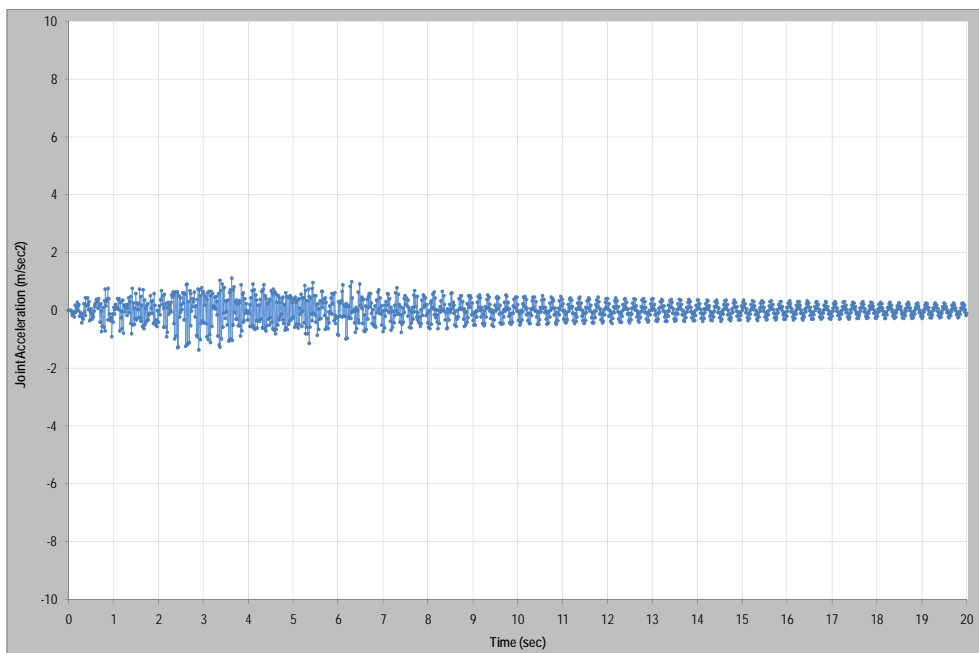


Figure A.15 Joint acceleration vs. time graphic of E5-10 analysis model with a speed of 75 m/sec

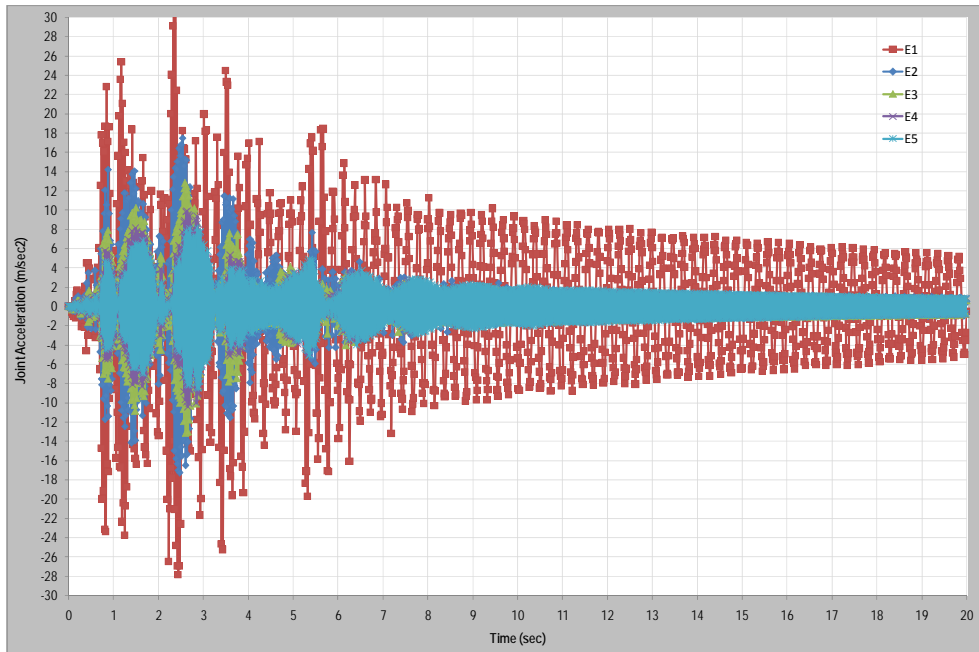


Figure A.16 Combined Joint acceleration vs. time graphic of analysis models without mass damping under a speed of 75 m/sec

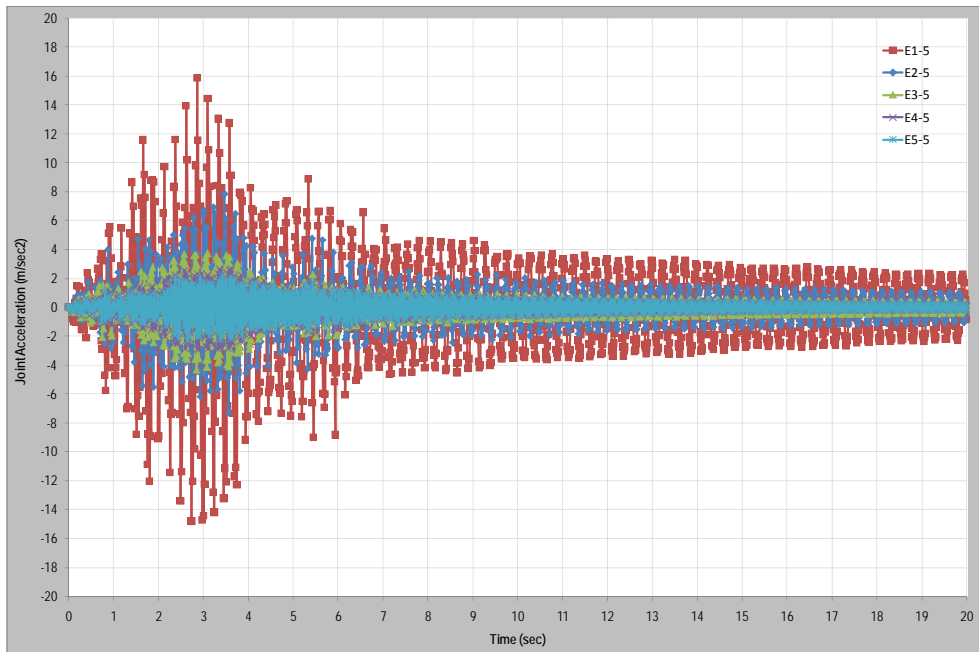


Figure A.17 Combined Joint acceleration vs. time graphic of analysis models with 5% mass damping under a speed of 75 m/sec

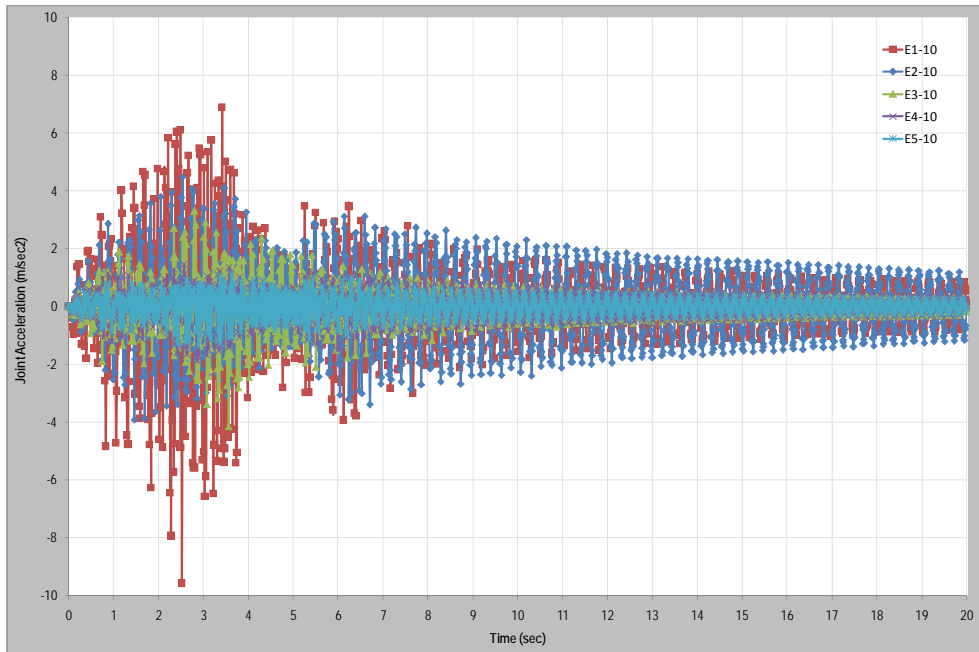


Figure A.18 Combined Joint acceleration vs. time graphic of analysis models with 10% mass damping under a speed of 75 m/sec

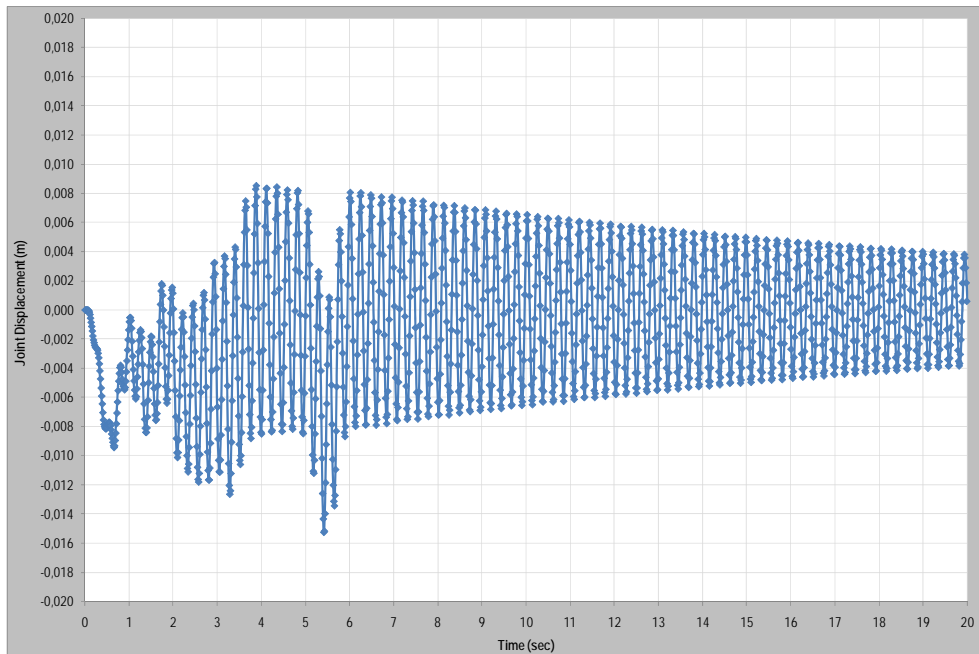


Figure A.19 Joint Displacement vs. time graphic of E1 analysis model with a speed of 75 m/sec

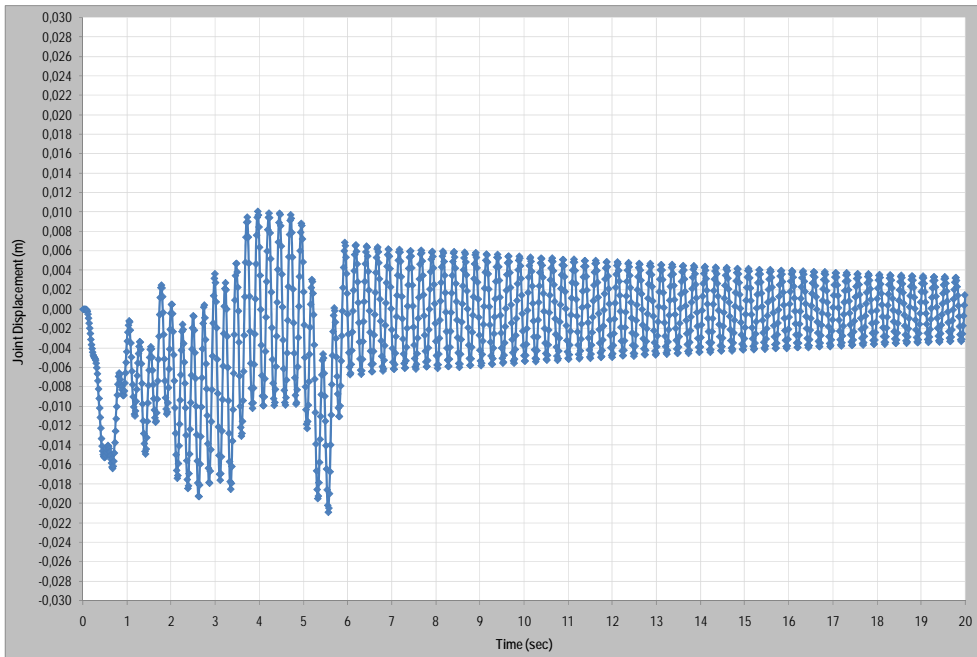


Figure A.20 Joint Displacement vs. time graphic of E1-5 analysis model with a speed of 75 m/sec

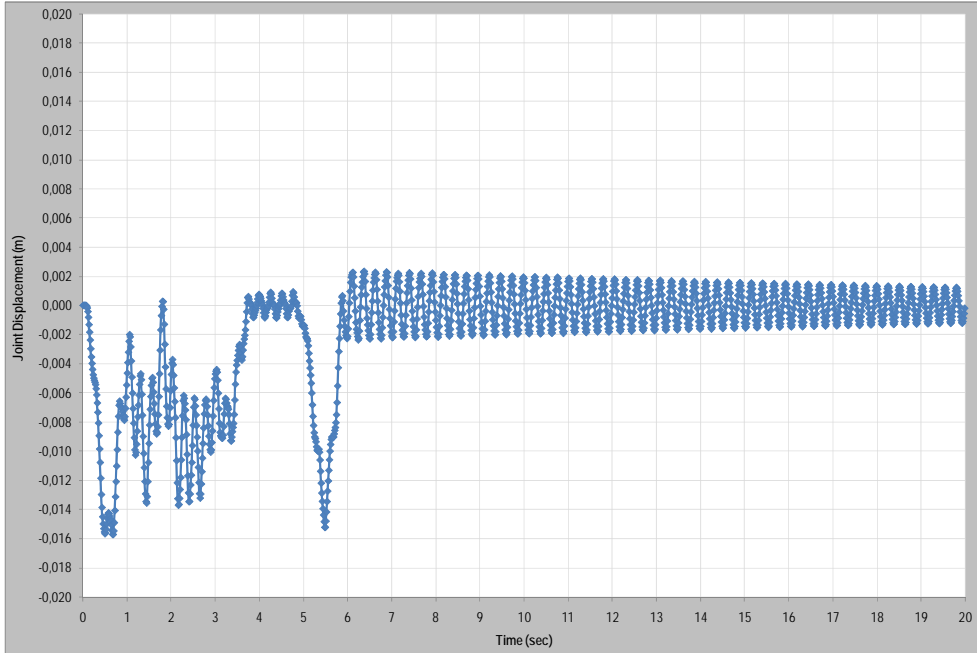


Figure A.21 Joint Displacement vs. time graphic of E1-10 analysis model with a speed of 75 m/sec

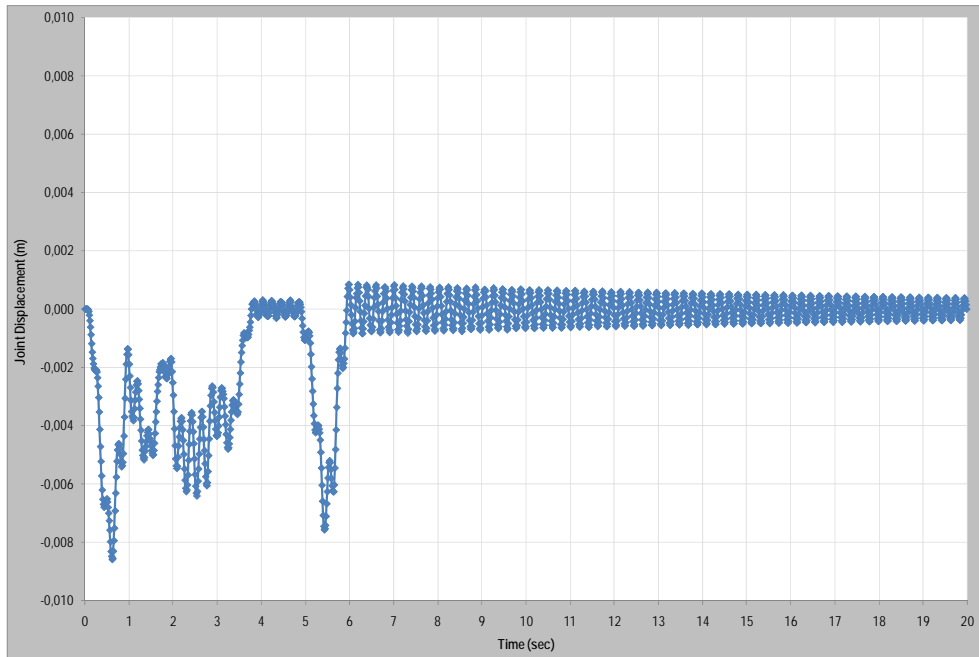


Figure A.22 Joint Displacement vs. time graphic of E2 analysis model with a speed of 75 m/sec

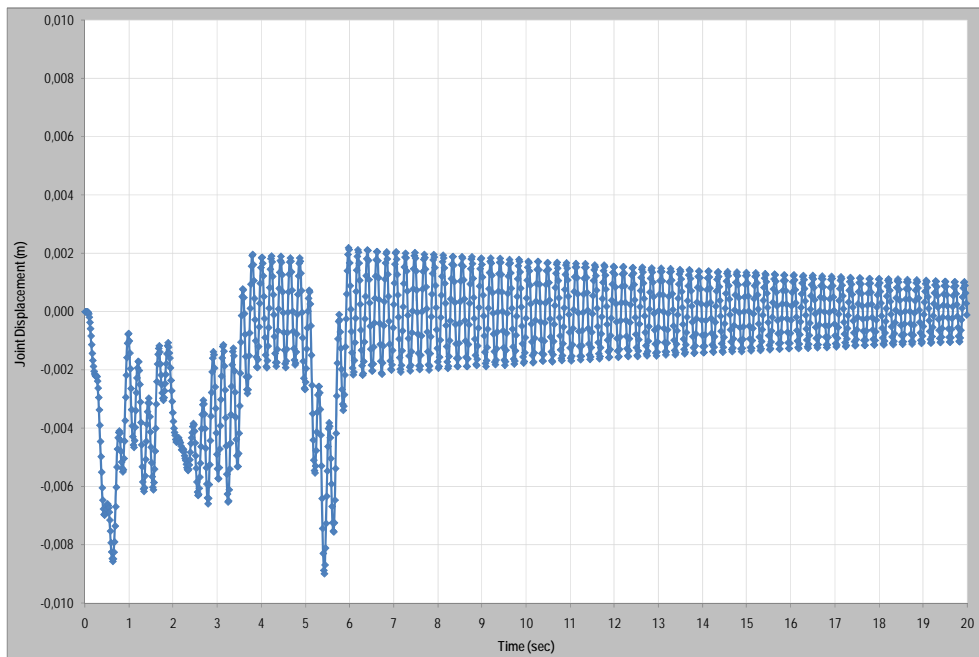


Figure A.23 Joint Displacement vs. time graphic of E2-5 analysis model with a speed of 75 m/sec

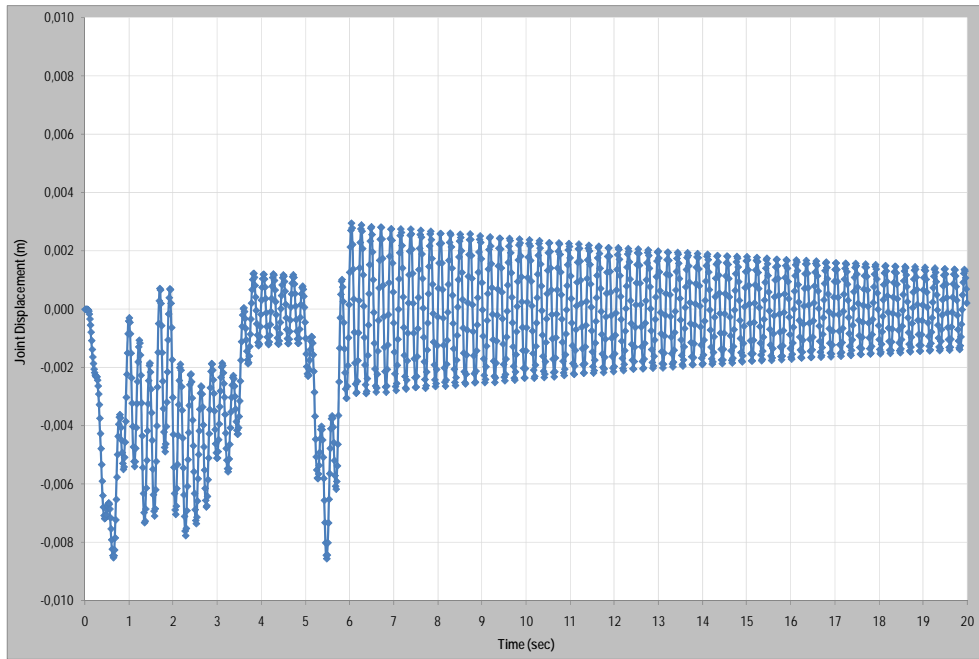


Figure A.24 Joint Displacement vs. time graphic of E2-10 analysis model with a speed of 75 m/sec

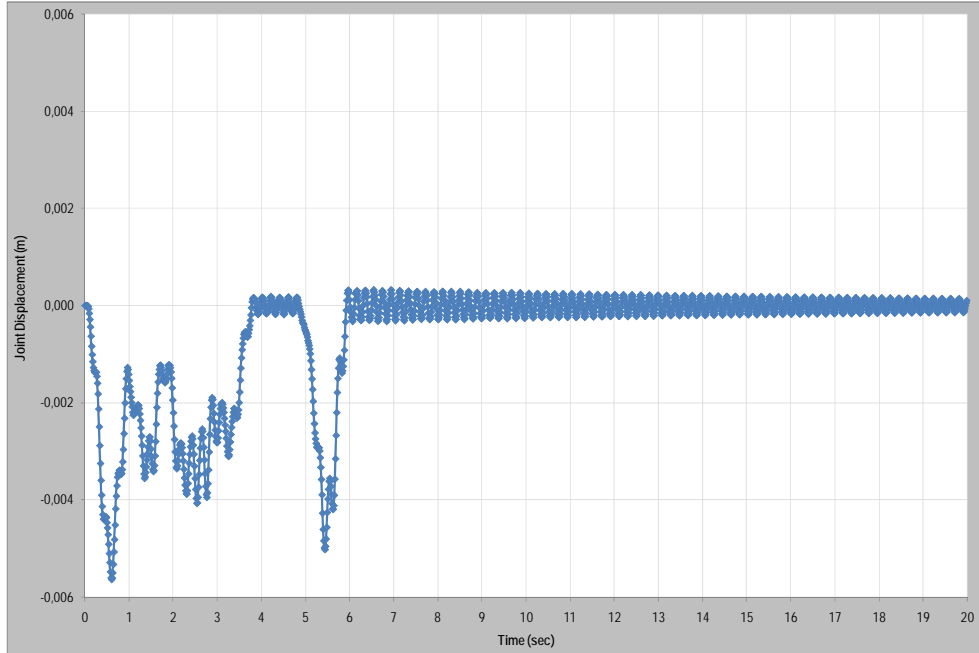


Figure A.25 Joint Displacement vs. time graphic of E3 analysis model with a speed of 75 m/sec

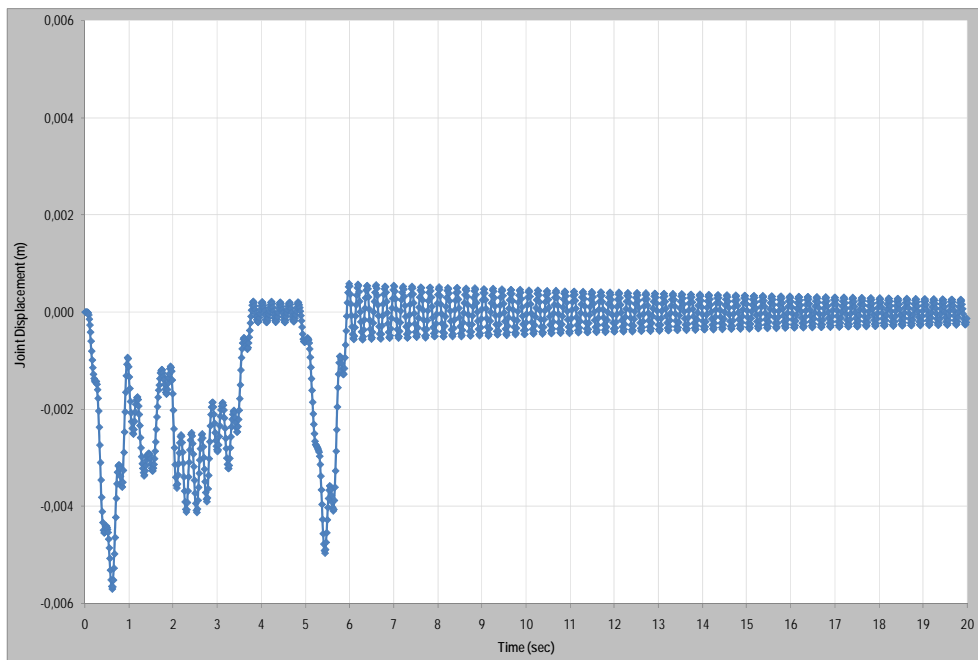


Figure A.26 Joint Displacement vs. time graphic of E3-5 analysis model with a speed of 75 m/sec

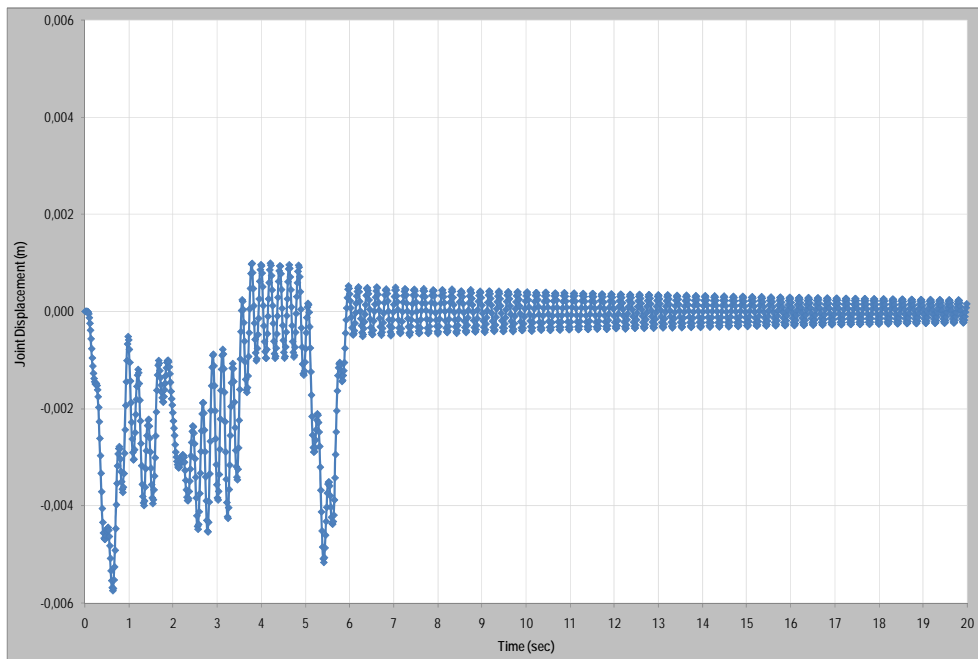


Figure A.27 Joint Displacement vs. time graphic of E3-10 analysis model with a speed of 75 m/sec

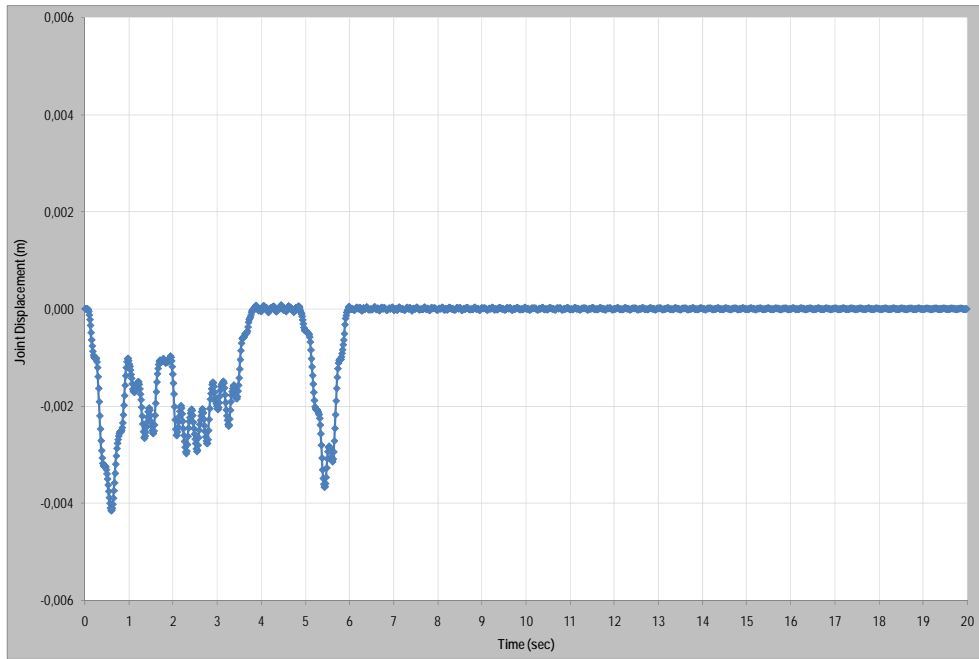


Figure A.28 Joint Displacement vs. time graphic of E4 analysis model with a speed of 75 m/sec

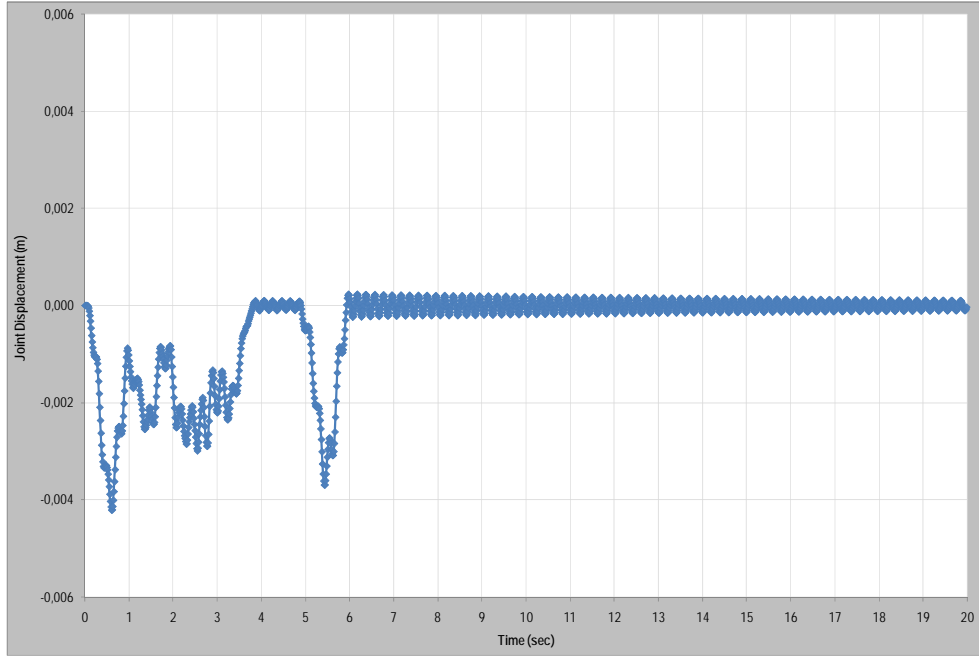


Figure A.29 Joint Displacement vs. time graphic of E4-5 analysis model with a speed of 75 m/sec

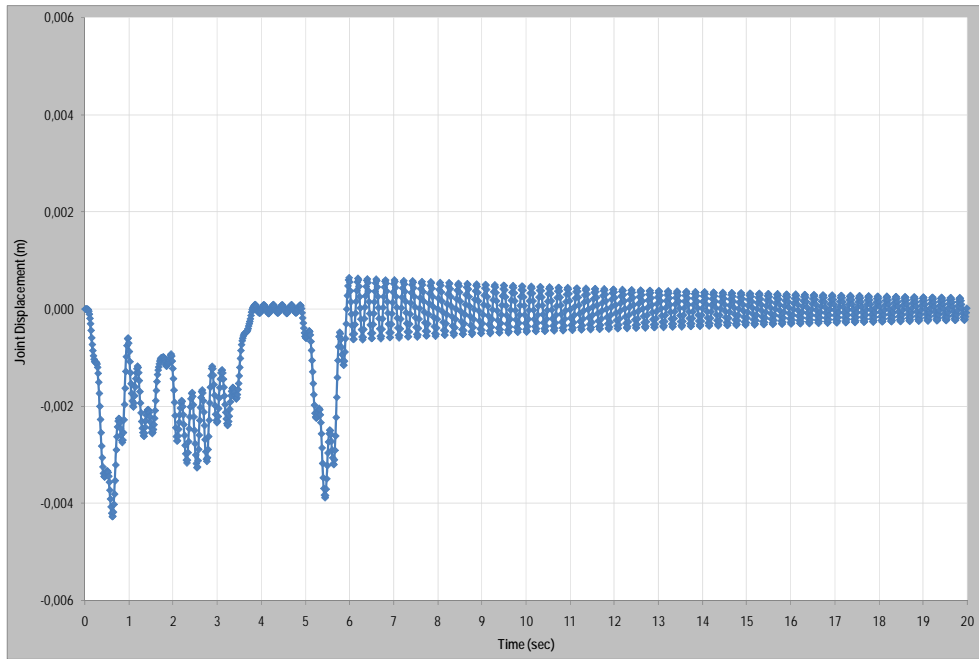


Figure A.30 Joint Displacement vs. time graphic of E4-10 analysis model with a speed of 75 m/sec

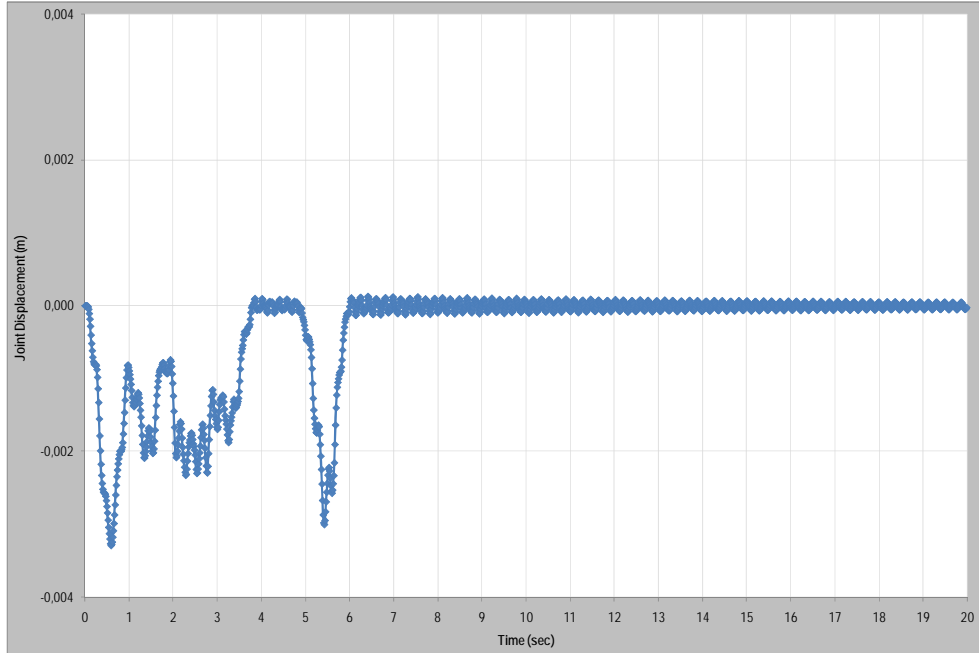


Figure A.31 Joint Displacement vs. time graphic of E5 analysis model with a speed of 75 m/sec

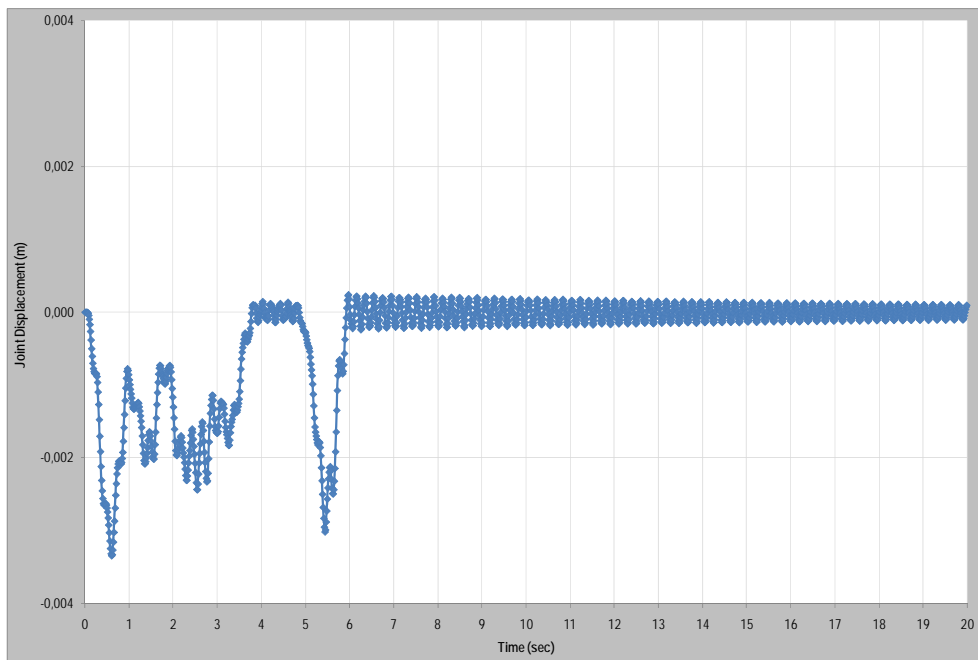


Figure A.32 Joint Displacement vs. time graphic of E5-5 analysis model with a speed of 75 m/sec

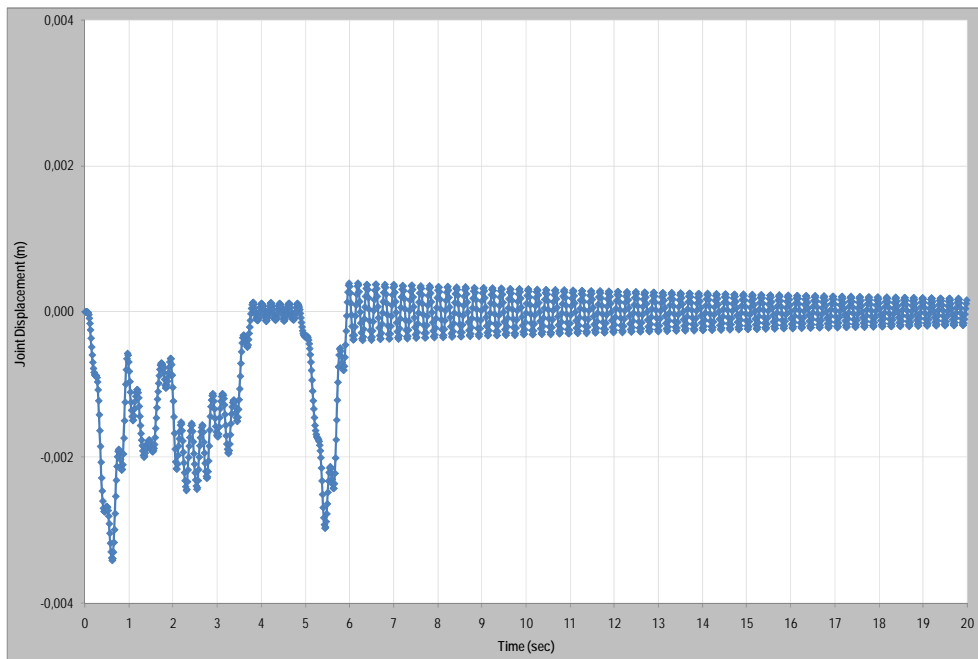


Figure A.33 Joint Displacement vs. time graphic of E5-10 analysis model with a speed of 75 m/sec

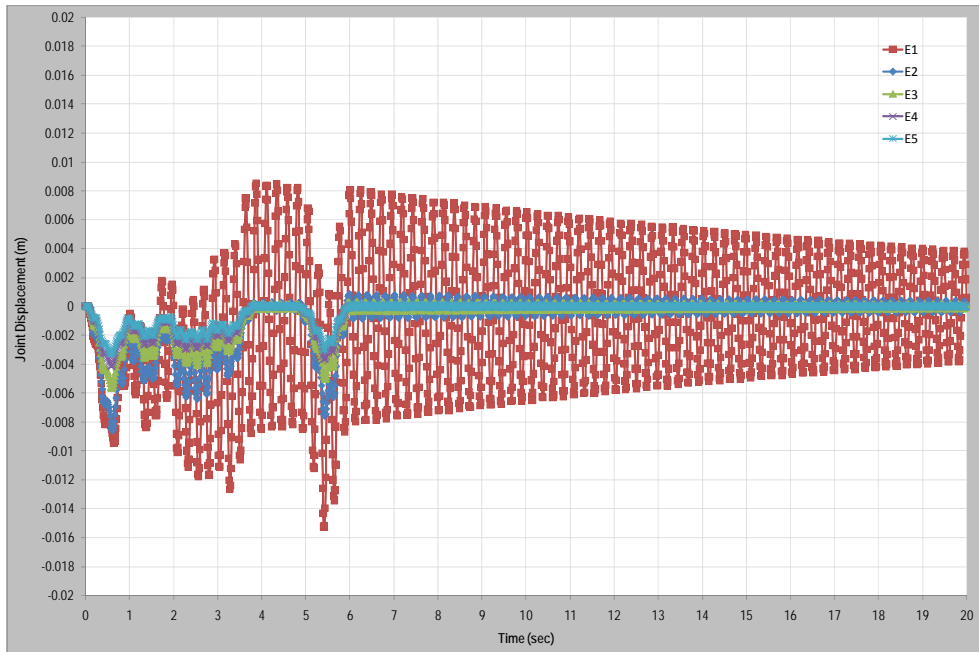


Figure A.34 Combined Joint displacement vs. time graphic of analysis models without mass damper under a speed of 75 m/sec

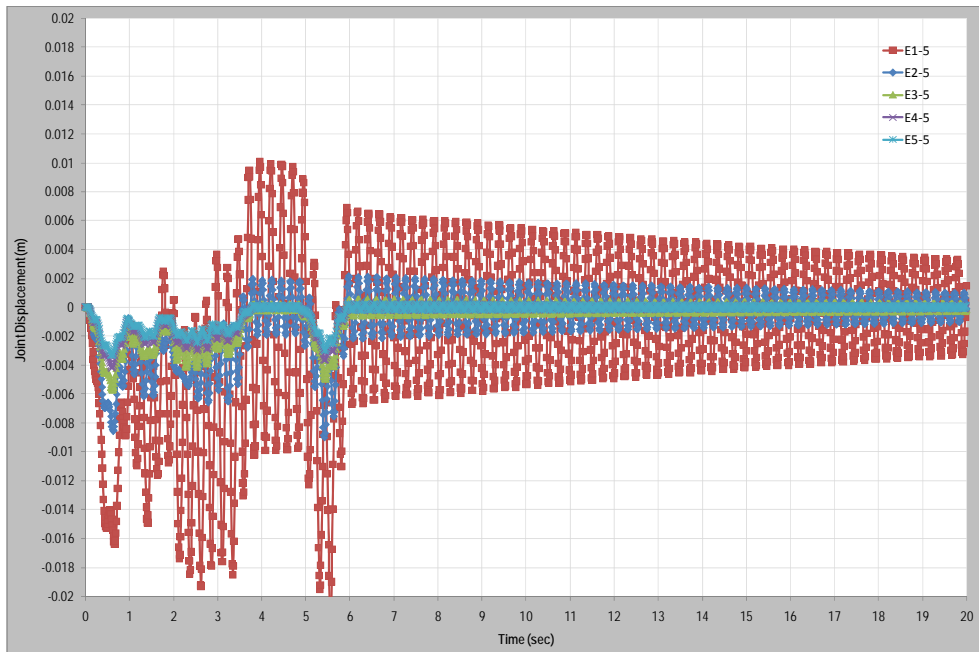


Figure A.35 Combined Joint displacement vs. time graphic of analysis models with 5% mass damper under a speed of 75 m/sec

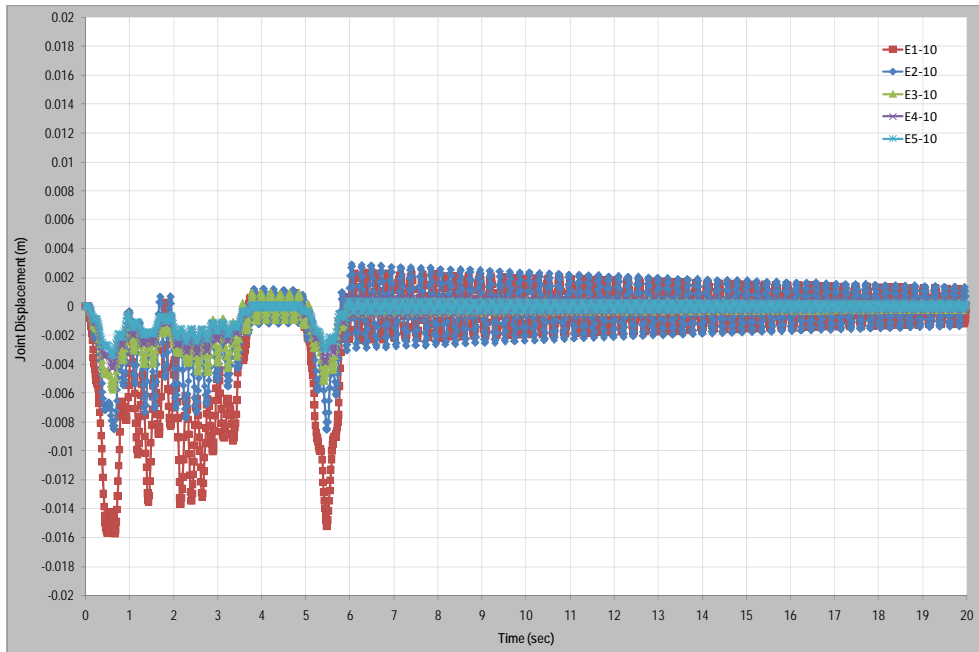


Figure A.36 Combined Joint displacement vs. time graphic of analysis models with 10% mass damper under a speed of 75 m/sec

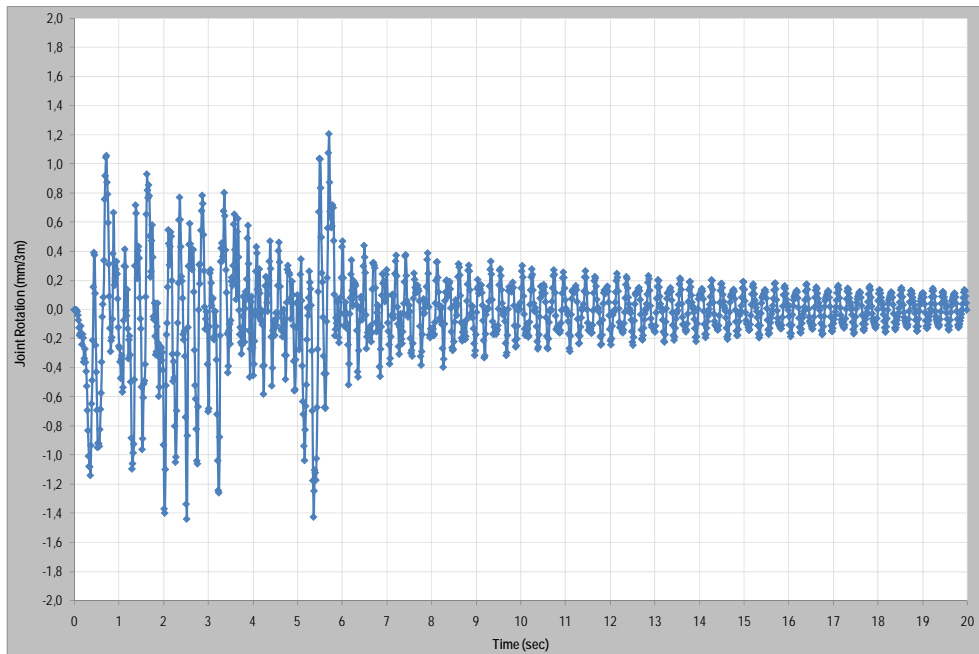


Figure A.37 Joint rotation vs. time graphic of E1 analysis model with a speed of 75 m/sec

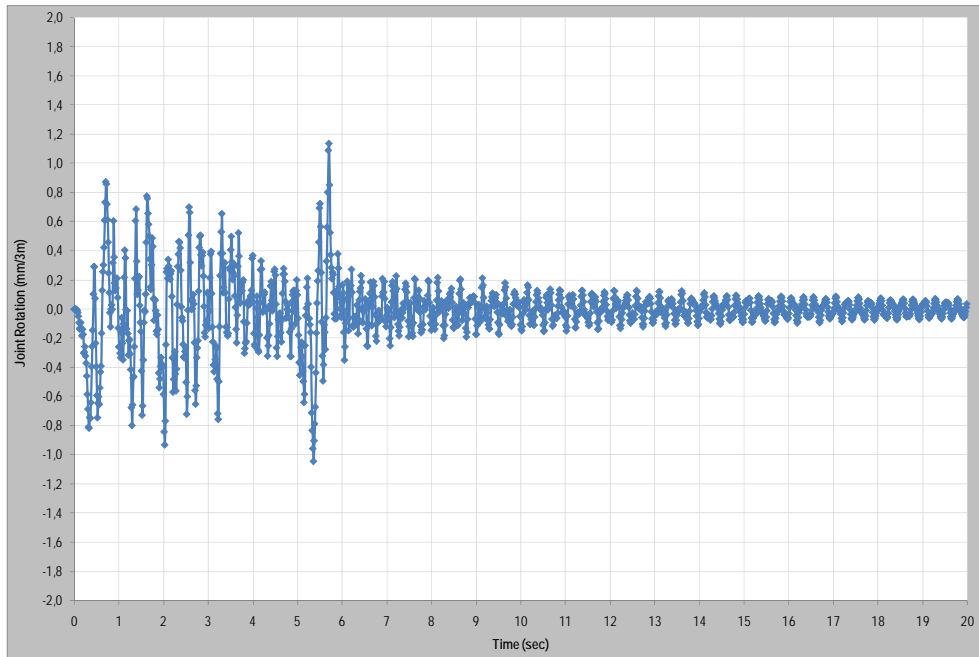


Figure A.38 Joint rotation vs. time graphic of E1-5 analysis model with a speed of 75 m/sec

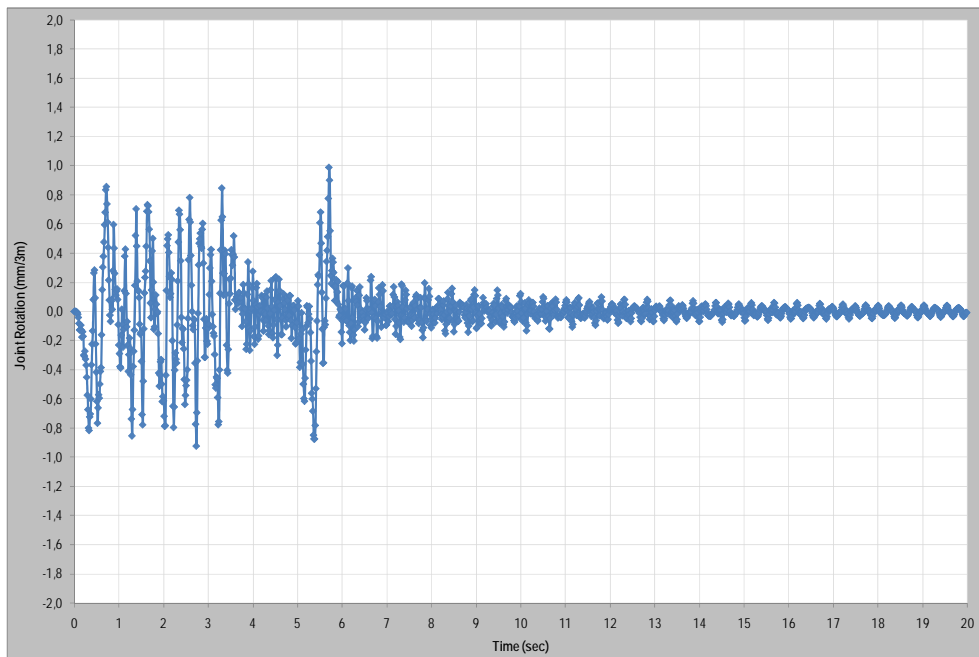


Figure A.39 Joint rotation vs. time graphic of E1-10 analysis model with a speed of 75 m/sec

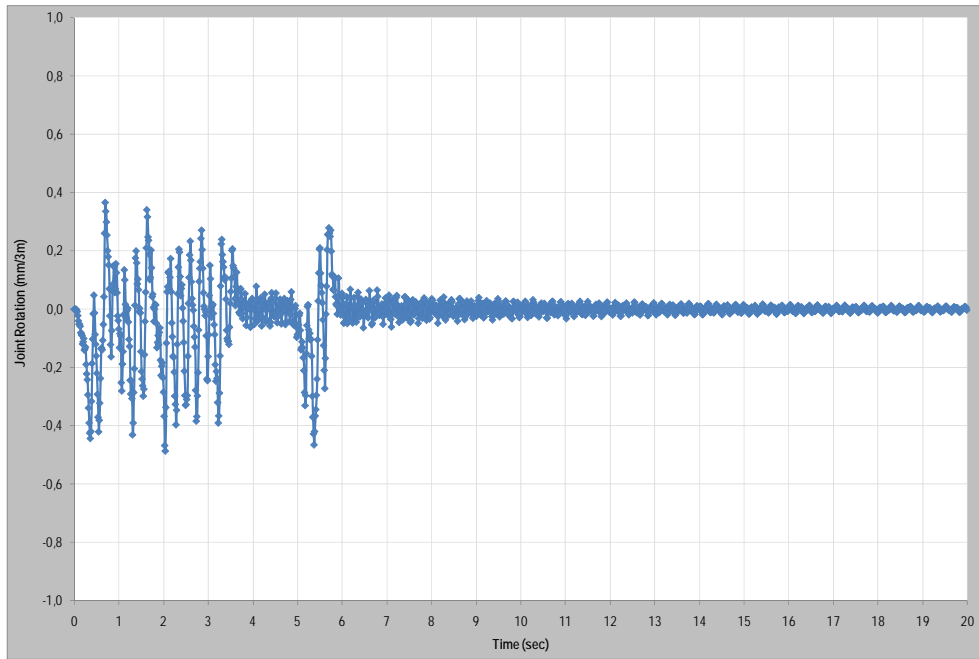


Figure A.40 Joint rotation vs. time graphic of E2 analysis model with a speed of 75 m/sec

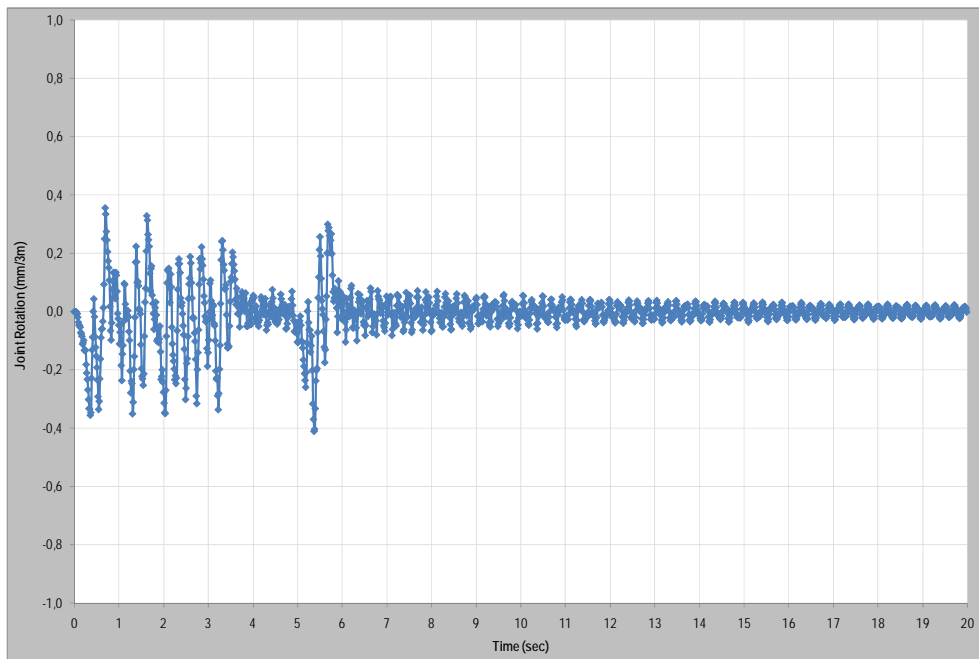


Figure A.41 Joint rotation vs. time graphic of E2-5 analysis model with a speed of 75 m/sec

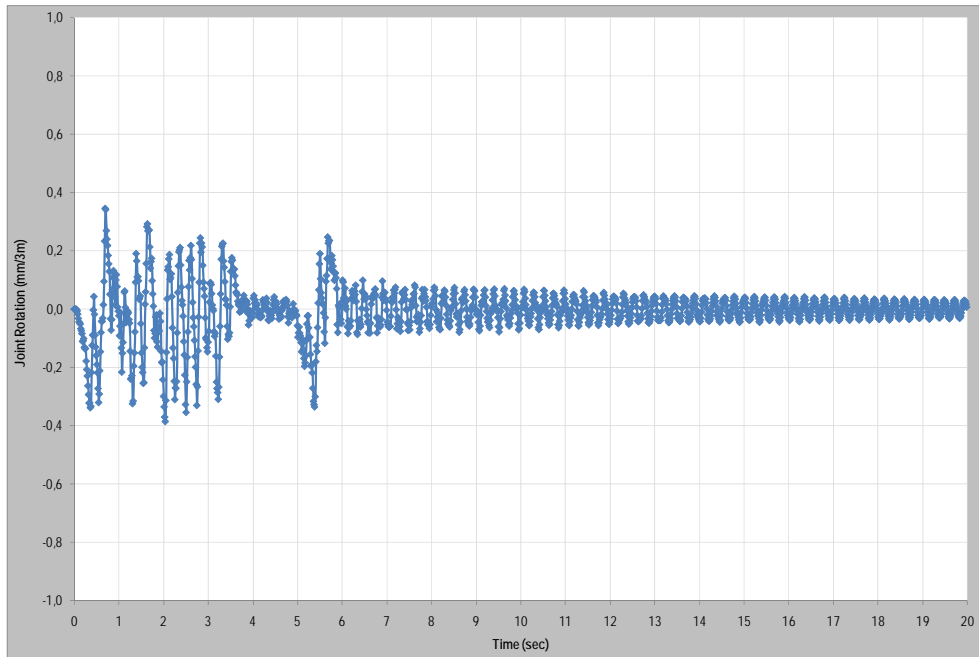


Figure A.42 Joint rotation vs. time graphic of E2-10 analysis model with a speed of 75 m/sec

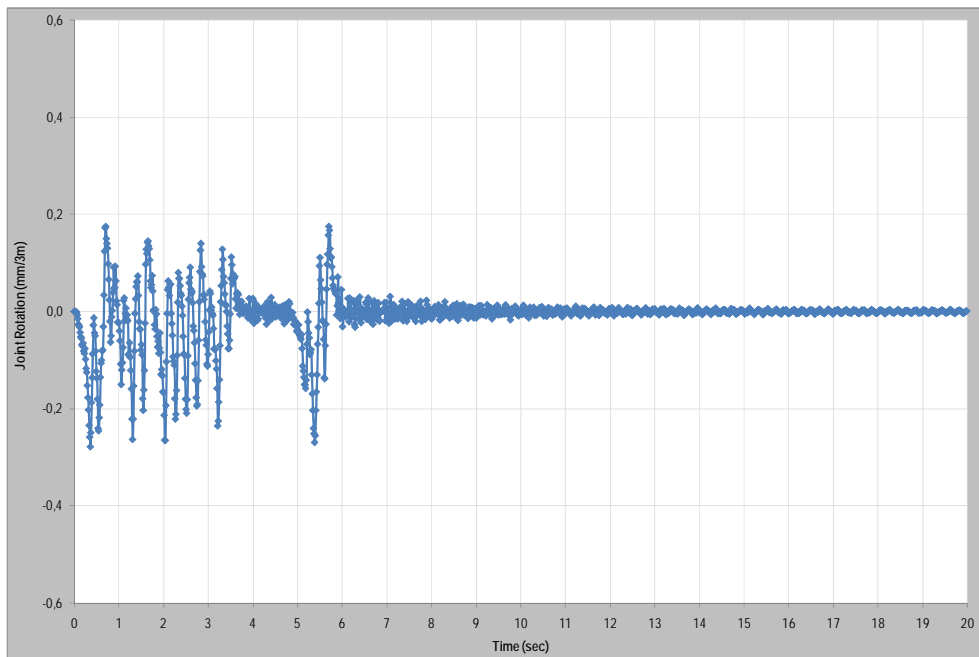


Figure A.43 Joint rotation vs. time graphic of E3 analysis model with a speed of 75 m/sec

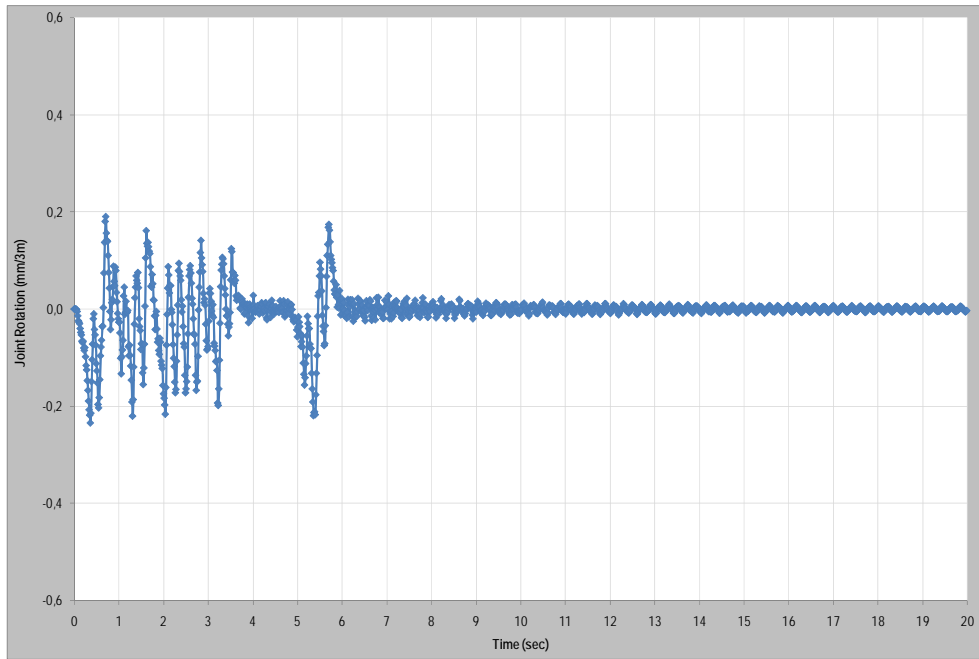


Figure A.44 Joint rotation vs. time graphic of E3-5 analysis model with a speed of 75 m/sec

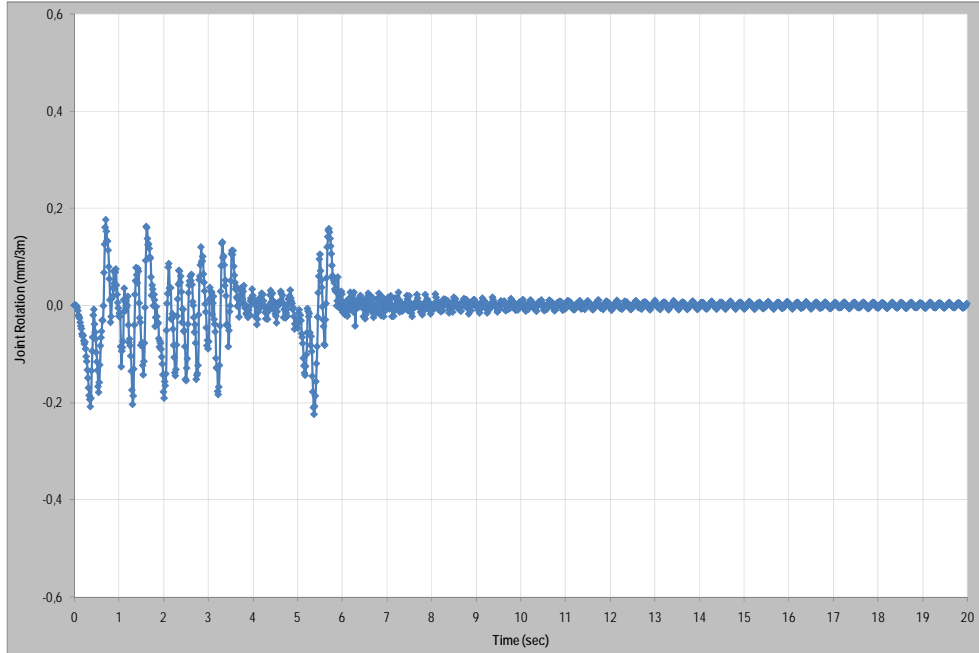


Figure A.45 Joint rotation vs. time graphic of E3-10 analysis model with a speed of 75 m/sec

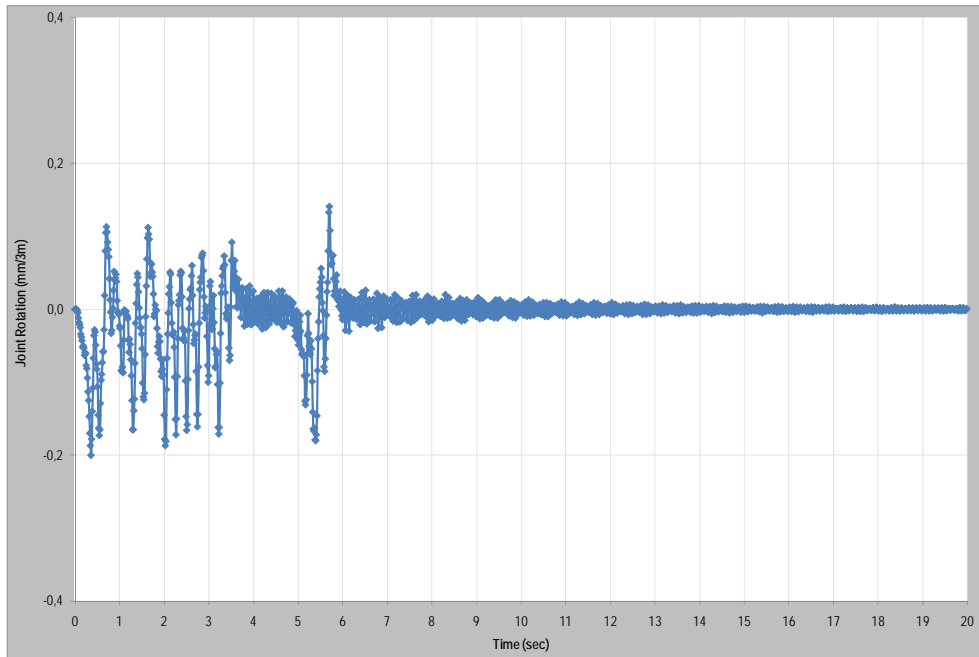


Figure A.46 Joint rotation vs. time graphic of E4 analysis model with a speed of 75 m/sec

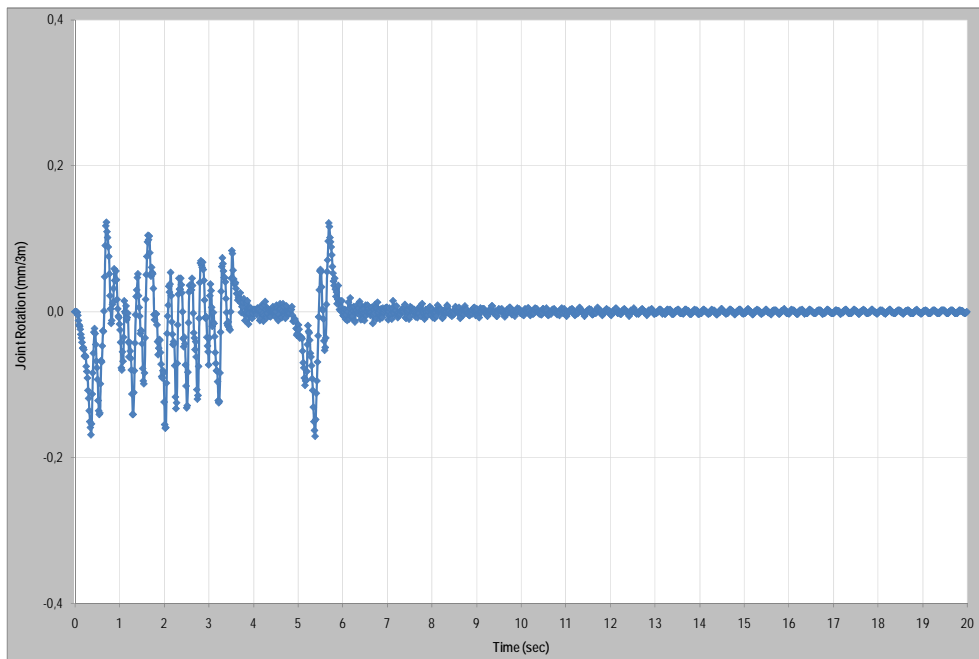


Figure A.47 Joint rotation vs. time graphic of E4-5 analysis model with a speed of 75 m/sec

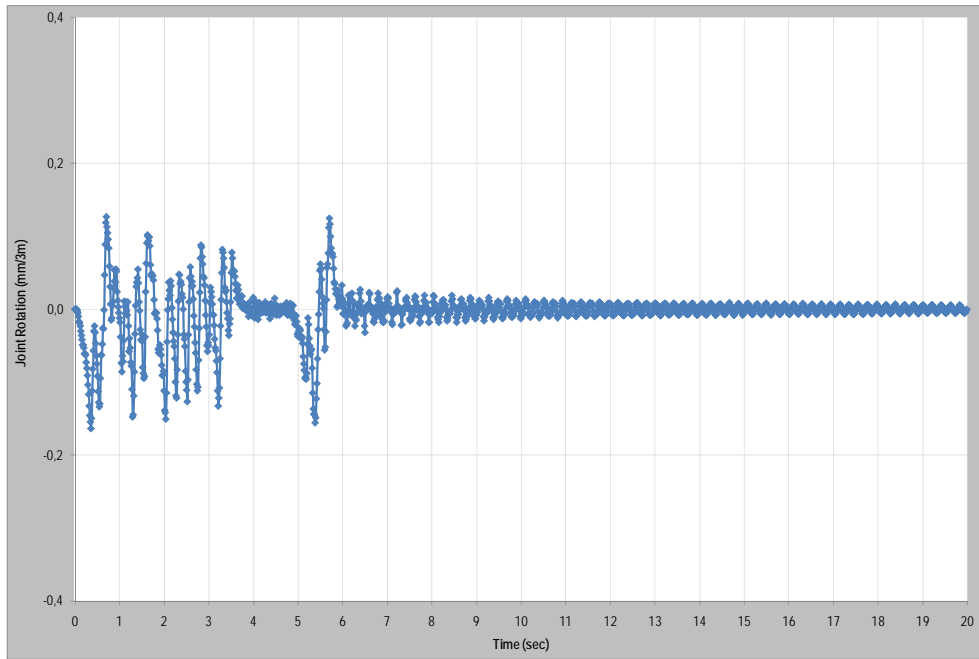


Figure A.48 Joint rotation vs. time graphic of E4-10 analysis model with a speed of 75 m/sec

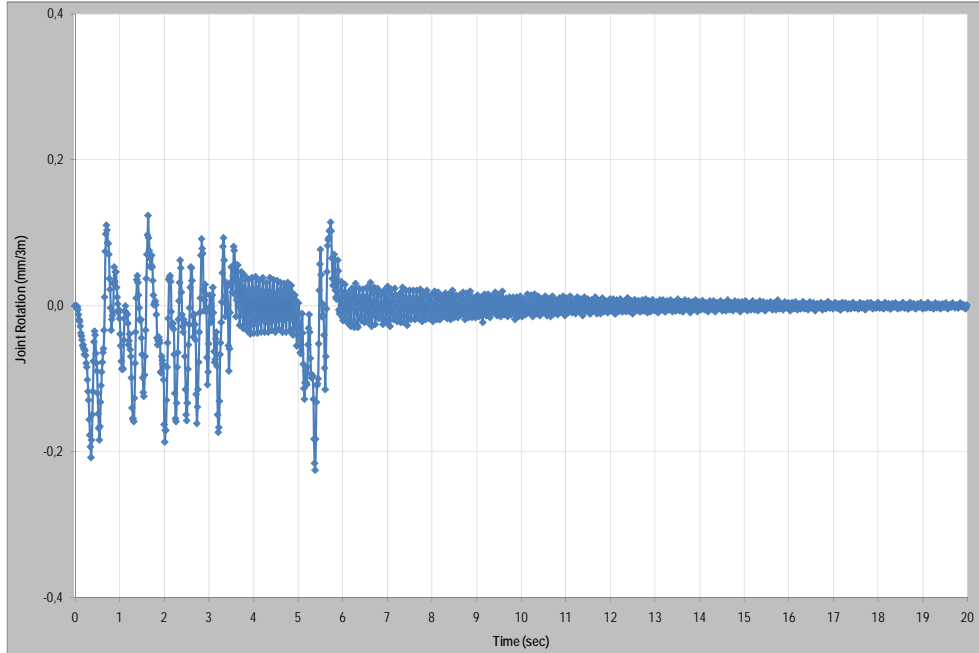


Figure A.49 Joint rotation vs. time graphic of E5 analysis model with a speed of 75 m/sec

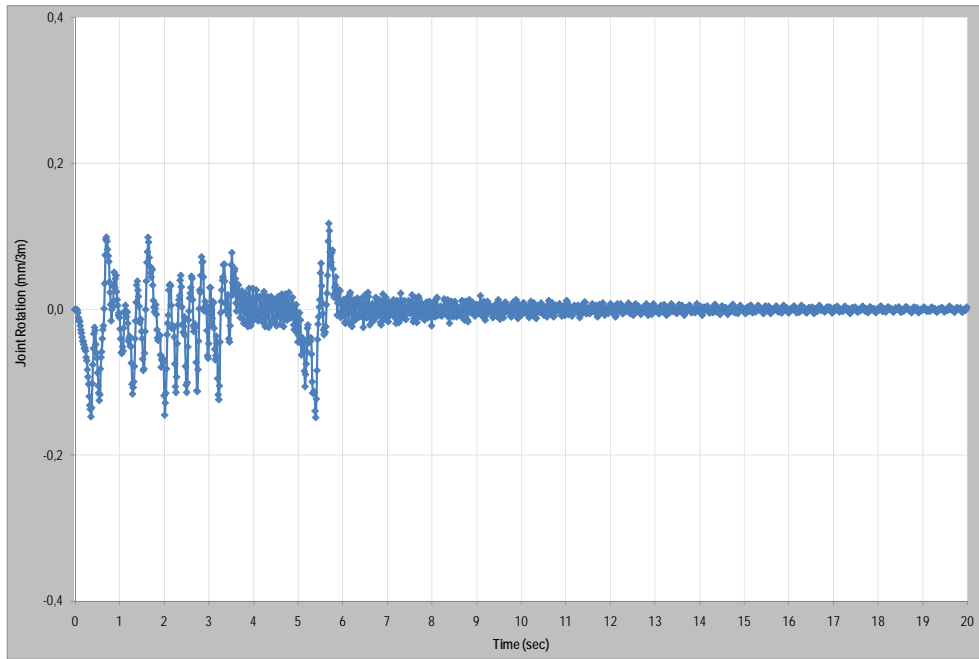


Figure A.50 Joint rotation vs. time graphic of E5-5 analysis model with a speed of 75 m/sec

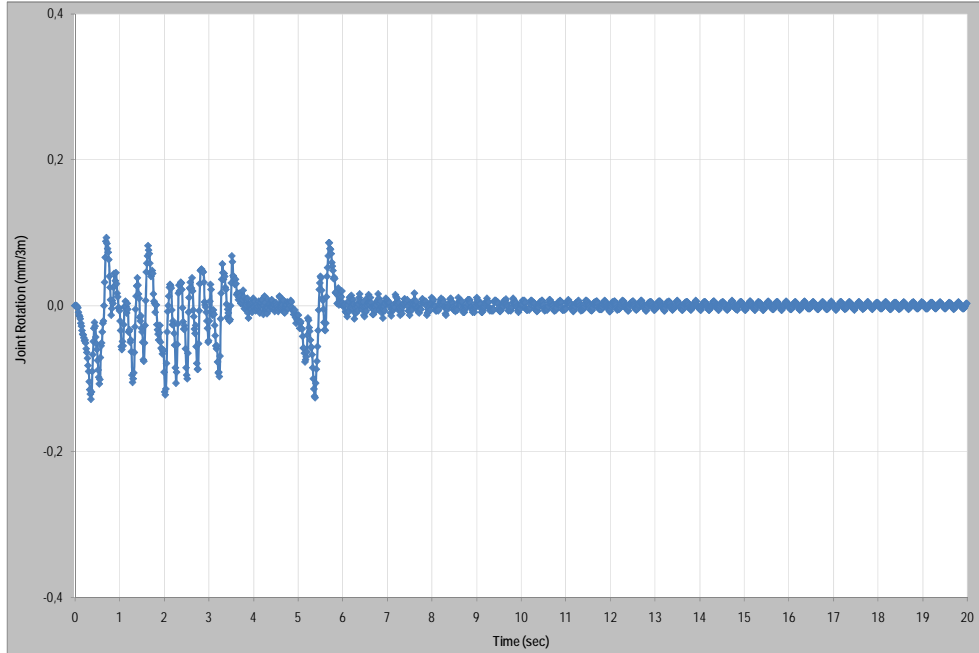


Figure A.51 Joint rotation vs. time graphic of E5-10 analysis model with a speed of 75 m/sec

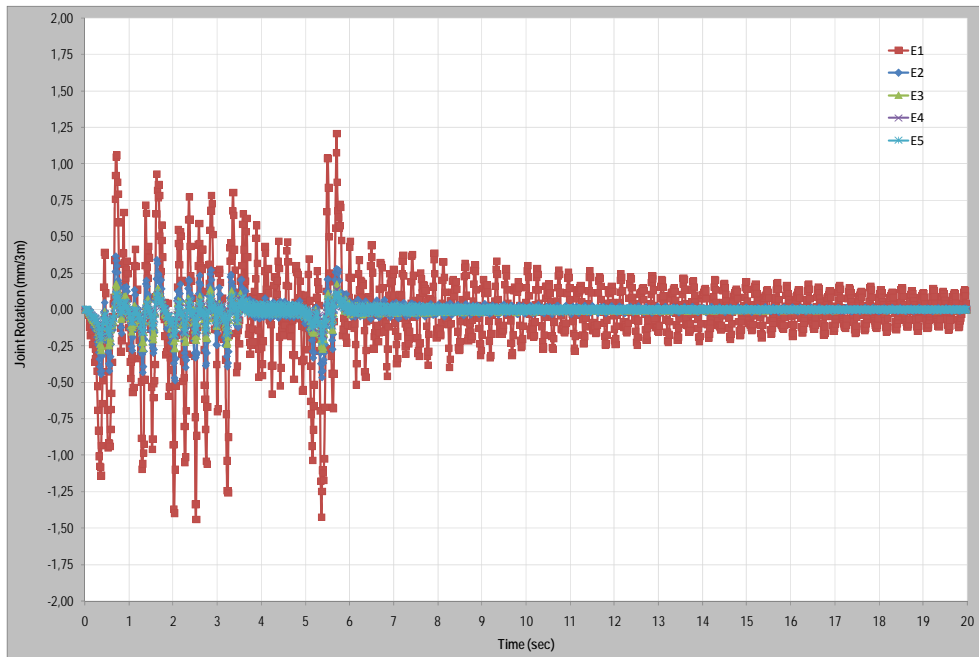


Figure A.52 Combined Joint rotation vs. time graphic of analysis models without mass damper under a speed of 75 m/sec

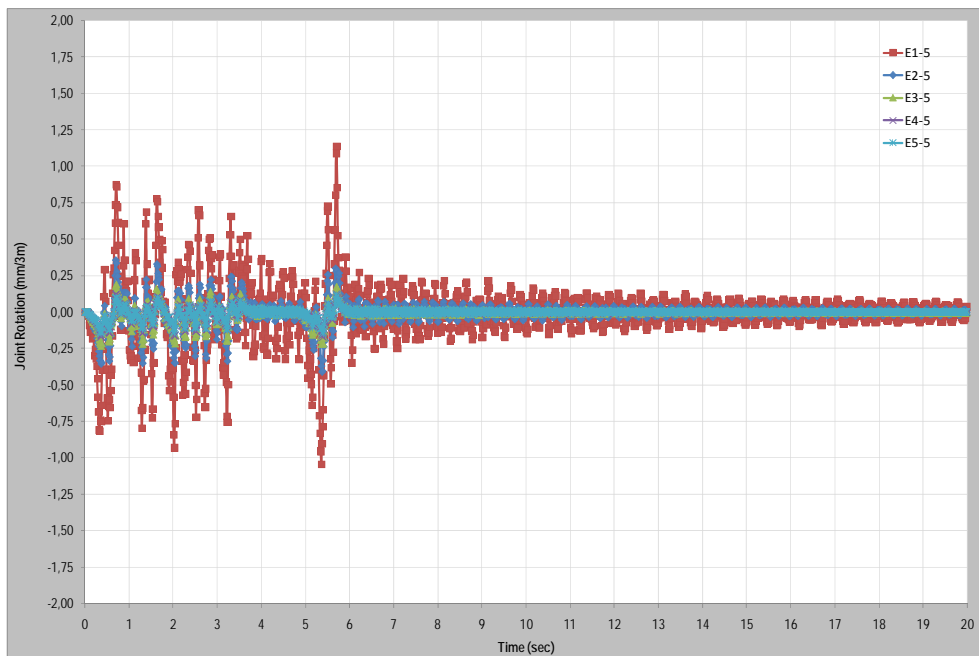


Figure A.53 Combined Joint rotation vs. time graphic of analysis models with 5% mass damper under a speed of 75 m/sec

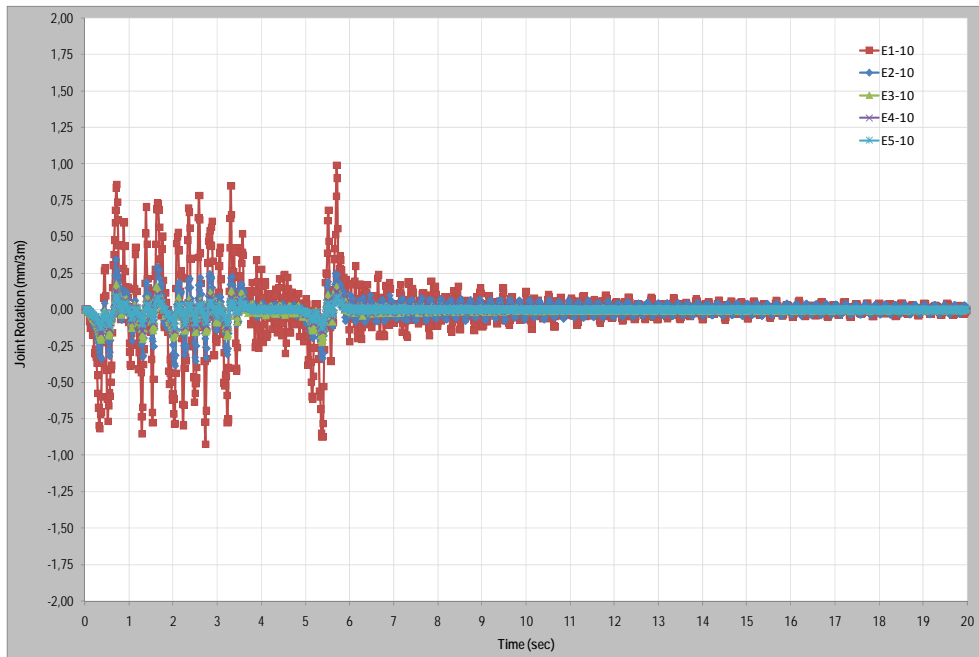


Figure A.54 Combined Joint rotation vs. time graphic of analysis models with 10% under a speed of 75 m/sec

A.2. Moving Suspension Mass Model Analysis Graphs

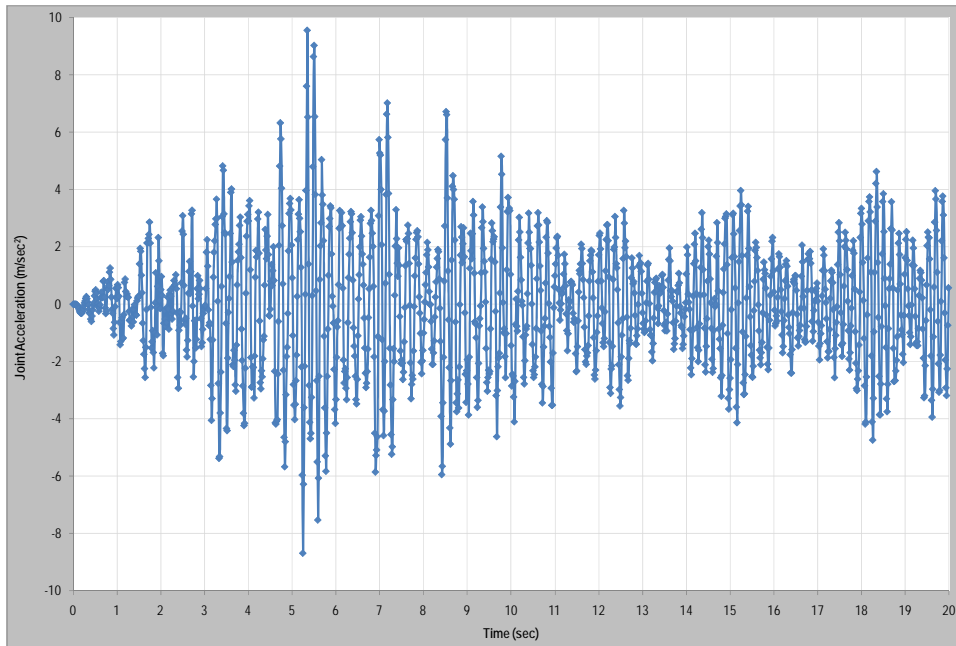


Figure A.55 Joint acceleration vs. time graphic of E1 analysis model with a speed of 70 m/sec

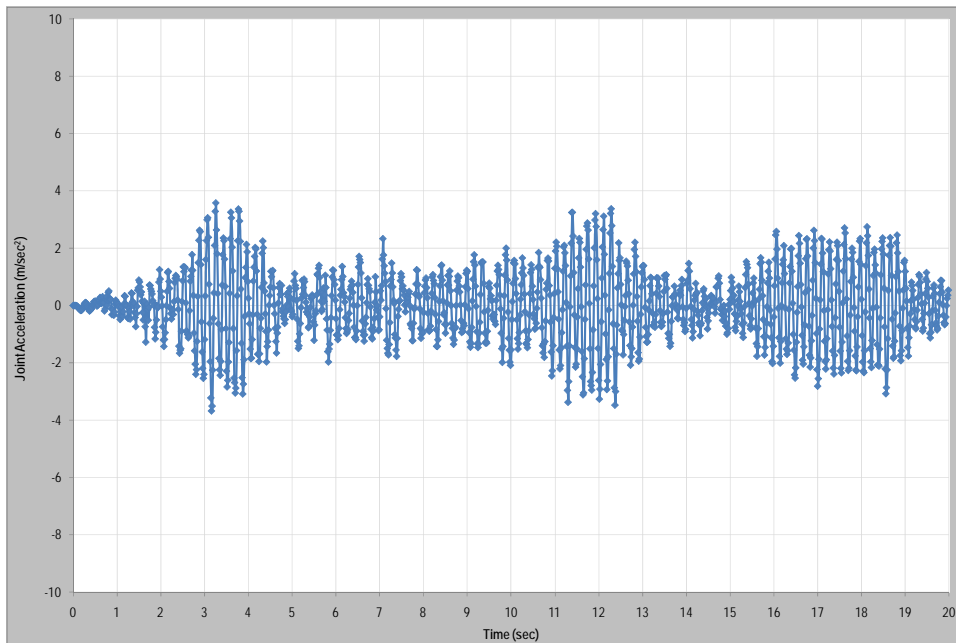


Figure A.56 Joint acceleration vs. time graphic of E2 analysis model with a speed of 70 m/sec

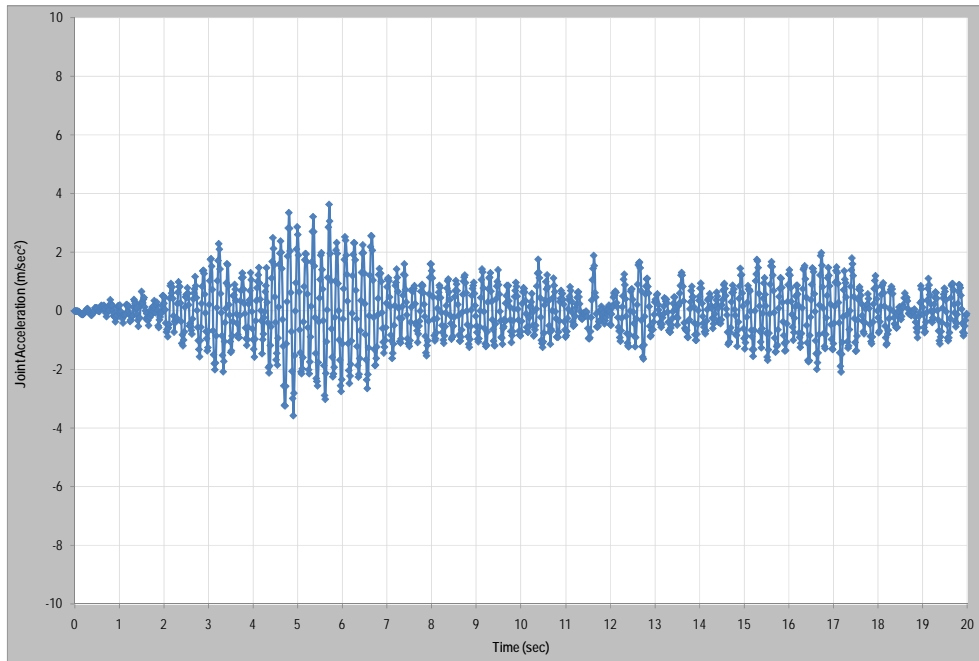


Figure A.57 Joint acceleration vs. time graphic of E3 analysis model with a speed of 70 m/sec

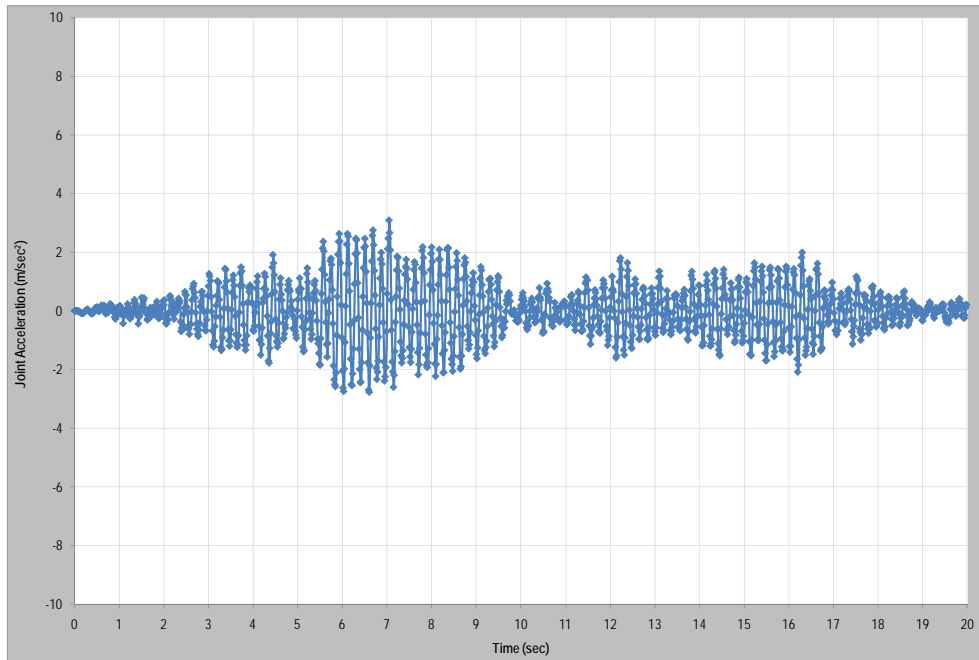


Figure A.58 Joint acceleration vs. time graphic of E4 analysis model with a speed of 70 m/sec

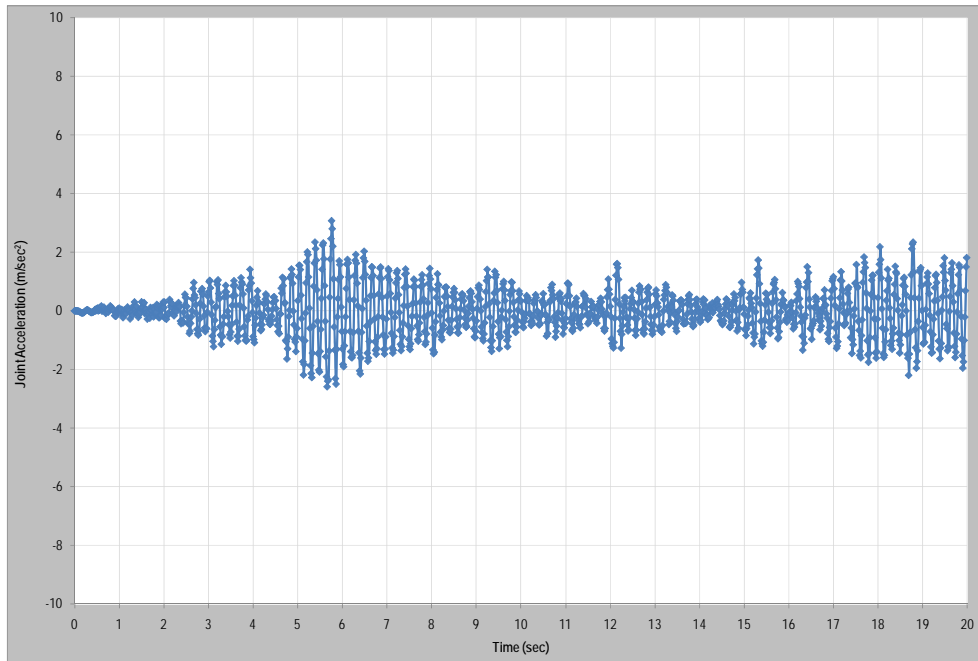


Figure A.59 Joint acceleration vs. time graphic of E5 analysis model with a speed of 70 m/sec

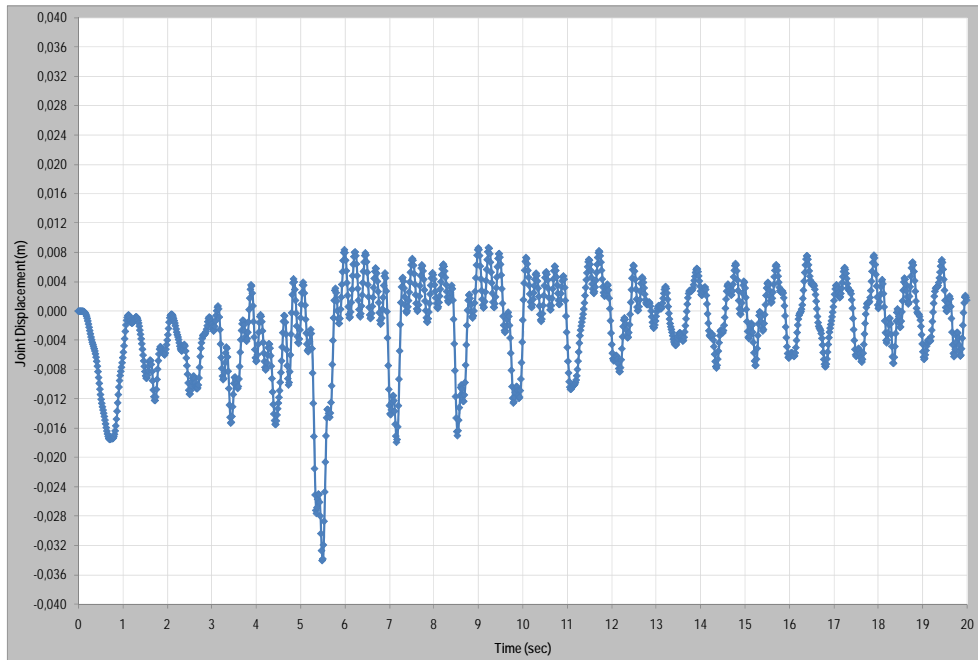


Figure A.60 Joint displacement vs. time graphic of E1 analysis model with a speed of 70 m/sec

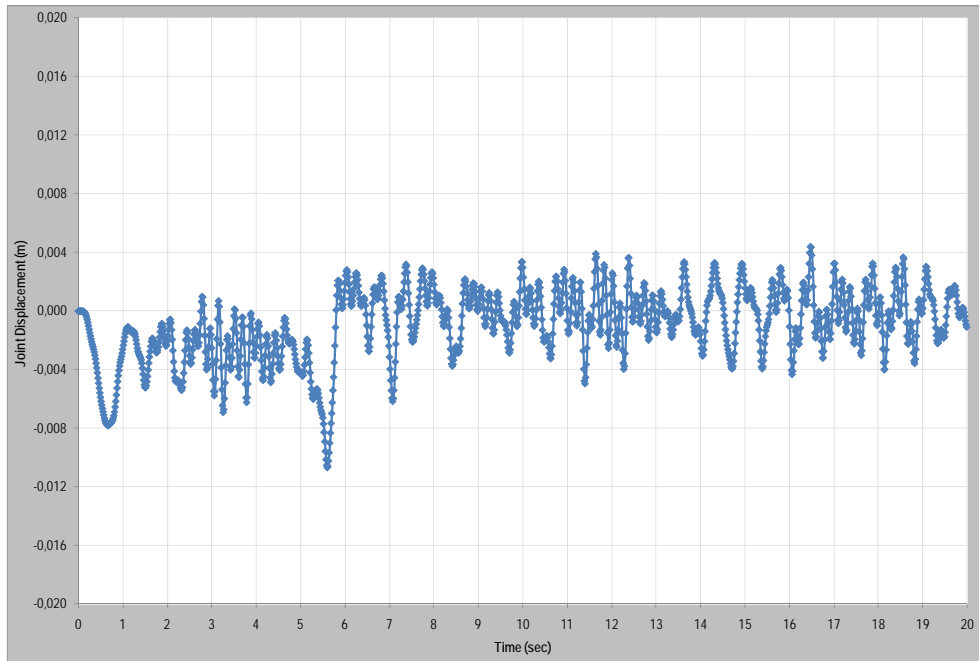


Figure A.61 Joint displacement vs. time graphic of E2 analysis model with a speed of 70 m/sec

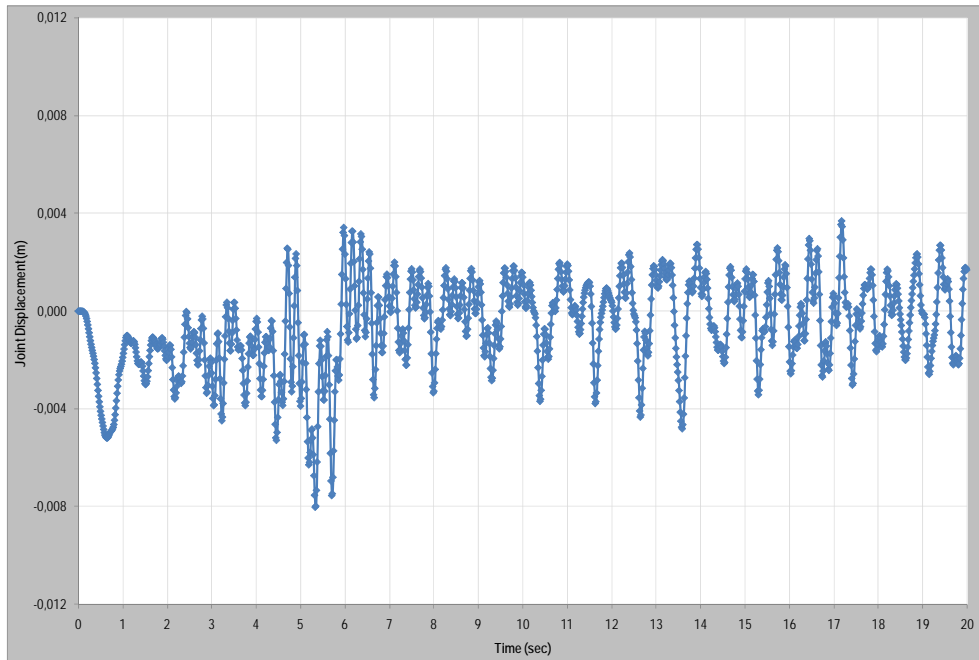


Figure A.62 Joint displacement vs. time graphic of E3 analysis model with a speed of 70 m/sec

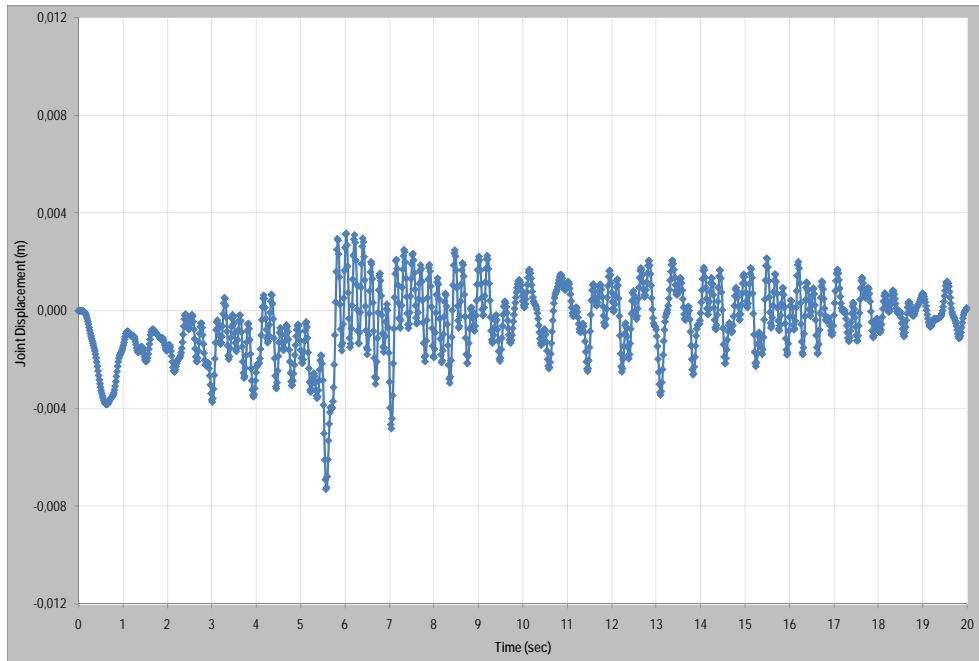


Figure A.63 Joint displacement vs. time graphic of E4 analysis model with a speed of 70 m/sec

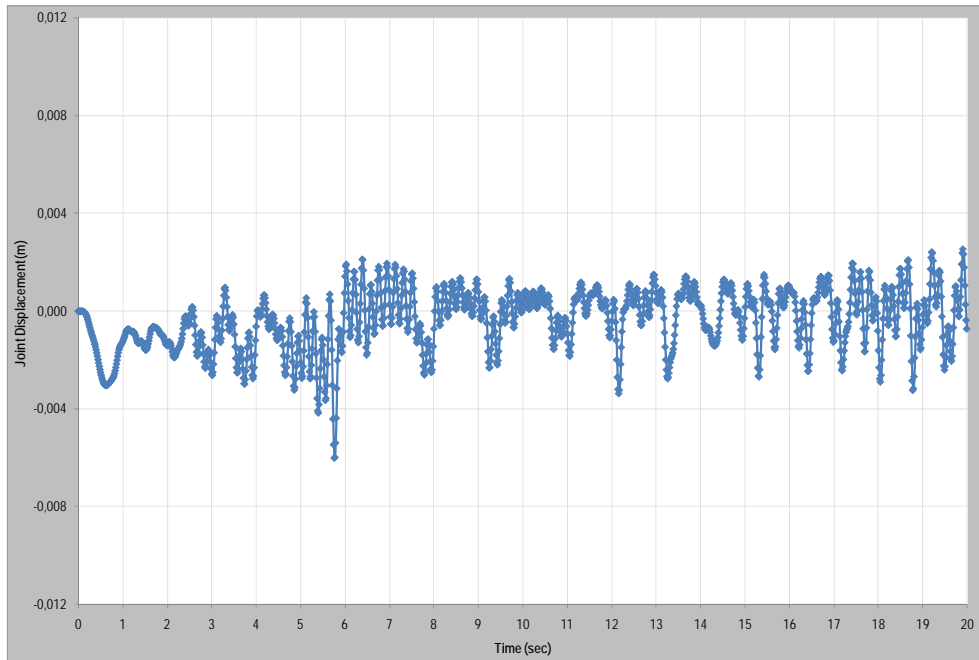


Figure A.64 Joint displacement vs. time graphic of E5 analysis model with a speed of 70 m/sec

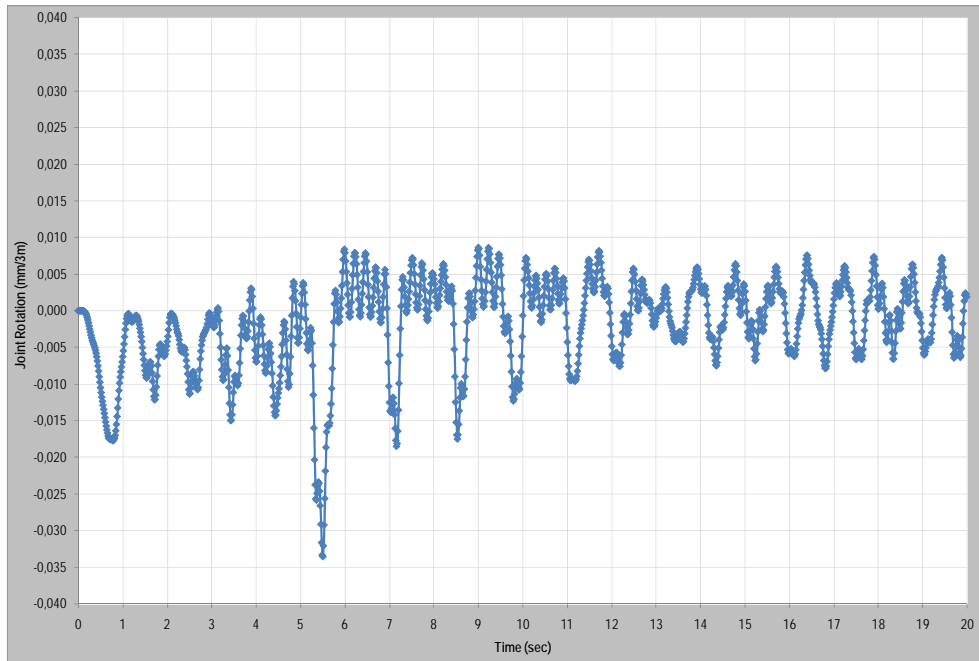


Figure A.65 Joint rotation vs. time graphic of E1 analysis model with a speed of 70 m/sec

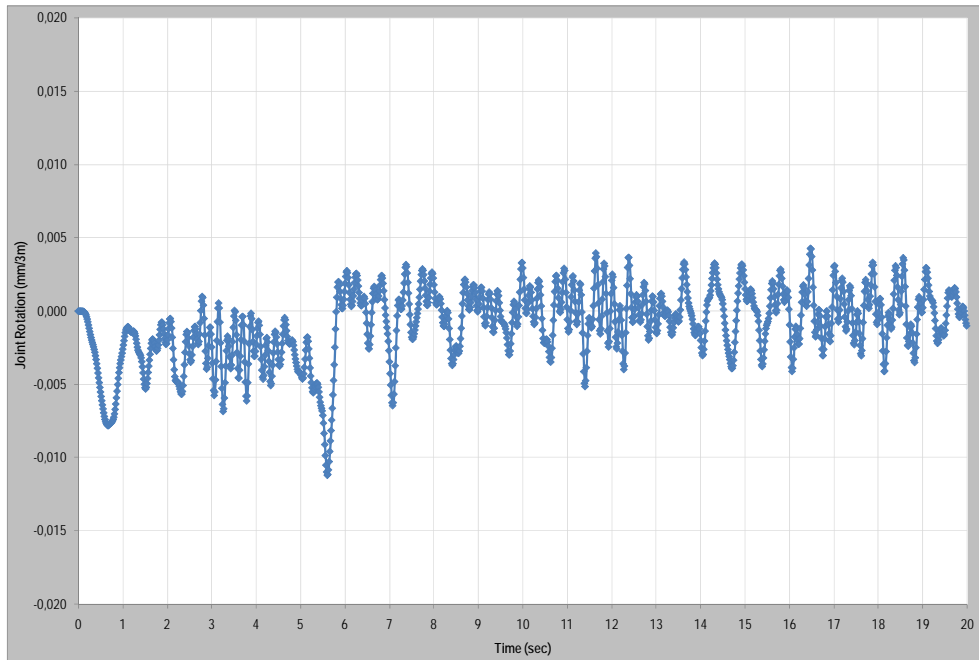


Figure A.66 Joint rotation vs. time graphic of E2 analysis model with a speed of 70 m/sec

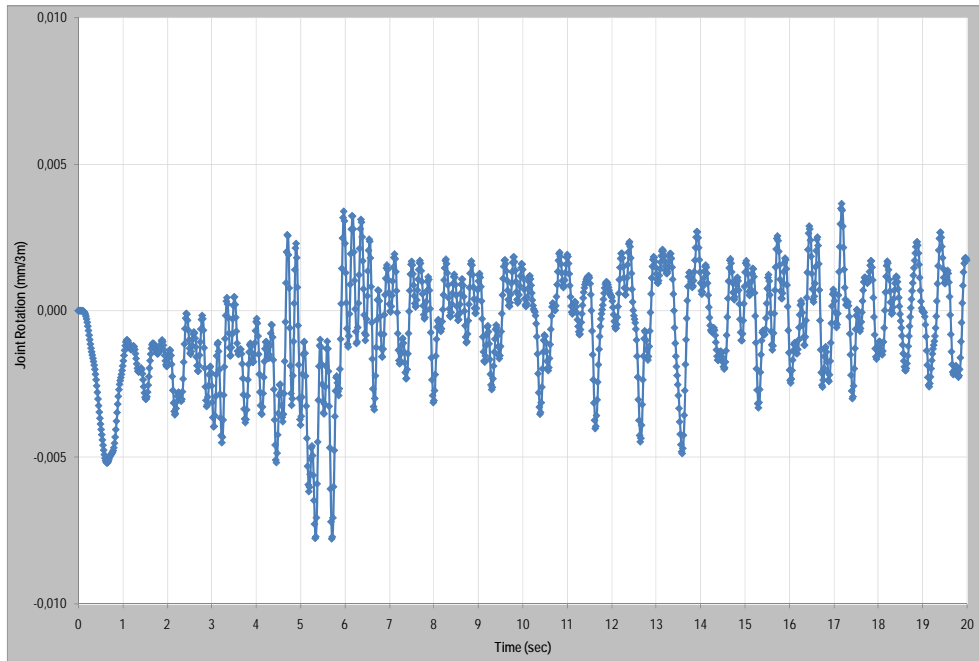


Figure A.67 Joint rotation vs. time graphic of E3 analysis model with a speed of 70 m/sec

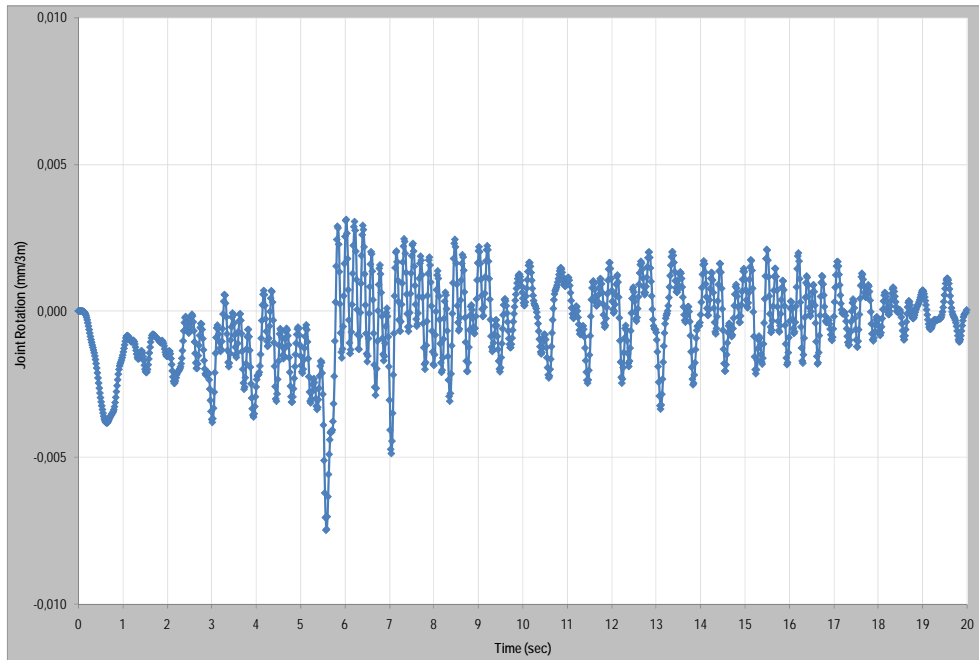


Figure A.68 Joint rotation vs. time graphic of E4 analysis model with a speed of 70 m/sec

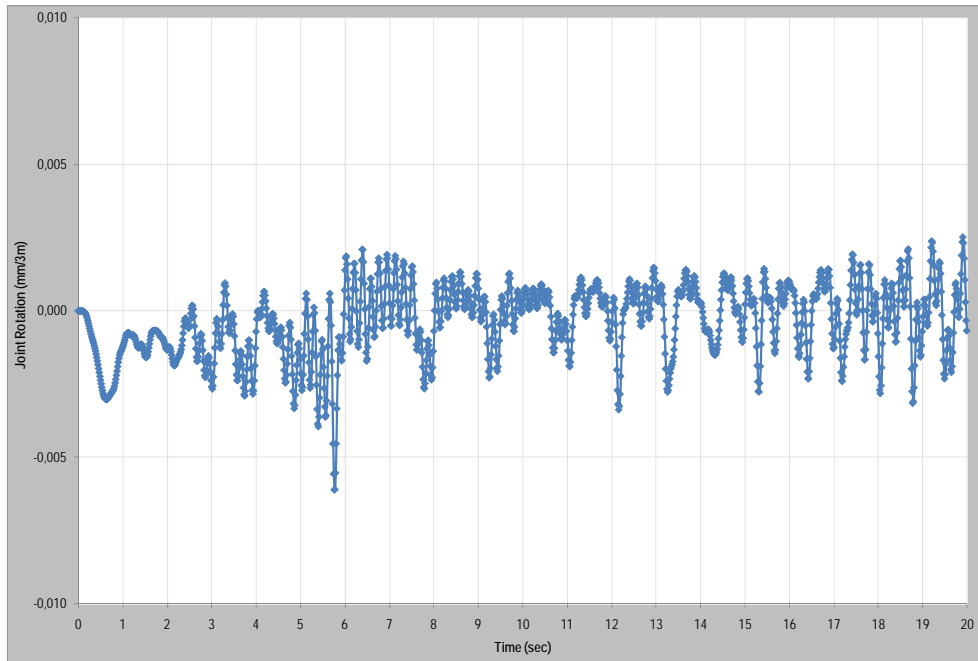


Figure A.69 Joint rotation vs. time graphic of E5 analysis model with a speed of 70 m/sec



Figure A.70 Combined Joint acceleration vs. time graphic of analysis models with a speed of 70 m/sec

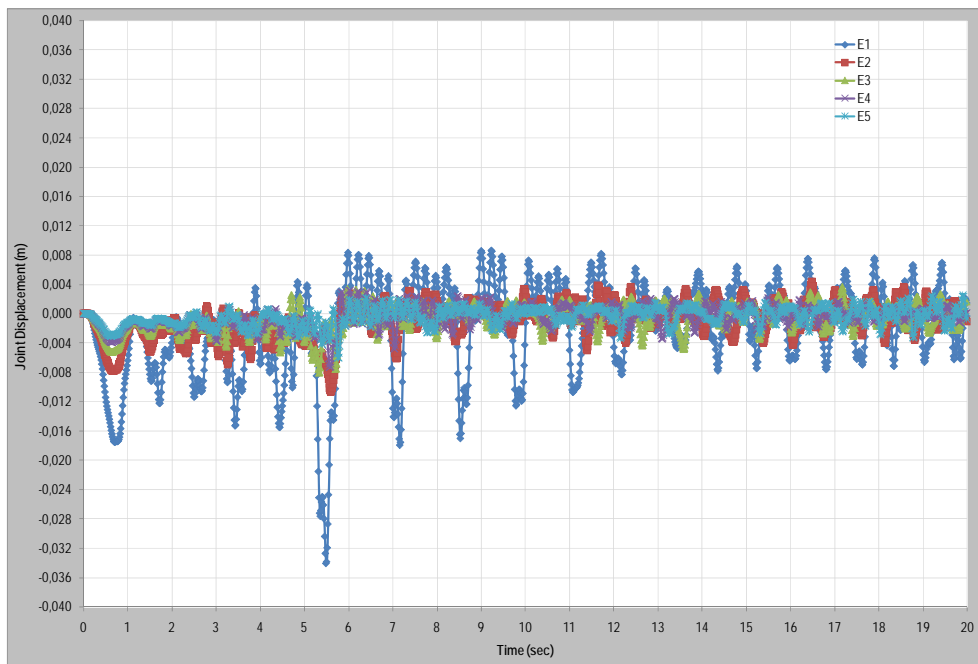


Figure A.71 Combined Joint acceleration vs. time graphic of analysis models with a speed of 70 m/sec

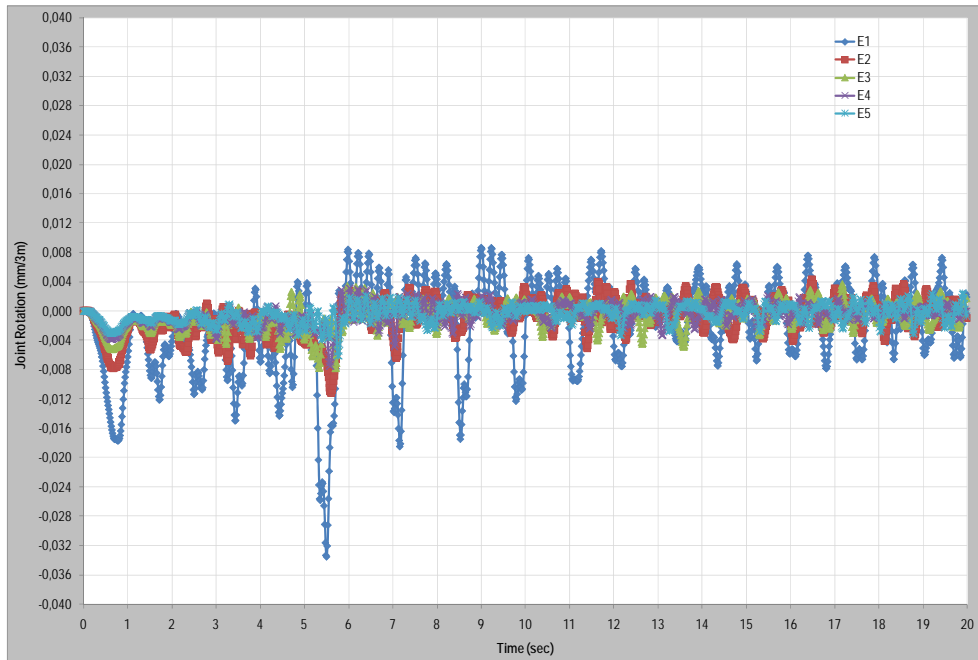


Figure A.72 Combined Joint acceleration vs. time graphic of analysis models with a speed of 70 m/sec